ABSTRACT

Title of Dissertation: OPTICAL AND THERMAL SYSTEMS FOR AUTOMATION OF POINT-OF-CARE ASSAYS

John Goertz
Doctor of Philosophy, 2018

Dissertation directed by: Professor Ian M. White
Department of Bioengineering

Modern medicine has detailed 70,000 different diagnoses; the 21st century challenge is bringing those diagnoses to over 7 billion people. This phenomenal feat requires precision biosensing strategies that minimize necessary training and manual effort while maximizing portability and affordability. Microfluidic strategies, both fabricated chips and paper-based devices, held the promise to facilitate point-of-care diagnostics but have been inadequate for many applications due to the trade-off between bulky pumps or limited control and complexity. This dissertation details novel strategies that control the progression of biochemical reactions with high functionality, portability, and ease-of-use.

First, I will describe an amplified signaling reaction that leverages both positive and negative feedback loops to achieve optically-regulated control. This assay, termed "Peroxidyme-Amplified Radical Chain Reaction" enables naked-eye detection of catalytic reporter DNA structures at concentrations across five orders of magnitude

down to 100 pM while eliminating the need for manual addition of hydrogen peroxide common to other such detection reactions.

Next, I will describe the development of a platform for thermal regulation of generic reactions. To address the need for a broadly capable automation platform that provides equal utility in the lab and field alike, we recently developed “phase-change partitions”. In our system, purified waxes segregate reagents until incremental heating melts the partitions one by one, causing the now-liquid alkane to float and allowing the desired reagents to interact with the sample on demand. This tight control over reaction progression enabled us to construct hands-free detection systems for isothermal DNA amplification, heavy metal contamination, and antibiotic resistance profiling. My work has demonstrated a broadly capable suite of assay control systems with the potential to enable simple, inexpensive automation of a broad array of chemical and biological analysis across human medicine, environmental surveillance, and industrial chemical synthesis.

OPTICAL AND THERMAL SYSTEMS FOR AUTOMATION OF POINT-OF-CARE ASSAYS

by

John Phillip Goertz

Dissertation submitted to the Faculty of the Graduate School of the
University of Maryland, College Park, in partial fulfillment
of the requirements for the degree of
Doctor of Philosophy
2018

Advisory Committee:
Associate Professor Ian M. White, Chair
Associate Professor Jason Kahn
Assistant Professor Huang-Chiao Huang
Professor Don DeVoe
Professor Srinivasa Raghavan

Dedication

To Ron and Carrie Goertz. My parents instilled in me a passion for science from an early age, while allowing me the freedom to choose my own path in life. As a teacher, my dad loved giving exciting demonstrations that captivated the audience, an appreciation of the instructive power of visual presentations that stuck with me and can be seen in many of the experiments shown here. As a marine veterinarian, my mom conveyed to me the power, beauty, and fragility of the natural world, a view that has shaped my perspective on the ways my research can contribute to saving it. The values that both my parents imparted to me gave me goals in life, a purpose, a desire to focus my career on finding ways to help those people less fortunate.

To Jennifer Goertz, whose enthusiasm has always been infectious, whose trust has always driven me to be the best role model I can, and whose confidence has always made me reach higher.

To Alex Ivovic, whose support has helped me through the hardest parts of graduate school, whose joy has reminded me to live my life outside of the lab, and whose love has always embraced the best and worst parts of who I am.

I love you all.

Acknowledgements

I could not have completed the work presented in this thesis on my own. I am deeply indebted to my lab mates for their input during group meetings, the frequent spontaneous brainstorming sessions, the manuscript revisions, and the idle musings that led to the research presented here. Drs. Wei Yu, Eric Hoppmann, and Kunal Pandit, as well as Sean Vergile, helped me get started in the lab, laying the foundation for the rest of my doctoral work. Dr. Stephen Restaino, Imaly Nanayakkara, Alessandra Zimmermann, and Hieu Nguyen all have contributed immensely to my success in graduate school, providing feedback, fresh perspectives, and new ideas.

My advisor and mentor Dr. Ian White allowed me the freedom to explore my own ideas during my doctoral work, no matter how crazy they may have seemed. Many failed, some succeeded, and through it all I learned what it takes to develop something remarkable, something with a chance of making a difference. His guidance instilled in me a solid foundation of biosensing fundamentals, inspired me with some harebrained ideas of his own, and somehow managed to solidify my desire to become a professor myself.

The undergraduates I worked with helped me in many ways, assisting with experiments, asking questions that challenged my hypothesis, and teaching me what it takes to teach others. This includes Eden Paul and Carolyn Lane, though our work together was neither published nor presented in this thesis. This includes Adam Berger, Megan Dang, Connor Hall, and Aliyah Taule. And most of all this includes Kenya Colvin, who performed much of the experimentation in Chapter 6, and Andrew Lippe,

who provided assistance to Chapter 6 and performed much of the experimental in Chapter 5. You've all helped me more than you know.

Dr. Jason Kahn, whose biochemical insight was particularly helpful during the development of Chapter 3 but also continuously helped me gain a better understanding of nucleic acid interactions, knowledge that will serve me well in the future.

Finally, to the Fischell Family, whose Fellowship support allowed me to attend this graduate program and gave me the freedom to pursue my own research ideas, untethered to any grant.

Table of Contents

List of Figures

1 Introduction

In many ways, this is a story about hydrogen peroxide. How it's used, how it's transported, the myriad ways it's generated, how we can get around it, how we can harness it, and how we can simply make it easier to work with. This oxidizing agent has enabled a vast array of biosensing reactions, qualitative and quantitative, high-tech and low-resource. Through catalysis by enzymes such as horseradish peroxidase or by DNA analogues such as G-quadruplex hemin aptamers, H_2O_2 is used to produce colored solutions, fluorescent molecules, electrochemical currents, and chemiluminescent glows. The literature is replete with physical and biochemical strategies for isolating a catalytic reporter in proportion to the analyte of interest, or generating such a reporter in response to the presence of the analyte, so that a final addition of H_2O_2 allows detection and potentially quantitation of the target. Many of these strategies seek to alleviate the burden of expensive, bulky instrumentation, making their assay more portable and less labor-intensive than traditional tests.

Yet that final step, the manual introduction of our oxidative friend, is so often overlooked. It is a difficult friend, to be sure: never one to play nice with others, it could ruin essential assay reagents if added too early, and its unstable temperament makes it difficult to store dry and prone to decomposition even when stored wet. And so, as we will see, a veritable cornucopia of elegant biochemical schemes have been developed for the amplification and detection of trace amounts of analyte only to end with manual addition of hydrogen peroxide. Such a required intervention complicates translation of the assay to even a well-equipped clinical laboratory setting, in which high-throughput, highly-parallelized systems reign through minimization of technician input for

maximization of productivity. Manual interactions are an even greater impediment to use in a rural, resource-poor setting, where trained workers, and their time and attention, are at a premium, spread thin as a result of crippled infrastructure. The need to perform numerous steps by hand prevents exciting new technologies from reaching those who need them most, those left behind by the exciting new technologies of the past. I want to change that. This thesis is a collection of ways we can start to change that.

Chapter 2 begins with an overview of the biochemical reactions I allude to above. I will describe the state-of-the-art approaches for amplifying and detecting a target molecule of interest, focusing on those suitable for (or at least intended for) the point-of-care. I will then detail strategies for automating such reactions through the simple application of heat. While many traditional systems rely on electrical or mechanical automation, the flexible and non-contact nature of thermal automation offers many advantages.

The remainder of this thesis details various engineering solutions to improving the capabilities and accessibilities of molecular diagnostics and (bio)chemical detection. Chapter 3 presents a biochemical solution to the need for manual addition of hydrogen peroxide that leverages green light to produce it *in situ* through multiple nested positive and negative feedback loops. Chapter 4 describes Phase-Change Partitions, a novel platform for thermal automation, radical in its simplicity, that offers a high degree of control over a diverse range of multi-step reactions amenable to a variety of heating systems and instrumentation. The potential of this platform is illustrated through thermal automation of reactions for isothermal DNA amplification, heavy metal ion

detection, and antibiotic resistance characterization. Chapter 5 provides a strategy for achieving the temperature control necessary to actuate these partitions in a field setting, without electricity, and demonstrates successful multi-step DNA amplification in this manner. Chapter 6 extends the capabilities of thermal automation through phase-change partitions to include *in situ* convective mixing, removing the need for manual agitation. Finally, Chapter 7 presents the re-engineering of the layered phase-change partitions into self-contained capsules, offering improved robustness, modularity, and manufacturability.

2 Literature Review: Amplified and Automated Strategies for Point-of-Care Assays

2.1 The ELISA

A discussion of point-of-care diagnostics must inevitably start with immunoassays. Since the late 20th century, human diagnostics have been dominated by the immunoassay, in particular the enzyme-linked immunosorbent assay (ELISA) (Lequin, 2005). The high affinity and exquisite selectivity of antibodies for their targets has enabled highly sensitive detection of a broad range of clinically relevant analytes. Often used to test for patient exposure to a specific antigen, the basic ELISA consists of a plate decorated with the antigen and an enzyme, typically horseradish peroxidase, conjugated to an antibody specific to human IgG. Patient serum is applied to the plate so that the relevant antibodies bind to the immobilized antigen. After several washes, a solution of enzyme-linked antibody is applied and allowed to interact with the patient antibodies. Unbound labeling antibodies are washed away, then a substrate solution is added along with H_2O_2, producing a color change proportional to the amount of patient antibodies trapped in the "sandwich" between immobilized antigen and labeling antibody.

It should quickly become apparent that this assay has many drawbacks that impair its use at the point-of-care (Drain et al., 2014; Gubala et al., 2012; Yager et al., 2008). Multiple wash cycles and extended incubations are difficult to achieve in a setting where trained human capital is at a premium. The tools and instrumentation required are often too bulky to be portable, while the proteins and reagents involved must be carefully stored to avoid deterioration. Finally, the ratio of reporter molecules (HRP) to target is typically one-to-one or only slightly higher, limiting the detection limit. Yet

for all these drawbacks, it is difficult to overstate the importance of the ELISA on clinical diagnostics. As alluded to in Chapter 1, hydrogen peroxide embodies the key advantages and the prominent disadvantages of the ELISA. H_2O_2 added at the end of the assay enables a visible color change that is highly sensitive to the analyte concentration. However, it must be added manually so that the color-generating reaction doesn't begin prematurely and because it may impact antigen-antibody binding. Accordingly, a great degree of effort has been spent trying to replicate the success of this assay through a platform more amenable to point-of-care diagnostics.

This literature review will focus on two aspects of those efforts. First, I will describe the evolution of catalytic G-quadruplex DNA structure to improve upon the reporter enzyme itself. This functional nucleic acid structure enables the same colorimetric detection scheme as HRP, yet exhibits greater stability, greater substrate diversity, and greater flexibility. Leveraging such catalytic DNA to engineer an amplified assay for visible biosensing is the subject of Chapter 3 of this dissertation. Next, I will present an overview of strategies for thermal reaction automation. Automation of reagent-handling can remove many of the manual steps from assays such as the ELISA, improving their usability, while doing so through thermal actuation provides a convenient platform amenable to a range of settings. Development of my own systems for thermal automation is the subject of the remaining chapters of this dissertation.

2.2 G-quadruplex Amplification Systems for Point-of-Care Diagnostics

2.2.1 Structure and function

Although G-quadruplexes as structural motifs had been known about for some time (Arnott et al., 1974; Gellert et al., 1962; Howard et al., 1977), it wasn't until twenty years ago that their catalytic properties were discovered. While attempting to identify

an aptamer capable of catalyzing porphyrin metalization, Travascio et al. (1998) discovered the G-quadruplex sequences PS2.M and PS5.M. They found that these sequences could bind with hemin (iron protoporphyrin IX) and catalyze its ability to facilitate the H_2O_2-driven oxidation of 3,3',5,5'-tetramethylbenzidine (TMB). Since then, a great number of hemin-binding G-quadruplex sequences with peroxidase-mimicking properties (here referred to as peroxidymes for brevity) have been identified, varying in their structure (parallel/antiparallel unimolecular/multimolecular) and catalytic activity. While basal catalytic activity is lower than that of HRP, peroxidymes exhibit significantly greater thermal (Guo et al., 2017; Ito and Hasuda, 2004) and solvent stability (Abe et al., 2012).

The most active G-quadruplex structures typically form from single-stranded sequences with tandem runs of three guanines separated by a minimal number of other nucleotides (Burge et al., 2006; Nakayama and Sintim, 2012). As shown in Figure 1, each guanine forms a planar G-quartet with guanines from the other sets via hydrogen bonding between the van Hoogsteen face of the nucleotides, rather than the canonical

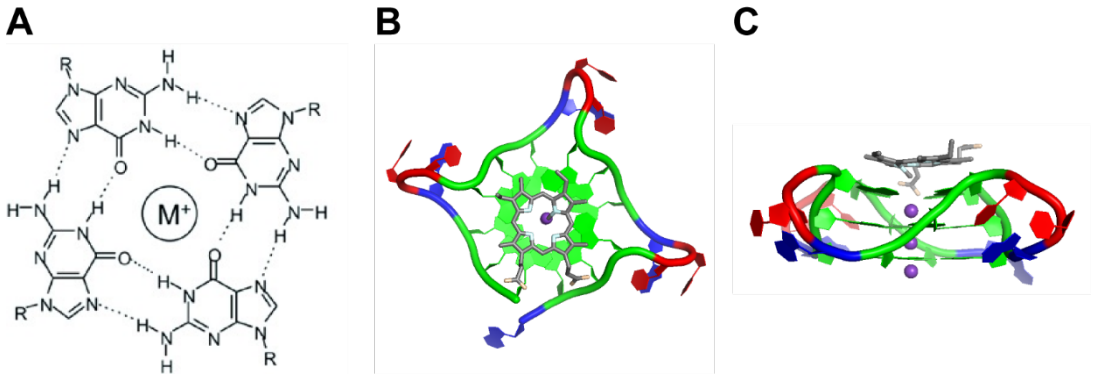

Figure 1. A) Planar G-tetrads nucleated by a metallic cation (M+) stack to form G-quadruplexes (image by Julian Hupert, https://commons.wikimedia.org/wiki/File:G-quadruplex.jpg). **B)** Top and **C)** side view of a G-quadruplex complexed to N-methyl mesoporphyrin IX (PDB 4FXM), a structurally similar compound to hemin. Guanines are indicated in green, thymines in red, adenines in blue, and potassium ions as purple spheres.

Watson-Crick face (Burge et al., 2006). The stacking of three or more such G-quartets forms a G-quadruplex, nucleated around one or more monovalent cations; most reports employ Na^+, K^+, or NH^{4+} (Nakayama and Sintim, 2012, 2009b). Hemin then stacks on top of one of the external faces of this structure, facilitated by a planar structure similar to that of the G-quartets (Li et al., 2009a; Shumayrikh et al., 2015). The ability of peroxidymes to catalyze hemin-mediated redox reactions stems from the formation of a coordination complex between the central iron of hemin and a nucleotide in the DNA sequence (Li et al., 2009a, 2016; Stefan et al., 2012). This is analogous to the mechanism of catalysis in HRP, for which a histidine provides such coordination (Newmyer et al., 1996).

Peroxidymes are capable of catalyzing redox interactions between a wide range of "fuel" and "reporter" substrates (in the sense of H_2O_2 and TMB, respectively). This includes colorimetric (TMB, ABTS, Stefan et al., 2012), fluorescent (Amplex Red, dichlorofluorescein diacetate, tyramine, Nakayama and Sintim, 2009a), chemiluminescent (luminol, Li et al., 2008), and electrochemical (ferrocene, Tang et al., 2012) reporters, as well as oxidative (H_2O_2, Travascio et al., 1998) and reductive (NADH, Golub et al., 2011) fuels; G-quadruplexes have indeed been found to be capable of mediating every reaction catalyzed by HRP, in addition to some reactions involving substrates sterically hindered from entering HRP's catalytic core (Yang et al., 2011). Apart from hemin, a variety of ligands have been identified that allow direct detection of the G-quadruplex structure via a change in the ligand's spectroscopic properties.

2.2.2 Biosensing and Amplification

There is a vast body of literature describing the use of peroxidymes as biosensors, which has been reviewed extensively (D. Chang et al., 2016; Gong et al., 2015; Kosman and Juskowiak, 2011; Neo et al., 2012; Roembke et al., 2013; Silverman, 2016; Teller and Willner, 2010; Willner et al., 2008). Here, I will give a brief overview of the primary strategies through which this is accomplished, for detection of metal ions, small molecules, nucleic acids, and proteins.

2.2.2.1 Direct Sensing

The most straightforward use of peroxidymes for sensing is to detect the nucleating cation itself or molecules that directly interact with the nucleating cation. Colorimetric potassium "sensors" have been designed in this way (Li et al., 2009c; Yang et al., 2010), as have sodium (Sun et al., 2016) and terbium (J. Zhang et al., 2011), while Rb+, Cs+, Sr^{2+}, Ba^{2+}, Pb^{2+} and have all been found to increase catalysis by some sequences towards some substrates (Nakayama and Sintim, 2012). Alternatively, "signal-off" sensors have been constructed via metal cations which exhibit high affinity to certain sequences (sufficient to competitively displace K^+, e.g.) but do not promote catalysis, or otherwise disrupt the G-quadruplex structure. Direct detection of Pb^{2+} (Li et al., 2010; Liu et al., 2014), Hg^{2+} (Li et al., 2009b), and Ag^+ (Kong et al., 2010; Zhou et al., 2010a, 2010b) has been achieved this way, as well as detection of ligands for those cations which prevent their insertion into the G-quadruplex, such as H_2S (Tang et al., 2016) and cysteine (Kong et al., 2010; Zhou et al., 2010a, 2010b). The majority of these sensors have been colorimetric in nature, utilizing ABTS or TMB.

Just as the "protein" aspect of HRP facilitates its use for detection of other proteins (through, e.g., production of streptavidin-HRP fusions and HRP-labeled antibodies),

the nucleic acid “aspect” of G-quadruplex catalysts makes them a natural reporter for detection of other nucleic acids. Sandwich assays have been designed in which a target sequence is immobilized to a surface via partially-complementary capture oligo, then labeled and detected with a peroxidyme sequence extended to include an “arm” complementary to the exposed region of the target (Pavlov et al., 2004). Several DNA sequence-specific sensors have been engineered by designing probe oligos which trap a reporter G-quadruplex-forming sequence into an inactive double-stranded conformation, only to be displaced by a target sequence complementary to the probe oligo (Xiao et al., 2004; L. Zhang et al., 2011; Zhou et al., 2012). Alternatively, researchers have designed split peroxidymes: two halves of the parent sequence that are each extended with oligos complementary to neighboring regions of a target. These split peroxidymes are unable to associate into catalytic structures in solution unless brought into close proximity by the target (Darius et al., 2010; Deng et al., 2008; Nakayama and Sintim, 2009b).

Aptamers are short DNA or RNA oligos which are engineered to bind to a particular target with high affinity and specificity (Ellington and Szostak, 1990; Jayasena, 1999; Mairal et al., 2008; Tuerk and Gold, 1990). They naturally present an attractive biorecognition motif for use in tandem with G-quadruplexes, and have been extensively employed for detection of a variety of targets, ranging from small molecules (Ruscito and DeRosa, 2016; Stojanovic et al., 2001), proteins (Fan et al., 2008; Ma et al., 2014), or even whole cells (Wang et al., 2017; W. Zhao et al., 2011).

Some aptamers (notably the thrombin aptamer and MUC-1 aptamers) themselves adopt catalytic G-quadruplex structures in the presence of their target, offering a

straightforward strategy for detection (Hua et al., 2013; Li et al., 2008; Yang et al., 2015). Aptamer sequences have also been simply extended to include the peroxidyme sequence, enabling detection via a sandwich assay (Du et al., 2011).

The same displacement strategy described above for detection of DNA sequences through complementary probe oligos has been applied for detection of aptamer targets: the aptamer constitutes the probe sequence, trapping a partially-complementary G-quadruplex in an inactive conformation until binding to its target, at which point the G-quadruplex is released into an active conformation (J. Jiang et al., 2013; Yang et al., 2012; L. Zhang et al., 2011; Zhou et al., 2012).

2.2.2.2 Amplified Detection

The direct sensing strategies described above are limited in their detection sensitivity by the one-to-one ratio of G-quadruplex reporter to target molecules. While the peroxidyme continuously produces signal (to an extent, Yang et al., 2011), this rate of signal growth is nonetheless insufficient to detect trace analyte quantities. To improve the sensitivity of peroxidyme-driven sensing systems, many authors have leveraged the wealth of nucleic acid amplification strategies (Deng and Gao, 2015; Ness et al., 2003; Reid et al., 2018) to generate numerous peroxidyme copies in response to each target molecule.

The displacement strategy described above, wherein a peroxidyme sequence is caged within a DNA structure and released by competition of a different oligo, can be extended to produce a cascading, self-propagating system. Hybridization Chain Reaction (HCR) (Chemeris et al., 2008; Dirks and Pierce, 2004) leverages two or more metastable DNA hairpins that are stable in solution together until one is unfolded by a

target sequence, exposing a region of one hairpin capable of unfolding the other. Unfolding this second hairpin exposes a region capable of unfolding the first, so the cascade results in long chains of concatenated probe sequences. The loop region of these hairpin sequences can be modified such that a G-quadruplex forms upon unfolding (Dong et al., 2012; Shimron et al., 2012; Wu et al., 2015). Catalytic Hairpin Assembly (CHA) (Y. Jiang et al., 2013) operates under a similar principle, except that multicomponent DNA complexes are rearranged from a non-signaling to a signaling conformation without concatamerization, and has been leveraged in isolation (Zang et al., 2015) or in tandem with HCR (Wu et al., 2016) to produce active peroxidymes.

While enzyme-free amplification systems have the advantage of simplicity, flexibility in storage, and potentially cost over enzyme-based strategies, they are often "leaky", exhibiting high background due to substrate DNA synthesis impurities and their inherent instability. As such they often achieve worse sensitivity than the comparably stable enzyme systems. In these systems, the peroxidyme is either liberated from a trapped conformation (Cheglakov et al., 2006; Yang et al., 2014), reconstituted from a "split" conformation (Darius et al., 2010), or generated *in situ* from a complementary sequence (Bhadra et al., 2014). Polymerase Chain Reaction, the gold standard for nucleic acid amplification described in depth in the next section, has been extensively used for amplified generation of catalytic G-quadruplexes in a target-specific manner (Bhadra et al., 2014; Cheglakov et al., 2006; Darius et al., 2010; Seok et al., 2014; Yang et al., 2014). Finally, isothermal amplification strategies have been engineered to synthesize the peroxidyme sequence in parallel with the target amplicon through Rolling Circle Amplification (RCA) (Bi et al., 2010; Liu et al., 2016; L. Tang

et al., 2012; Wen et al., 2012; Zeng et al., 2013), Exponential Amplification Reaction (EXPAR) (Nie et al., 2014; Y. Xu et al., 2016), and Helicase-Dependent Amplification (HDA) (Pollet et al., 2012).

2.2.3 Conclusion

Catalytic G-quadruplexes are a highly versatile biochemical reporter for a wide range of biosensing schemes. Amenable to a broader substrate selection than HRP, they present a flexible tool compatible with a variety of detection settings and platforms. They have been used both for direct detection and as the product of amplified detection reactions. However, while they improve upon these factors compared with HRP, they retain a chief limitation: the manual addition of H_2O_2. With few exceptions (Golub et al., 2011), every reaction described above required manual addition of H_2O_2 as its final step. Often, this is not as simple as add-and-read: typically, the reaction must be developed for anywhere from 10 to 30 minutes or more. Strategies for getting around this central limitation by automating the delivery of reagents are the subject of the next section of this chapter.

2.3 Thermal control of biochemical reactions[1]

Facilitated by numerous strategies for achieving temperature control in a highly flexible variety of form-factors, researchers have developed an array of systems that leverage thermoresponsive physical and biochemical transitions to control the progression of biochemical reactions. Meltable barriers have been used to block fluidic channels or as capsular shells, segregating reagents until the appropriate thermal

[1] This section is being submitted for publication as a review article. As such, it contains references to my own work described in later chapters of this dissertation.

stimulus is applied. Thermoresponsive polymers have been used to control substrate diffusion or to modulate enzyme activity. Complementary to these thermal control strategies, many approaches have been developed systems for portable heat regulation, from chemical to electrical heating. Here, we review the breadth of these various developments, highlighting their advantages and disadvantages and identifying ways in which they may be integrated to a complement each other.

2.3.1 Introduction

Biochemical detection leverages the interplay of biology, materials science, chemistry, and physics for the recognition, transduction, amplification, and detection of the target molecule in a complex biological matrix. The numerous demands of sample preparation and signal generation require the design of assays with several interdependent nodes, each performing their individual function in isolation before passing on the sample to a subsequent stage. Traditional systems are comprised of several separate steps carried out and strung together manually. However, this piecemeal approach leads to high costs and labor demands, impairing the accessibility of such assays to poor populations and rural settings. On the other hand, integration of the various components into a single platform, the output of each stage seamlessly and automatically forming the input to the next, has the potential to alleviate these disparities and empower the translation of laboratory assays to the field. Microfluidic devices were developed to achieve this goal, but the extensive pumps and other peripheral equipment required impairs the true portability and accessibility of such miniaturized systems (Whitesides, 2006). The capillary action of paper has similarly enabled construction of highly portable assays (Martinez et al., 2010; Yager et

al., 2008), but in isolation they are limited in the complexity they support and the degree of control they allow. To expand the capabilities of these systems or even to supersede them, a diverse array of thermally-actuated strategies have been developed that take advantage of the manifold means of regulating temperature. These techniques employ physical barriers and biochemical modifications to achieve thermal control, comprising a highly capable toolkit for integrated reaction automation.

The evolution of polymerase chain reaction (PCR) is illustrative of the overall evolution of thermally controlled reactions. This elegant biochemical system is itself a form of thermal automation: DNA strands are separated at high temperatures and replicated at lower temperatures by Taq, a thermostable polymerase isolated from a bacterium that inhabits thermal hot springs (Saiki et al., 1988). PCR is the gold-standard approach for nucleic acid amplification and detection, a now-ubiquitous technique by which specific DNA sequences are replicated exponentially to produce sufficient quantities for diagnostics, forensics, sequencing, synthetic biology, and many other applications. The simplest form of the assay is not without drawbacks, however, and myriad efforts have been devoted to leveraging physical and biochemical transitions modulated by the requisite temperature changes to improve the fidelity and usability of the reaction. This review will begin with an overview of the most popular modifications to PCR, both physical and biochemical approaches. We will then discuss related strategies found in more generic platforms for biochemical control. Finally, we will review techniques for achieving the thermal control itself in a portable format.

2.3.2 Hot-start PCR

"Hot-start" PCR is perhaps the most widely-used form of thermal reaction regulation. Central to this reaction is oscillating the sample between 95 °C, at which target DNA duplexes are separated, and ~60 °C, where short DNA primers anneal to the separated strands are extended enzymatically, replicating the target sequence exponentially (Figure **2**A). The annealing temperature is critical to exert selection pressure for primer binding towards the perfectly-complementary target region and away from nearly-complementary off-target regions (it should be noted that some PCR protocols for specific target/primer combinations specify separate temperatures for primer annealing and enzymatic extension, but the difference between these temperatures is irrelevant to our discussion). Due to its exquisite sensitivity, any off-target interactions between the primers and undesired sequences can significantly impair the specificity of the reaction, potentially overwhelming on-target interactions. Early incarnations of the assay encountered problems during the initial warm-up phase: at intermediate temperatures, primers could bind to nearly-complementary regions, either within sample DNA or within the primers themselves (Figure **2**B). While comparably weak, these off-target interactions created kinetic traps that led to replication of the wrong sequence. To avoid these complications, reactions were prepared without the polymerase and heated to the denaturation temperature, at which point polymerase and/or primers was added manually. In addition to being cumbersome and labor-intensive, exposing the reactions to the environment at this stage risked contamination by either "wild" DNA or aerosolized DNA products from previous reactions.

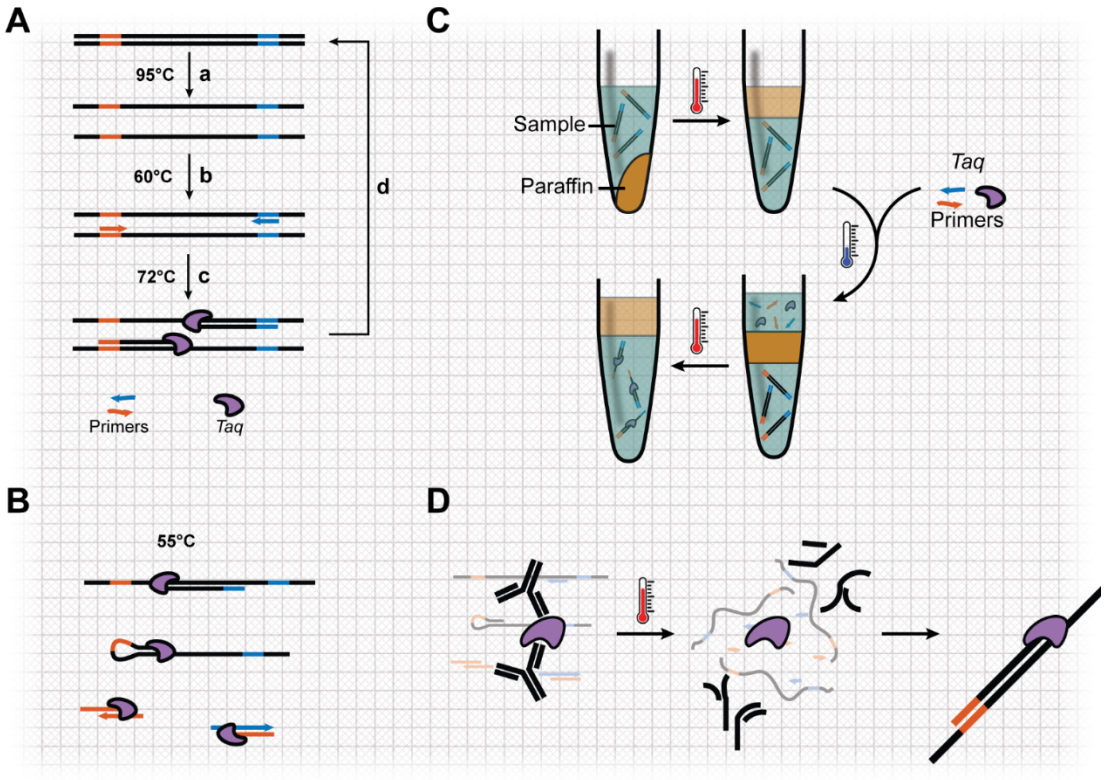

Figure 2. Hot-start Polymerase Chain Reaction. **A)** PCR exponentially replicates a target DNA sequence by cycling through thermally-controlled stages: (a) denaturation of duplex DNA, (b) annealing of short primer sequences, (c) extension of the primers by a polymerase, and (d) repeating the cycle to further replicate the newly-synthesized strands (Saiki et al., 1988). **B)** At intermediate temperatures experienced while the reaction is warming up, off-target priming, secondary structures, and primer dimers can lead to replication of undesired sequences, impacting the sensitivity and specificity of the reaction (Chou et al., 1992). **C)** A physical solution for engineering a "hot-start" reaction that avoids these complications is to use a wax barrier to separate the polymerase from the sample until a high enough temperature is reached to melt the wax (Hébert et al., 1993). **D)** A biochemical approach is to engineer antibodies to inhibit the polymerase's activity that denature at high temperatures (Kellogg et al., 1994).

2.3.2.1 Wax-assisted hot-start

An early solution to manual addition of reagents in such a "hot-start" system was to separate the enzymes from the bulk reaction using wax (Chou et al., 1992; Hébert et al., 1993) (Figure **2**C). A sample solution was placed in reaction tubes along with the appropriate buffer and dNTPs as well as a piece of paraffin wax with a suitably high

melting point. The tube was heated to melt the wax and then cooled, forming a solid layer of wax that effectively sealed the sample solution below, after which a second solution containing primers and polymerase were added on top of this barrier. The solutions remained isolated from each other until the melting point of the wax was reached (designed to be near the desired annealing temperature), at which point the now-liquid wax is displaced by the enzyme solution above and floats, allowing the two solutions to mix and the reaction to proceed. In this application, the wax plays the dual roles of separating the reagents until the desired temperature is reached and, after it melts and floats to the top of the aqueous solutions, acting as a vapor barrier that prevents evaporation of minute reaction volumes (typically 10-50 µL) at elevated temperatures. Purpose-built wax beads were sold under the brand name Ampliwax PCR Gems (Chou et al., 1992), but have since been discontinued; simple paraffin wax was found to be equally effective, as only the sterility and not the precise volume of the wax barrier is strictly necessary (Hébert et al., 1993). Ampliwax beads were also used to achieve one-pot, two-step reverse-transcriptase PCR (RT-PCR) for amplification of RNA sequences (Sears and Khan, 2003). The reverse transcription reaction (wherein RNA is enzymatically copied into complementary DNA) took place above the solid wax barrier, which was then melted to begin PCR.

2.3.2.2 Biochemical-assisted hot-start

While wax barriers provided a simple method of thermally regulating initiation of PCR, they impaired assay throughput. To reduce the burden on the user of forming the wax barriers, biochemical approaches to hot-start PCR were found. Soon after the introduction of Ampliwax beads, engineered antibodies were used as thermolabile inhibitors of Taq polymerase (Kellogg et al., 1994). The antibodies prevented primer

extension by the enzyme until they heat-denatured, at which point polymerase activity was restored (Figure **2**D). Later adaptations replaced the antibodies with aptamers (Lin and Jayasena, 1997; Noma et al., 2006), single-stranded nucleic acid sequences engineered to bind to a specific target under desired conditions (Ellington and Szostak, 1990; Tuerk and Gold, 1990). Aptamers are advantageous to antibodies due to their abiotic discovery, ease of synthesis, and flexibility to be tailored to specific interaction conditions (Jayasena, 1999; Mairal et al., 2008; Zimbres et al., 2013). Aptamers have also been used to engineer "warm start" Bst polymerase that is inhibited until reaching 50-60 °C (New England Biolabs, 2017) extending the benefits of thermally-regulated reaction initiation to isothermal nucleic acid amplification techniques such as loop-mediated isothermal amplification (LAMP) and exponential amplification reaction (EXPAR) (Reid et al., 2018; Tanner et al., 2012). Other biochemical strategies include utilizing Taq mutants that exhibit reduced activity at moderate temperatures (Kermekchiev et al., 2003), designing primers to lock themselves within blunt-end hairpin configurations until the appropriate target-annealing temperature is reached (Kaboev et al., 2000), and finally employing an additional enzyme (typically RNAse HII) to cleave non-extendible protecting groups off primer 3' ends at the appropriate temperature (Dobosy et al., 2011).

The various strategies for achieving hot-start PCR present archetypes for thermal control of other reaction systems. As we will expand upon below, the most widely-used approach for a thermally-automated platform is to physically separate reagents after or until a certain temperature is reached. Waxes are often used to accomplish such a burst valve, although in some instances the working solution itself is frozen and/or thawed.

The second category of thermal control systems leverages biochemical transitions at elevated temperatures, analogous to antibody or aptamer-inhibited Taq. In one model, the swelling characteristics of thermosensitive polymers have enabled sequestration of compounds for controlled-release; in another, the polymers are conjugated to enzymes such that the folding state of the protein, and thus its activity, is dependent on the folding state of the polymer. While the physical-separation approach offers the advantages of simplicity and low cost, the biochemical approach may be preferable for integration of several independently thermoresponsive components in a highly compact, all-aqueous system.

2.3.3 Physical Transitions

The most straightforward method of thermal reaction control is simply to physically separate reagents with a barrier that melts at a specified temperature. As in the example of wax-assisted hot-start PCR, paraffin has been the primary means to achieve this, as an encapsulant of reagents or as a valve in a fluidic channel. Alternatively, the thermal control over fluid flow has been achieved by leveraging the volume change of a melting material (again, typically paraffin) to fashion a pump. This section will discuss strategies such as these that exploit the physical transition of materials at certain temperatures.

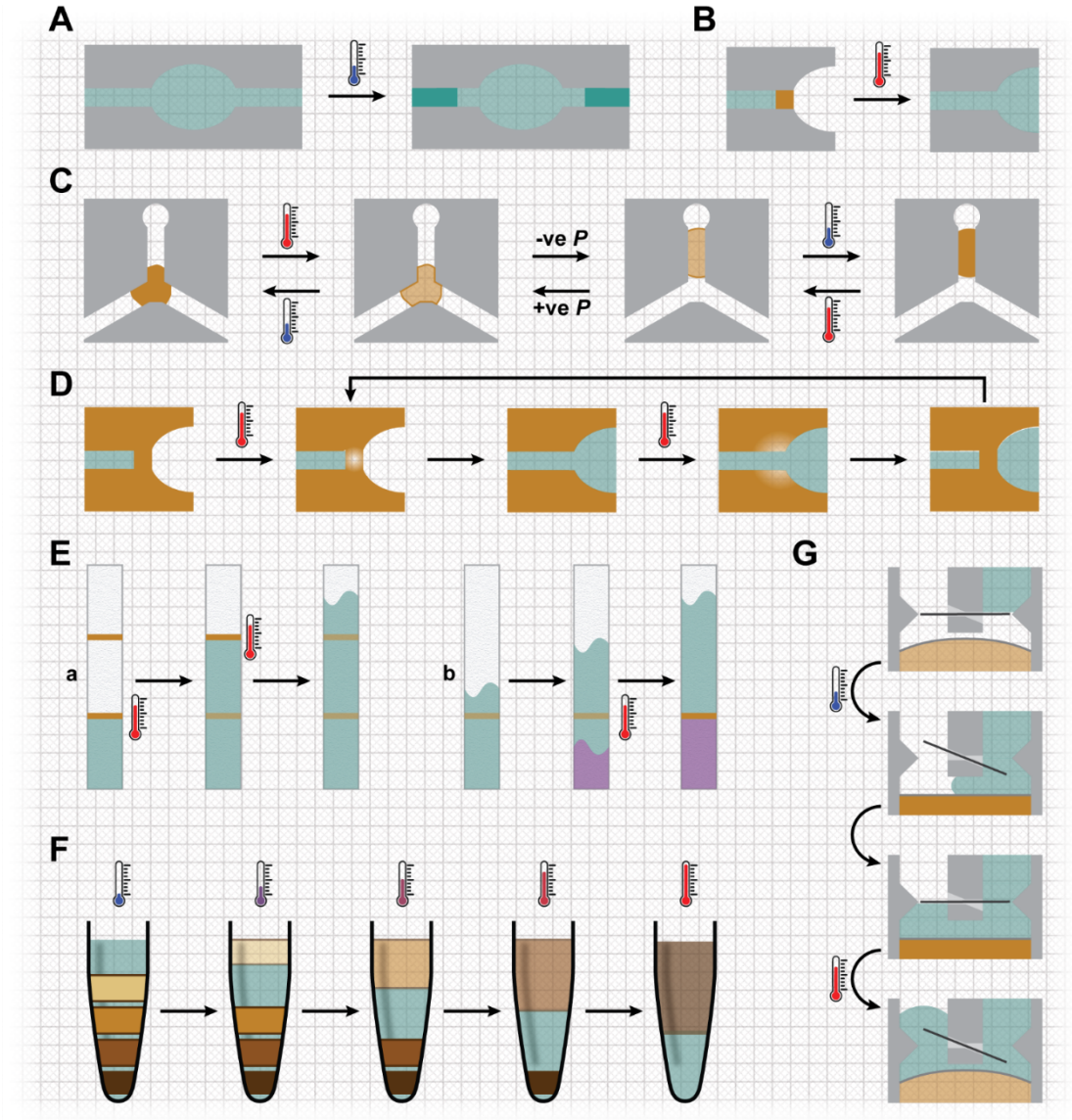

Figure 3. Physical valves and pumps. **A)** The simplest thermal valves freeze portions of the working solution (Chen et al., 2005) or **B)** use a wax plug to obstruct flow (Lee et al., 2009). **C)** Positive and negative pneumatic pressure can be used to reposition a "latchable" wax plug (Liu et al., 2004). **D)** Channel walls can be fabricated directly out of wax and cyclically opened and closed with localized heating (Díaz-González et al., 2016). **E)** Wax valves can be printed onto paper in either (a) closed-to-opened or (b) opened-to-closed configuration, actuated with localized heating (Phillips et al., 2016). **F)** Different purified alkanes can be layered in a tube to segregate various reagent zones until the respective melting temperature is reached (Goertz and White, 2018). **G)** The volume change accompanying wax melting/freezing can be leveraged with a mechanical one-way valve to create a pump (Sim et al., 2003).

2.3.3.1 Fluidic control

Microfluidic devices have emerged as highly capable systems for sample manipulation and reaction control (Whitesides, 2006). Sub-millimeter channels fabricated within (typically) polymer monoliths enable the miniaturization of biochemical reactions with numerous steps at high throughput. This aqueous reaction solution provides a natural medium capable of arresting fluid flow when cooled. Such freeze-thaw phase-change valves, leveraging water/ice transitions in the working solution, have been constructed using thin-film electric cooling devices (Chen et al., 2005; Gui and Liu, 2004; He et al., 2001) (Figure **3**A). Pneumatic control is often used to drive fluid flow through microfluidic devices, and it has been combined with microfabricated heaters to cyclically melt, reposition, and solidify a wax plug to block or open a primary fluidic channel, either directly or through an elastomer membrane (Liu et al., 2004; Pal et al., 2004; Yang and Lin, 2007) (Figure **3**E). A key advantage of this thermo-pneumatic approach is that it is "latchable": only switching the valve requires energy (to melt and reposition the plug), not maintaining the valve in one state or another. Rather than using wax to seal a channel made from a different material, which can pose interfacial problems and difficulties in fabrication, Díaz-González et al., (2016) constructed microfluidic channels within molded wax sandwiched between glass plates (Figure **3**D). Embedded thin-film heaters could directly melt the wax between two regions to open a new channel or could melt the wax adjacent to a channel to close it, with multiple actuation cycles possible.

Centrifugal microfluidic systems rely on the centripetal acceleration provided by a spinning (typically disk-shaped) platform to replace the pumping systems used to drive fluid flow through traditional microfluidic channel systems. Fluid motion is governed

by channel geometry as well as rotation speed and direction (Gorkin et al., 2010), but extended incubations of a sample within a particular chamber is difficult to achieve with only these variables. To achieve such control, paraffin wax was embedded with ~10 nm iron oxide nanoparticles (referred to as Ferrowax), which could then be melted with a 1.5 W laser, enabling both valve actuation and thermal lysis of bacteria (Cho et al., 2007; B. S. Lee et al., 2009) (Figure **3**B). The twelve separate valves actuated this way in four stages facilitated a sample-to-answer colorimetric immunoassay system. Such a thermally-automated valve system likely led to a far simpler centrifugal disk design than could be achieved with passive valves, but at the significant added cost of a high-powered laser and the accompanying power requirements and spatial control system. To accomplish similar control without requiring the spatial resolution of a laser, Abi-Samra et al., (2011) employed high- and low-melting paraffin to achieve multistage liquid handling in CD microchannels, and Kong et al., (2015) used various temperature cycles to melt, solidify, and re-melt wax valves with a similar goal.

Paper-based devices have emerged to enable passive fluidic networks capable of processing small fluidic volumes. The capillary action of paper (or a similar fibrous/porous membrane) drives fluid motion along its length, the kinetics of which can be tuned through channel geometry and additives (e.g., sugar barriers or surfactant accelerators). However, in most cases the timing of network components is dictated by design and not adjustable at the point-of-use, often limited to short reaction times. Phillips et al., (2016) used a wax-ink office printer to create thermally-actuated barriers to capillary flow (Figure **3**E). During printing, wax only minimally penetrated the paper substrate, creating “open” valves that permitted fluid flow but could be “closed” by

heating (41 °C or 48 °C for 15 or 25 seconds for nitrocellulose or chromatography paper, respectively), presumably to allow the wax to fully penetrate the membrane. Subsequent heating "opened" the valve, allowing an advancing fluid front to displace a portion of the now-molten wax and continue to flow downstream.

The authors achieved independent actuation of as many as six sequential valves spaced ~5 mm apart, although high spatiotemporal control over heating was necessary since all valves were composed of the same material. The authors demonstrated the ability of their valves to enable thermal automation of a gold-enhanced lateral flow immunoassay (LFIA), in which an enhancement solution was separated from the primary antigen-immunogold-capture reaction by a wax valve that was then melted to initiate enhancement, improving the visibility of the signal.

Lafleur et al., (2016) leveraged wax valves for sample flow control through both flexible tubing and a paper network. Their device enabled lysis, amplification, and multiplexed detection of bacteria from directly from a nasal swab. Chemical heat aided lysis and actuated the tubing valve, while a custom printed circuit board provided the heating necessary for amplification and actuation of the paper valve.

Recently, our group extended the idea of reaction control via phase transitions to create a generic platform amenable to thermal automation of a wide range of assays (Goertz and White, 2018). Instead of relying solely on paraffin waxes – which are heterogeneous in composition and display broad, often multimodal melting transitions – we employed purified alkanes (octadecane, eicosane, docosane, tetracosane) that exhibited well-defined melting transitions. Aqueous reagent layers were interspersed with hydrocarbon barriers (formed by deposition of molten alkane), each displaying a

lower melting point than the one beneath. These partitions could then be melted one by one to introduce specific reagents to the sample solution on demand (Figure **3**F). As many as four sequential reactant additions were demonstrated, and this tight control over reaction progression enabled us to construct hands-free detection systems for isothermal DNA amplification, heavy metal contamination, and antibiotic resistance profiling.

Notably, this "phase-change partition" technology is not only compatible with already-ubiquitous thermocyclers intended for PCR, but the broad separation of alkane melting points mean that less precise (and less expensive) means of temperature control (e.g., water baths, consumer kitchen water-heaters, meal-ready-to-eat field ration heaters) are sufficient for thermal automation of such assays. Other hydrophobic substances may be able to be used in place of or in tandem with purified alkanes – we found that purified fatty acids performed well as thermally-actuated barriers, but shorter chains exhibited non-negligible solubility at elevated temperatures that may potentially impact reaction conditions (unpublished data). While thermally stable, this platform is susceptible to mechanical disruption. The interface between the wall and the solidified alkanes is a natural weak point that can be dislodged through rough handling. Furthermore, this platform is, naturally, only compatible with reactions in which the entire volume carries over from each step to the next. Many assays dictate transfer of a small portion from an initial reaction to a significantly larger volume of subsequent reactants in order to minimize incompatibilities between reaction buffers and components. Such assays would obviously have to be re-designed to be adapted to this platform.

In addition to using meltable materials to block fluid flow, researchers have reported the use of paraffin as thermally-actuated pump, wherein the volume (and pressure) change resulting from the melting/freezing of heterogeneous and homogeneous alkane waxes drives fluid motion (Ogden et al., 2014). A representative example of a phase-change pump can be found in Sim et al., (2003). A silicon rubber membrane separates a sealed actuator chamber, containing water and a heating element, from a pumping chamber with one-way valves on either end (Figure **3**G). Activating the heater vaporized the actuating water, deflecting the silicon membrane into the pumping chamber and expelling fluid downstream; subsequent deactivation of the heater led to condensation of the actuating water, relaxing the silicon membrane and drawing upstream fluid into the pumping chamber. Similarly, Mamanee et al., (2006) and Yoo et al., (2007) leveraged thermal expansion of air to deflect PDMS and construct a peristaltic micropump for microfluidic systems. To construct a solid-liquid phase-change actuator, Liu et al., (2018) embedded paraffin within a matrix of expanded graphite and nickel microparticles, producing a microactuator that was self-sealed (within the graphite pores) and could be heated inductively (due to the electrical conductivity of the graphite and the magnetic permeability of the nickel) to achieve up to nearly 400 μm actuation height.

2.3.3.2 Encapsulation

An alternative approach controlling flow of a reaction solution through a network of reagent zones is to create self-contained compartments with meltable walls. This

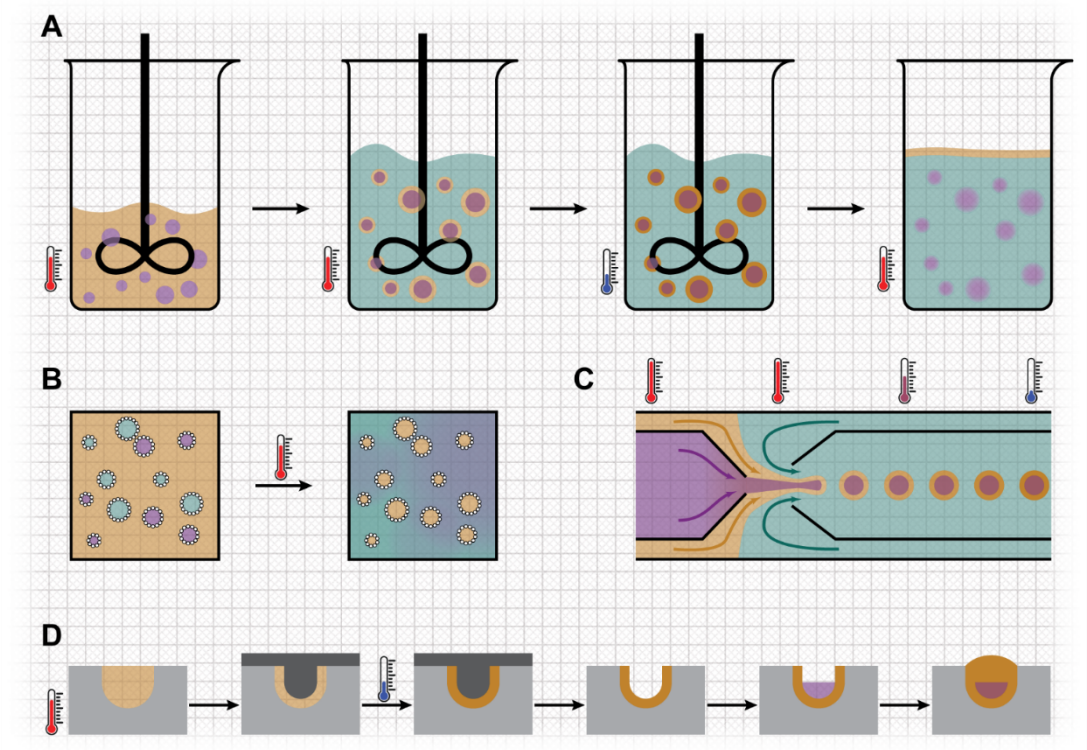

Figure 4. Physical encapsulation strategies. **A)** For bulk emulsion encapsulation, the core is first dispersed in molten shell material. This single emulsion is then mixed into a hot "continuous" phase to produce a double emulsion (e.g., water-in-oil-in-water), which is then rapidly cooled to solidify the shells. The core-shell microcapsules can be subsequently melted to release the cargo (Taguchi et al., 2014. **B)** In a Pickering emulsion, nanoparticles stabilize the oil-water interface. These emulsions undergo phase inversion at high temperatures, transitioning from a water-in-oil emulsion to an oil-in-water emulsion and allowing different cargo solutions to mix (Binks et al., 2005). **C)** Capillary microfluidics enables tight control over core-shell dimensions and monodispersity. An aqueous core phase is introduced to a co-flowing molten shell phase. Counter-flowing continuous phase pinches the coaxial streams into droplets, which are rapidly cooled to form core-shell microcapsules (Sun et al., 2010). **D)** Mesoscale capsules can be cast in arbitrary shapes. Molten shell material is poured into a cast, then a stamp is fixed in place to form a hollow cavity. When the stamp is removed, the capsule is filled with cargo, then capped with additional shell material (Goertz et al., submitted).

strategy has the potential to improve manufacturability of thermally-controlled systems by enabling modular, asynchronous assembly of the complete assay system rather than the sequential construction required by many wholly integrated systems.

Wax encapsulation has been achieved through bulk emulsion and spray-cooling methods. Taguchi et al., (2014) prepared a water-in-oil-in-oil double emulsion of aqueous azur B in paraffin wax prepared in silicone oil and tuning the leakage behavior by increasing the amount of surfactant (Poem J0021) (Figure **4**A). Mellema et al., (2006) employed a similar melt dispersion-emulsion strategy. Industrial techniques such as fluidized bed spray-coating have also been used to produce wax capsules (Jozwiakowski et al., 1990; Knezevic et al., 1998), but the stability and monodispersity of such encapsulations is often poor.

Instead of traditional molecular surfactants, nanoparticles have been used to stabilize the oil-water interface in so-called Pickering emulsions (Chevalier and Bolzinger, 2013; Pickering, 1907; Ramsden, 1904). Such emulsions are naturally sensitive to temperature, as oil-in-water emulsions formed at room temperature undergo catastrophic phase inversion at elevated temperatures to form water-in-oil emulsions (Binks et al., 2005) (Figure **4**B). Greater control over thermal behavior of Pickering emulsions has been achieved by employing as the colloidal stabilizer micro/nanoparticles surface-coated by or entirely comprised of pNIPAAm (Destribats et al., 2012; Monteux et al., 2010; Ngai et al., 2005; Tsuji and Kawaguchi, 2008; Zhang et al., 2010; Zoppe et al., 2012) or poly[2-(dimethylamino)ethyl methacrylate] (PDMAEMA (Tang et al., 2014; Zoppe et al., 2012).

Vreeland and Locascio (2003) synthesized liposomes containing aqueous cargos through a freeze-thaw cycling method. The liposomes were then passed through a microchannel superimposed with a static temperature gradient. While below the melting point of the lipid chain, in the gel phase, the liposomes exhibited low permeability, as they did above the melting point, in the fluid phase; in the region of the melting point, however, the disordered membrane released its cargo into the microchannel. Tuning the poles of the thermal gradient offered spatial control over this behavior.

Microfluidics has enabled fabrication of small thermoresponsive compartments with tighter control over size and homogeneity than that afforded by conventional emulsion methods. Sun et al. (2010) used a flow-focusing capillary microfluidic device to produce water-in-oil-in-water (w/o/w) double emulsions where the “oil” phase constituted molten fatty glycerides, paraffin oil, or purified alkanes that hardened into a shell upon cooling (Figure **4**C). In their apparatus, the aqueous core phase was extruded in a thin stream into the co-flowing oil shell phase and pinched into separate droplets by an aqueous outer phase flowing antiparallel. After encapsulation in this manner, the core phase could be released into the supernatant by melting the shell. The droplets had to be rapidly cooled in an ice bath immediately following generation or the more-dense core would sink through the less-dense shell, leading to very thin capsule walls or premature coalescence with the outer phase. While no surfactant was necessary within the core phase (a crucial consideration for biochemical assays) it was necessary that the core contain approximately 50% glycerol to increase its viscosity to roughly that of the molten wax phase. By using dual-bore capillary tubes to inject

multiple core phases into the shell phase, they demonstrated the fabrication of wax compartments containing two distinct cores, and it is likely that higher-order multicompartment capsules could be generated as per similar approaches found in their and others' reports (Chu et al., 2007; Duncanson et al., 2012; W. Wang et al., 2014).

We recently reported the encapsulation of mesoscale volumes through casting of hollow wax capsules in a manner analogous to injection molding (Goertz et al., submitted) (Figure **4**D). Molds were either directly 3D printed or cast from a 3D-printed master, then filled with molten phase-change partitions, and joined with a 3D printed stamp to form cup-shaped structures. These cups could be filled with liquids, solids, or hydrogels, then capped, and sealed by immersion in a lower-melting phase-change partition. The capsules were stable against leakage and evaporation and were used to contain hazardous materials for thermally-automated sensing applications. The flexibility afforded by 3D printing should enable this principle to be expanded to other volumes, geometries, and applications.

2.3.4 Biochemical Transitions

In the biochemical archetype of hot-start PCR described above, antibodies or aptamers inhibited the enzymatic activity of Taq until being denatured or "melted" off. This principle of leveraging alterations in biochemical interactions at elevated temperatures has been harnessed to modulate the activity of other enzymes as well as to control flow through channels and for controlled-release of the entrapped of molecules. This has primarily been achieved through the use of thermoresponsive polymers. The vast range of such polymers and their applications has been reviewed previously (Klouda and Mikos, 2008; Roy et al., 2013; Trzebicka et al., 2017). By far

the most popular such polymer is poly(N-isopropylacrylamide) (pNIPAAm) (Heskins and Guillet, 1968; Klouda and Mikos, 2008; Roy and Gupta, 2003; Schild, 1992; S. Satarkar et al., 2010), although similar or even superior thermoresponsive properties have been identified in poly[2-(dimethylamino)ethyl methacrylate] (pDMAEMA)

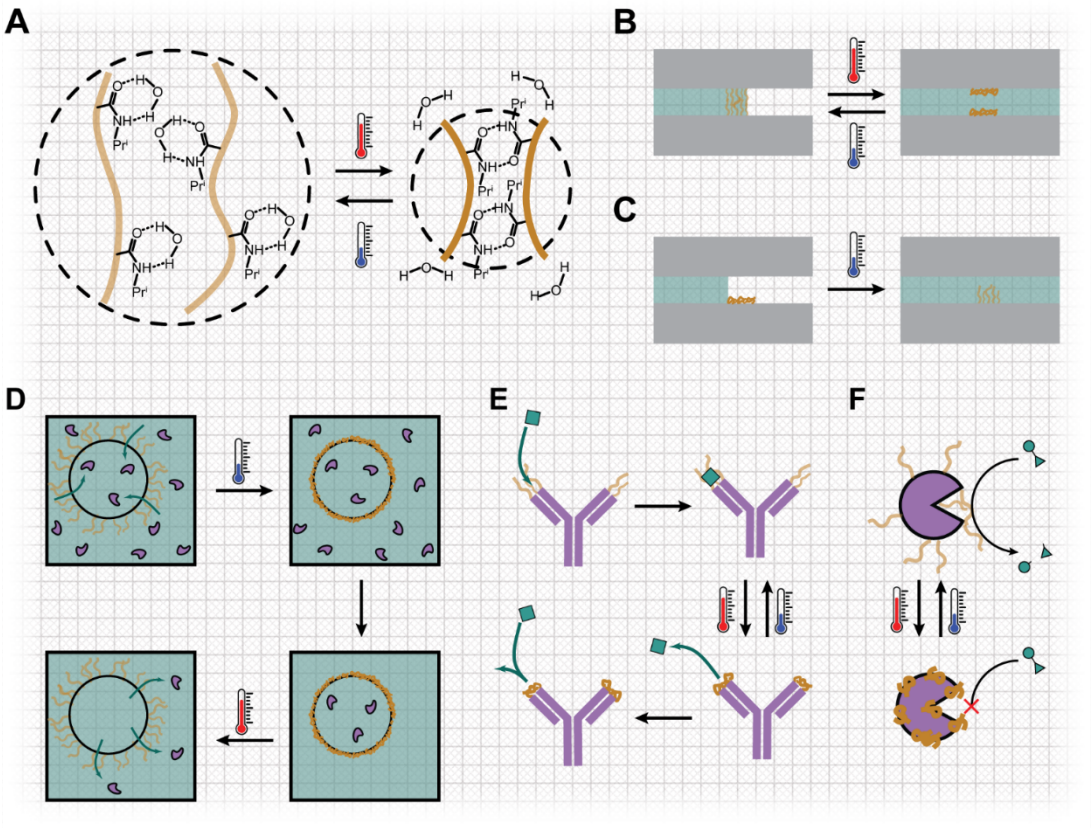

Figure 5. Biochemical strategies for thermal control. **A)** Thermoresponsive polymers such as pNIPAAm transition from forming hydrogen bonds with water at low temperatures to forming hydrogen bonds with other polymer units at high temperatures, with a corresponding decrease in volume and hydrophilicity (Weng and Xie, 2015). **B)** Under driven flow, a swollen polymer plug arrests fluid flow, while collapsed polymer permits flow (Yu et al., 2003). **C)** Under capillary flow, the hydrophobicity of the collapsed polymer prevents wetting of the channel wall, arresting flow, while swollen polymer permits wetting and corresponding flow (Londe et al., 2008). **D)** Polymer microcapsules are loaded with reagents at high temperature, prevent escape at low temperature, and release their cargo at high temperature (Ma et al., 2013). **E)** Polymer can be conjugated to binding proteins, permitting binding at low temperatures while prevent binding and releasing bound molecules at high temperature (Liu et al., 2008). **F)** Enzymes conjugated with polymer exhibit reduced catalytic activity at higher temperatures (Molawi and Studer, 2007).

(Glinel et al., 2003; Tang et al., 2014; Zoppe et al., 2012), 2-(2-methoxyethoxy)ethyl methacrylate (MEO2MA) and oligo(ethylene glycol) methacrylate (OEGMA) copolymers P(MEO2MA-co-OEGMA) (Lutz et al., 2006; Ma et al., 2013), poly(N-vinylcaprolactam) (pVCL) (Ramos et al., 2012), and poly(4-hydroxybutyl vinyl ether) (pHOBVE) (Sugihara et al., 2007). These polymers exhibit temperature-dependent swelling, optically and diffusively permeable at low temperatures but collapse at temperatures above the lower critical solution temperature (LCST, ~32 °C for pNIPAAm), undergoing a corresponding hydrophilic-to-hydrophobic transition (Figure **5**A). Polymers which exhibit the reverse behavior, swelling at high temperatures while collapsing at low, are less prevalent (Roy et al., 2013).

2.3.4.1 Valves

The polymer pNIPAAm has also been used to create a thermo-responsive valve (Figure **5**B). At temperatures above the polymer's LCST it forms intramolecular hydrogen bonds, rendering it hydrophobic, while below the LCST those hydrogen bonding sites are available to external molecules, rendering it hydrophilic. Yu et al. (2003) leveraged this transition to obstruct or permit fluid flow through a microchannel via a pNIPAAm plug (Figure **5**B). Londe et al. (2008) tuned the wettability of the floor of a microchannel with the polymer (Figure **5**C), enhancing the hydrophobic state with the superhydrophobic surface agent (1H,1H,2H,2H-perfluorooctyl) silane deposited on top of the pNIPAAm and enhancing the hydrophilic state through a polyelectrolyte network assembled layer-by-layer beneath.

PMIPAAm was similarly employed in a capillary microfluidic system, in which the temperature-dependent swelling of the polymer completely blocked the channel and

could be oscillated repeatedly (Idota et al., 2005). Capillaries could also be coated in such a way that the swollen polymer did not block flow, but the hydrophobic surface of the contracted polymer could trap hydrophobic molecules in solution, releasable upon re-swelling (Idota et al., 2006).

Buchholz et al. (2001) used solution-phase copolymers of diethylacrylamide and dimethylacrylamide to create a "viscosity switch" for capillary DNA sequencing. Dispersed in the sample solution, the polymer matrix offered low viscosity at high temperatures, ideal for rapid loading of the capillary, and high viscosity at room temperature, achieving adequate sieving of the DNA oligos.

2.3.4.2 Microcapsules

Thermoresponsive polymers have been used extensively to create core-shell microcapsules, entrapping molecules at high temperatures that diffuse out at lower temperatures (Glinel et al., 2003; Suzuki et al., 2001; Zarket and Raghavan, 2017) (Figure **5**D). A representative example of this approach can be found in Ma et al. (2013). Capsules were also formed by coating silica nanoparticles with random copolymer branches of 2-(2-methoxyethoxy)ethyl methacrylate (MEO2MA) and oligo(ethylene glycol) methacrylate (OEGMA). Removing the silica core via HF etching produced hollow capsules responsive to both pH and temperature that could be stimulated to load and subsequently release cargo molecules. The transition temperature could be tuned to 38, 47, and 56 °C by varying the stoichiometry of the copolymer components.

2.3.4.3 Biomolecular Interactions

Thermoresponsive polymers have also been tethered directly to enzymes and other proteins to thermally modulate their folding structure, accessibility to substrates, and/or

catalytic activity. (Ding et al., 2001) conjugated poly(N,N-diethylacrylamide) (pDEAAm) to streptavidin. The unfolded polymer shielded the protein's binding site such that attachment of biotinylated proteins was dependent on size and temperature: small proteins (protein G, MW 6.2 kDa) could bind at any temperature, intermediate proteins (BSA, MW 66 kDa) could bind only above the LCST, and large proteins (IgG, MW 150 kDa) were unable to bind at any temperature; thermally-triggered release of bound molecules was also possible.

Liu et al. (2008) conjugated carboxyl-terminated pNIPAAm via carbodiimide/hydroxysuccinimide (EDC/NHS) chemistry to antibodies immobilized on an electrode surface, creating an immunoassay that could be operated above the LCST and refreshed below the LCST (Figure **5**E). While antigen-antibody binding was reduced by 83% upon reducing the temperature, and minimal hysteresis was observed across several cycles, there was no comparison against binding to unmodified antibody.

Golden et al. (2010) modified both antibodies and a filtration membrane with pNIPAAm via RAFT (Reversible Addition-Fragmentation chain Transfer) polymerization. Above the LCST the membrane was semi-permeable, allowing unmodified solution molecules through while obstructing passage of conjugated antibodies and their complexes with antigen and labeled detection antibodies; below the LCST, the membrane lost this sieving action. This enabled ~40-fold concentration of target antigen with 84% total recovery, facilitating clinically-relevant immunosandwich detection of a malaria antigen with a total assay time of ten minutes.

Lee and Park (2008) conjugated copolymers of pNIPAAm and glucosyoxylethyl methacrylate to trypsin to allow moderate thermal modulation of its activity and

improve its thermal stability (although basal enzymatic activity of conjugates was <30% of unmodified trypsin), while Molawi and Studer (2007) employed a different polymerization strategy to prepare pNIPAAm-trypsin conjugates with completely suppressed activity above the LCST (although basal enzyme activity was not compared to unmodified trypsin) (Figure **5**F).

Similarly, De et al. (2008) conjugated pNIPAAm to BSA via RAFT polymerization. Basal esterase activity of the protein was reduced by less than 10%, and several thermal modulation cycles of esterase activity were achieved. However, the degree of deactivation above the LCST was rather minimal: below the LCST, enzyme activity was ~90% that of unmodified protein; above the LCST, it was reduced to ~75%.

2.3.5 Portable Temperature Control

Thermal control is attractive for many applications in part due to its flexibility. Myriad systems exist for regulating temperature, and heating can be accomplished in a portable, compact device with a minimum of peripheral equipment. Many strategies have been developed for such portable temperature control, particularly for the purpose of maintaining the necessary temperatures for isothermal nucleic acid control. In this section, we will explore approaches for inexpensive, portable temperature regulation, including compact electronics and electricity-free systems.

2.3.5.1 Electrical

The Arduino platform has provided a compact, modular, low-cost, easily-programmable microcontroller for a variety of thermally-based diagnostics. It offers the potential to not only record and control temperature changes but also modulate/record optical signals, actuate mechanical components, communicate with

Bluetooth devices, geotag samples, and interface with Internet systems. Reaction systems leveraging an Arduino have been used for LAMP detection of *Pseudomonas syringae peponis* (Velders et al., 2018) as well as Zika, chikungunya, and dengue viruses (Priye et al., 2017); PCR detection of *Bacillus subtilis*, *Neisseria gonorrhoeae*, Ebola virus, and drug-resistant *Staphylococcus aureus* (Priye et al., 2016; Restaino and White, 2018; Wong et al., 2015); RPA detection of *Chlamydia trachomatis* (Ereku et al., 2018); as well as paper-based detection of creatinine in whole blood (Tseng et al., 2018). While the Arduino itself is small, portable, and low-cost, the power necessary for cyclic temperature ramping may be difficult to realize in a truly field-compatible manner. Dedicated portable electrical heating devices have also been constructed for multi-step thermal sample processing and isothermal amplification (Dou et al., 2017; Lafleur et al., 2016). Finally, solar heat was used to achieve PCR in an Arduino-controlled centrifugal microfluidic device for sample-to-answer detection of Kaposi's Sarcoma herpesvirus (Jiang et al., 2014).

2.3.5.2 Chemical

Phase-change materials (PCMs) have been used extensively as passive temperature regulators. A PCM is simply a material with a desired melting point (typically between 10 °C and 90 °C) and a high latent heat of fusion: as the material melts, the temperature inside remains approximately constant. Thus, PCMs provide thermal buffers around their melting point, relaxing the demands of a tightly-controlled heating source. There is a vast body of literature devoted towards characterizing and manipulating such materials for solar heating and “smart” construction and textile composites (Farid et al., 2004; Yuan et al., 2014; Zalba et al., 2003). The most common materials include paraffin-like waxes (Fang et al., 2010a; Li et al., 2013; Sarı et al., 2015, 2014), fatty

acids (Alva et al., 2017; Chen et al., 2013; Fang et al., 2011, 2010b; Latibari et al., 2013; Pielichowski and Flejtuch, 2003; Pourmohamadian et al., 2017; Song et al., 2014; Yuan et al., 2014; Zhang et al., 2012), and hydrated salts (Liu et al., 2017; Ryu et al., 1992a; Shin et al., 2015). Typically, the PCM is encapsulated, either in a core-shell microstructure or within a porous matrix. Doing so improves the thermal conductivity of the PCM, prevents leakage to facilitate re-use, mitigates supercooling (cooling of a liquid below its freezing temperature due to a lack of nucleation), and prevents irreversible phase separation during melting (in the case of hydrated salts) (Farid et al., 2004; Ryu et al., 1992a; Yuan et al., 2014).

Aided by the flexibility afforded by PCMs, researches have developed numerous "non-instrumented" devices that precisely heat biochemical reactions without the use of electricity. (Kubota et al., 2013) constructed a reaction platform based on a thermos with a PCM-filled aluminum sample-holder insert, supplying heat by pouring in boiling water to perform LAMP-mediated detection of *Salmonella enterica*. The heat released by hydration of CaO has also been leveraged for detection of HIV (Curtis et al., 2012), malaria DNA (LaBarre et al., 2011, 2010), and for lysis of *Staphylococcus epidermidis* (W. Liu et al., 2018).

Another approach has been to utilize "Meal Ready to Eat" (MRE) heaters (Buser et al., 2015). Developed for safely cooking military field rations without electricity or fire, MRE heaters consist of fine granules of a MgFe alloy to which saline is added. The resulting galvanic corrosion is highly exothermic, with an approximately 15-fold greater energy density than the CaO system (Buser et al., 2015). An additional advantage of this system is improved control over heating: the temperature profile can

be tuned by varying granule size, saline concentration, and saline delivery rate (Buser et al., 2015; Liu et al., 2011). This heating system has been used with various PCMs, typically within a vacuum thermos and often with the aid of a smartphone, for detection of *E. coli* (Liu et al., 2011), HSV-2 (Liao et al., 2016), Zika virus (Song et al., 2016), and malaria (Sema et al., 2015), and for lytic enzyme deactivation (Buser et al., 2016).

2.4 Conclusion

As seen above, microfluidic flow can be controlled through direct freeze/thawing of the primary solution or phase change of a pumping/valving solution. Similarly, reagents can be sequestered within capsules, released upon melting of the shell material. Paraffin is the most common material with which to achieve thermal flow control in microfluidic systems through phase transitions, either as a pump or a valve, thanks to its convenient melting temperature, structural stability, and low cost. However, due to its heterogeneous nature, paraffin exhibits multiple solid-state phase transitions below its canonical melting temperature in addition to a broad transition profile near the melting temperature, as revealed by differential scanning calorimetry (Ogden et al., 2014). Many of the above platforms would likely benefit from the relaxed technical considerations of instead using purified alkanes to achieve thermally automated multi-step fluid handling (Goertz and White, 2018) rather than relying on high spatiotemporal resolution in temperature control to achieve the same with paraffins. Octadecane, eicosane, docosane, tetracosane, and octacosane are relatively inexpensive (the intervening odd-numbered alkanes are typically much more expensive) and have distinct melting points (30 °C, 37 °C, 42 °C, 52 °C, and 65 °C, respectively). Furthermore, a greater variety of melting points within that range can be

achieved through eutectic mixtures, i.e. a mixture of two or more compounds with different melting points that (when formulated at precise ratios) exhibits a single melting transition lower than any of the constituents (Guo et al., 2004; Inoue et al., 2004a, 2004b; Sarı et al., 2015, 2014).

In contrast to thermal-control strategies that leverage physical transitions, those that exploit biochemical transitions are more complicated to implement. Additionally, while a wax plug can be designed large enough to perfectly sequester reagents, conformational changes in proteins and polymers are rarely perfect in their inhibition or release. However, direct modification of enzymes has the potential to enable highly compact thermally-controllable reactions with multiple integrated steps possible within a single solution. Polymer conjugation to proteins is likely to impair their maximum activity but has been shown capable of actually improving stability against chemical denaturants (Lucius et al., 2016). A potential drawback of thermoresponsive polymers, and biochemically-mediated thermal control in general, is that rarely is the desired transition dependent solely on temperature. Intermolecular and intramolecular interactions are influenced by the presence of electrolytes as well as the pH of the solution. Effective thermal control will require careful consideration of these parameters as well. Biochemical reactions, particularly those involved in exponential nucleic acid amplification, have very low tolerances for undesired enzymatic activity at the wrong stage of the assay. A thermoresponsive polymer strategy for modulating such enzyme activity will have to achieve correspondingly high degrees of inhibition; the modest control achieved in many of the reports examined above may prove insufficient. Additionally, it should be common practice to compare the maximal

activity of modified enzymes with that of unmodified; loss of activity can be compensated for by using proportionately more enzyme but doing so will add to the cost of the assay, on top of the higher unit cost of the modified enzyme itself. Finally, biochemical and physical strategies for reaction control can be augmented by selecting natural or engineered enzymes that are appropriately thermostable or thermolabile. Many thermostable enzymes exhibit sharply reduced activity at lower temperature, providing natural temperature control that can potentially be further tuned with polymer conjugation. Conversely, thermally-controlled reaction systems may also need to utilize biomolecules which retain their activity across a broad temperature range. Catalytic DNA structures are significantly less affected by temperature changes than many proteins (Ito and Hasuda, 2004), and some have been engineered specifically to retain activity at extreme temperatures (Guo et al., 2017; Nelson et al., 2005).

Many of the advantages of thermal automation are particularly beneficial to portable reactions for point-of-care diagnostics. Above, we examined reports for achieving the temperature control necessary in a portable format, from PCM-buffered chemical heating to low-power electrical heating. Oddly, few reports have combined portable heating with thermally-controlled reactions (Goertz et al., submitted; Lafleur et al., 2016), or leveraged physical and biochemical strategies in tandem. Portable heating systems have typically been used for driving isothermal nucleic acid amplification, rarely for actuation of physically meltable barriers or for modulation of biochemical thermal switches. Similarly, it seems that the compactness and modularity of thermoresponsive polymers conjugated to enzymes or microparticles could augment physical segregation strategies, with their capacity for perfect isolation of reactants.

The future of thermal control for biochemical assays will likely focus on achieving tight control over initiation of numerous sequential reaction nodes in a small, portable, low-cost manner. Such developments are poised to facilitate the application of such systems for field-ready environmental surveillance systems, bio/chemical warfare agent detection, and point-of-care diagnostics.

3 Peroxidyme Amplified Radical Chain Reaction (PARCR): Visible Detection of a Catalytic Reporter[2]

Here we circumvent the need for adding H_2O_2 manually by generating it *in situ* in tandem with several optically-driven feedback loops. Other attempts had been made prior to this to work to engineer a G-quadruplex reporter system without exogeneous H_2O_2. This included generation of a colorimetric signal through an H_2O_2-generating feedback loop centered around spontaneous thionitrobenzoic acid oxidation (Golub et al., 2013) – we attempted to replicate these results but observed only minimal concentration-dependence of the resulting signal, with high background. This strategy extends the NADH-driven G-quadruplex-mediated strategy (Golub et al., 2011), which in isolation yielded acceptable concentration-dependence but failed to produce a visible signal. For the purposes of point-of-care, a visible signal is most desirable because it relaxes the requirements of quantification instrumentation. This chapter describes the engineering of feedback loops to accomplish such a result.

3.1 Abstract

We present Peroxidyme Amplified Radical Chain Reaction (PARCR), a novel enzyme-free system that achieves exponential amplification of a visible signal. Typical enzyme-free amplification systems that produce a visible readout suffer from long reaction times, low sensitivity, and narrow dynamic range. PARCR employs photocatalyzed non-linear signal generation, enabling unprecedented one-pot, naked-eye detection of a catalytic reporter from 1 μM down to 100 pM. In this reaction, hemin-binding peroxidase-mimicking DNAzymes ("peroxidymes") mediate the NADH-driven oxidation of a colorless, non-fluorescent phenoxazine dye (Amplex

[2] This work was published in *Angewandte Chemie International Edition,* 56 (43) 2017, 13411-13415

Red) to a brightly colored, strongly fluorescent product (resorufin); illumination with green light initiates multiple radical-forming positive-feedback loops, rapidly producing visible levels of resorufin. We envision PARCR as an easy-to-use readout for a range of detection schemes, including aptamer labels, hybridization assays, and nucleic acid amplification.

3.2 Introduction

Chemical reactions that produce visible color changes have become indispensable to modern analytics and diagnostics (Boehle et al., 2017; Dehghan Esmatabadi et al., 2015; Dungchai et al., 2010; Hänscheid, 1999; H Esterbauer, 1996; Liang et al., 2010; Logu et al., 2001; Martinez et al., 2010; Mazzone et al., 2007), as evidenced by the widespread use of enzyme immunoassays (Porstmann and Porstmann, 1988; Rissin et al., 2010; Yolken, 1982), antibiotic-resistance assays (Boehle et al., 2017; Logu et al., 2001), nanoparticle-aggregation assays (Alivisatos et al., 1996; Hauck et al., 2010; Mazzone et al., 2007), and many others. Typically, the signals produced by these assays are directly proportional to analyte concentration (Porstmann and Porstmann, 1988; Sapan et al., 1999). However, linear signal gain systems such as these exhibit significantly worse sensitivity and dynamic range than exponential amplification systems, which are much less prevalent in the literature (Baker and Phillips, 2012; Gao et al., 2014; Jin et al., 2015; Mize et al., 1989; Obzansky et al., 1991). Additionally, these systems often require enzyme reporters and sensitive spectroscopic instrumentation to achieve maximum performance, limiting their applicability to a narrow range of laboratory settings. Here, we couple photochemical and biochemical feedback loops to achieve exponential signal gain in an enzyme-free

system, allowing naked-eye detection of a catalytic reporter across five orders of magnitude down to sub-nanomolar concentrations. The full dynamic range of this assay, termed Peroxidyme Amplified Radical Chain Reaction (PARCR), can be monitored with an LED and a simple cell phone camera. This reaction leverages the oxidative activity of catalytic nucleic acids in tandem with the photosensitivity of a redox-active fluorophore to exponentially generate fluorescence, rapidly producing a readily visible signal.

The oxidation-sensitive phenoxazine dye Amplex Red (**AR**, N-acetyl-3,7-dihydroxyphenoxazine) has been used for fluorometric detection via either HRP or HRP-mimicking DNAzymes (referred to here as "peroxidymes") (Golub et al., 2011; Nakayama and Sintim, 2009a; Zhou et al., 1997). This reaction, driven by either H_2O_2 or NADH, results in the oxidation of colorless, non-fluorescent AR to produce pink-colored, orange-fluorescent resorufin (**RSF**, 7-hydroxy-3H-phenoxazin-3-one). However, the resulting linear generation of RSF occurs too slowly to become visible to the naked eye within a reasonable timeframe for analysis. Additionally, phenoxazine dyes such as AR are known to be photolabile due to reactivity of the photoexcited fluorescent product with the precursor, a characteristic often cited as a detriment (Zhao et al., 2011; Zhao et al., 2012). The PARCR assay described here exploits this photosensitivity, exponentially generating visible levels of RSF via illumination of a solution containing hemin, NADH, AR, and a peroxidyme sequence ($C(TGGG)_4A$, referred to as "EAD")(Chang et al., 2016; Cheng et al., 2009; Nakayama and Sintim, 2009b) in ammonium-acetate-tris buffer (Figure 6). Peroxidymes, a key mediator of this system, bind to hemin upon adopting a G-quadruplex conformation. This complex

catalyzes similar redox reactions as HRP yet has numerous advantages as a catalytic reporter, including ease of chemical synthesis and modification, environmental stability, and ability to be biochemically synthesized *in situ* (Kosman and Juskowiak, 2011; Mairal et al., 2008; Tombelli et al., 2007; Travascio et al., 1998; J. Xu et al., 2016; Zhou et al., 2014).

3.3 Materials and Methods

Materials and Instrumentation. Hemin, NADH, catalase, resorufin, and Amplex Red (10-Acetyl-3,7-dihydroxyphenoxazine, purity ≥ 98%) were obtained from Cayman Chemicals (Ann Arbor, MI, USA). DNA was obtained from IDT (Coralville, IA, USA). The "EAD" peroxidyme sequence (5'-CTGGGTGGGTGGGTGGGA-3') was used for all experiments except where otherwise noted (see Table 1 for other sequences used).

Standard 96-well clear-bottom black-walled μClear microplates (medium binding) were obtained from Greiner (Kremsmünster, Austria), LightCycler 480 white-walled multiwell PCR plates from Roche (Basel, Switzerland). Clear-walled MicroAmp Optical 96-well reaction plates (ThermoFisher, Waltham, MA, USA) were used for all LED-excited experiments except where otherwise noted.

UV LEDs (5 mm XSL-365-5E) were purchased from Roithner LaserTechnik (Vienna, Austria) and visible LEDs (Screen Master 5 mm oval C566D) from Cree Inc. (Durham, NC, USA); all LEDs have a spectral width <20 nm. A power meter (843-R, Newport, Irvine, CA, USA or UVX-36, UVP, Upland, CA) was used to determine the current required for each LED to produce 250 $\mu W/cm^2$ at approximately 1 cm; for all other values intensity was assumed to be directly dependent on current. LEDs were

held approximately 1 cm above microplate well bottoms via a custom 3D printed ABS jig (Replicator 2x, MakerBot, New York, NY, USA).

A Nanodrop 1000 (Thermo Fisher, Halethorpe, MD) was used to verify stock concentrations of RSF (ε_{570} = 57 $mM^{-1}cm^{-1}$) and NADH (ε_{340} = 6.22 $mM^{-1}cm^{-1}$). Microplate fluorescence and absorbance measurements were performed with Spectramax M5 plate reader (Molecular Devices, Sunnyvale, CA, USA). RSF fluorescence was determined by measuring the emission of 590 nm light due to excitation at 530 nm with a 590 nm cutoff filter; NADH fluorescence was determined with 460 nm emission and 340 nm excitation and a 455 nm cutoff filter. Smartphone-based reaction monitoring was performed by illuminating 8-well PCR strips (Bio-Rad, Hercules, CA) with green LEDs and capturing time-lapse videos with a Galaxy S6 (Samsung, Seoul, South Korea) (5 ms exposure, ISO 50) using the Lapse It Pro app. MATLAB (MathWorks, Natick, MA, USA) was used for all data processing and analysis.

CutSmart Buffer, Klenow Fragment (5'-3' exo-), dNTPs, Nt.BbvCI were purchase from New England Biolabs (Ipswitch, MA, USA), and iQ Supermix from Bio-Rad. A LightCycler 480 II (Roche) was used for PCR.

Data Processing. To quantitatively compare amplification behavior, RSF fluorescence curves that reached a chosen reaction threshold (10^4 RFU) were fit with a modified version of a sigmoidal curve common to exponential reaction curve analysis (Liu and Saint, 2002):

$$F(t) = \frac{F_{max}}{1 + e^{\frac{t - t_c}{k}}} + m \cdot t + F_0 \quad (1)$$

where the fluorescence intensity F at a given time t is related to an initial and maximum fluorescence (F_0 and F_{max}, respectively), a linear offset with slope m, an exponential slope factor k, and the characteristic time t_c used to compare amplification rates (note that, in the pure sigmoid, t_c represents the time at which the fluorescence is half its maximum strength). Data points from the lag and exponential phases were used for fitting (Figure 13); all curve fits had a coefficient of determination $R^2>0.99$.

One-way ANOVA with Dunnett's critical value or one-tailed Student's T-test were used to determine statistical significance assuming $\alpha=0.05$, as appropriate. Significant comparisons are indicated by "*".

Optical Characterization. Initial characterization was performed in standard microplates with a final reaction volume of 100 µL. The peroxidyme sequence known as "EAD" (CTGGGTGGGTGGGTGGGA)(T. Chang et al., 2016; Cheng et al., 2009) was diluted to 300 nM with 1 µM hemin and 100 µM AR in ammonium buffer (500 mM NH_4OAc, 50 mM Tris, pH 7.5) (Nakayama and Sintim, 2009b). The reaction was initiated with the addition of NADH to a final concentration of 100 µM. To evaluate the wavelength-specificity of the photocatalyzed reaction, the reaction mixture was illuminated at 250 µW/cm^2 with LEDs of various colors: red (620 nm), yellow (591 nm), green (527 nm), blue (470 nm), and UV (365 nm). Yellow and green LEDs produced similar reaction rates at various optical intensities, but the green LED was capable of sustaining higher intensities than the yellow and was thus used for all subsequent experiments. Unless otherwise specified, all other experiments were performed under 1.5 mW/cm^2 green light. Excitation light provided by the plate reader

during fluorescence measurements did not significantly contribute to RSF generation (Figure 13).

It should also be noted that the PARCR system is sensitive to the optical characteristics of the reaction vessel: the reactions in Figure **15**C were conducted in clear PCR plates; faster reaction times and decreased sensitivity were observed in opaque, white-walled PCR plates (**Figure 14**D).

The pink solution color becomes noticeable to the naked eye and the orange fluorescence distinguishable from the green excitation light above 2.5 µM RSF; the high extinction coefficient and fluorescence quantum yield of RSF (57 $mM^{-1} \cdot cm^{-1}$ and 0.74, respectively (Bueno et al., 2002; Siu et al., 2014)) eliminate the need for excitation or emission filters for accurate detection.

Mechanistic Investigations and Detection Limit Determination. After initial optical characterization, all further experiments were performed in clear 96-well PCR plates with a reaction volume of 20 µL comprising, unless otherwise specified, 100 µM NADH, 300 nM hemin, and 20 µM AR in ammonium buffer (500 mM NH_4OAc, 50 mM Tris, pH 7.5) (see **Figure 14**, Figure **15**, Figure **18**, and **Figure 19** for reaction behavior under other conditions). Mineral oil was layered over reaction solutions to prevent evaporation over the course of the assay.

ABTS oxidation during PARCR was investigated in standard clear 96-well microplates with a reaction volume of 100 µL. 1 mM ABTS was included in reactions of 100 µM AR, 10 µM RSF, 1 µM EAD, and/or 1 µM hemin, as indicated. ABTS oxidation is typically monitored by an increase in absorbance at 420 nm. However, the

high amounts of RSF generated during PARCR contributed slightly to the absorbance at 420 nm, described by the equation $RSF_{420nm} = f_R*RSF_{570nm}+o_R$. Similarly, oxidized ABTS contributed slightly to the absorbance at 570 nm, described by the equation $ABTS_{570nm} = f_A*ABTS_{420nm}+o_A$. These coefficients were determined empirically to be $f_R = 0.1081$, $o_R = 0.1245$, $f_A = 0.3327$, $o_A = 0.08758$. To account for this, the absorbance at 420 nm due to oxidized ABTS ($ABTS_{420nm}$) was determined from the absorbance at 420 and 570 nm (A_{420nm} and A_{570nm}, respectively) with the following equation:

$$ABTS_{420nm} = \frac{A_{420nm} - f_R(A_{570nm} + o_A) + o_R}{f_A + 1} \quad (2)$$

ABTS concentration was determined using an extinction coefficient of ε^{420} = 32 $mM^{-1}cm^{-1}$ and the solution pathlength determined by the PathCheck feature of the plate reader.

Cell Phone Camera Image Processing. Processing of time lapse cell phone images was done in MATLAB. The (nonlinear) RGB coordinates representing each still image were converted to the (linear) L*a*b* colorspace via standard transforms,(Ginardi et al., 2014; Loh et al., 2011) the average value of each color coordinate was determined for each reaction well, then the Euclidean distance D between color coordinates of an image i and the initial image 0 was used to determine the degree of color change (Archibong et al., 2017; Shen et al., 2012):

$$D = \sqrt{(L_i^* - L_0^*)^2 + (a_i^* - a_0^*)^2 + (b_i^* - b_0^*)^2}. \quad (3)$$

In Situ Peroxidyme Generation. Two methods were used to generate the EAD peroxidyme sequence from a target DNA sequence, polymerase chain reaction (PCR)

and one-sided strand-displacement amplification (SDA). PCR reactions (3-minute "hot-start" followed by 40 cycles of a 30-second 95°C melt step and a 30-second 55°C anneal/extension step) comprised of 1x iQ Supermix, 250 nM forward and reverse primers, 100 µM NADH, 100 nM hemin, and 20 µM AR. Primers contained an antisense EAD sequence on the 5' end of the target-recognition sequence. Immediately following thermocycling, PCR reactions were exposed to green light and fluorescently monitored as above. SDA primers were designed to contain the recognition sequence for the nicking endonuclease Nt.BbvCI between an antisense-peroxidyme sequence and the target-recognition sequence. The reaction mixture consisted of 1x CutSmart buffer, 100 µM NADH, 300 nM hemin, 200 nM primer, 0.2 U/µL Klenow, 0.5 U/µL Nt.BbvCI nicking endonuclease, 500 µM dNTPs, 100 nM target DNA. Negative control reactions contained no enzymes and no target DNA. Primer and target DNA sequences for PCR and SDA reactions can be found in Table 1.

Table 1. DNA Sequences used in this manuscript. Nt.BbvCI recognition site is shown in bold, antisense-peroxidyme sequences are shown in green, and target-complementary regions in italics.

EAD Peroxidyme	CTGGGTGGGTGGGTGGGA
SDA Target	CACAAAAACAGCATATTGACGCTGGGAAAGACCAGAGATCCTGC TGTCTCTGCAACA*TCAATCCAGGCACAGAGCGCCGCAAGATG*
SDA Primer	TCCCACCCACCCACCCAG**GCTGAGG***CATCTTGCGGCGCTCTGTG CCTGGATTGA*
CatG4 Peroxidyme	TGGGTAGGGCGGGTTGGGAAA
PCR Target	*TTGGGACCATAAAACCTCATTCAC*TTTAACCGTTGCCTGCCAAC CAAATCGATAAACGCCCAG*GAAGCAGATGGAGTTGTCGGGTAT*
PCR Forward Primer	TTTCCCAACCCGCCCTACCCAAGAGAC*TTGGGACCATAAAACCT CATTCAC*
PCR Reverse Primer	TTTCCCAACCCGCCCTACCCAAGAGAC*ATACCCGACAACTCCAT CTGCTTC*

3.4 Results and Discussion

We found exponential generation of RSF fluorescence ($\lambda = 591$ nm) occurred most efficiently under yellow or green illumination (Figure 7A), which agrees well with RSF's excitation peak at 570 nm. NADH was also consumed during this reaction at a rate commensurate with RSF generation (Figure 7B), and both rates increased with illumination intensity (Figure 12). The RSF fluorescence data fit well to a modified sigmoidal curve, allowing quantitative comparison of reaction rate by a characteristic time t_c (Equation 1 and Figure **13**). To examine the nature of this exponential behavior, we investigated the interaction of photoexcited RSF and AR alone in buffer. In agreement with previous reports (Zhao et al., 2012), we found that RSF was produced at an exponentially increasing rate from a buffered solution of AR under illumination with green light; spiking RSF into this solution accelerated this reaction in a concentration-dependent manner (Figure 8A). This suggests that, independent from the activity of peroxidymes in solution, photochemical positive feedback results in the production of RSF from solutions of AR. Additionally, this demonstrates that "dark" peroxidyme production of RSF feeds into this self-propagating reaction. Including ABTS led to generation of the colored oxidation product $ABTS^{\cdot+}$ only when AR, RSF, and peroxidyme were all present (Figure 8B), and the presence of EAD and hemin accelerated production of RSF from AR under illumination (Figure 8C). Together, these data suggest production of H_2O_2 during the photooxidation of AR feeds back into "dark" production of RSF by peroxidymes, contributing biochemical positive feedback within the PARCR system.

Although the presence of peroxidymes dramatically accelerated RSF production there was no correlation between EAD concentration and t_c for a fixed hemin concentration (**Figure 14**B), so the addition of NADH was required to produce adequate resolution and sensitivity. Including NADH in the reaction mixture in fact delayed signal generation in solutions of AR alone, AR spiked with RSF, or AR and peroxidyme together (Figure 8C), despite the fact that higher NADH concentrations promoted faster dark reaction rates (Figure **15**). Indeed, in all reactions observed, the onset of exponentially increasing signal generation occurred only after NADH was depleted and the rate of NADH depletion is in fact a good predictor of the characteristic time t_c of RSF fluorescence generation (**Figure 13**B). This is perhaps unexpected since NADH drives RSF production in the dark reaction; however, NADH can also reduce photoexcited ^{3}(RSF)* to RSF$^{\bullet-}$, which subsequently returns to ground-state RSF via oxidation by molecular oxygen, producing H_2O_2 (B. Zhao et al., 2011). Accordingly, NADH depletion in solution with AR, RSF, or peroxidyme individually is similar to basal levels, but it is accelerated in the presence of AR and RSF together and dramatically accelerated in the presence of AR, RSF, and peroxidyme together (Figure 9) . This suggests that while NADH enables “dark” production of RSF, it also inhibits the photocatalyzed reaction, leading to slow signal growth while NADH remains in solution. Once illumination is removed, the reaction returns to the slow signal change characteristic of the dark reaction (**Figure 16**). An advantage of this latter phenomenon is that it enables a relatively stable color record of reaction progress once illumination ceases.

Taken together, our data and others' results suggest the following mechanism for PARCR (Figure 6) (Golub et al., 2011; B. Zhao et al., 2011; Zhao et al., 2012; Zhou et al., 1997). In the dark portion of the reaction, NADH drives the continuous peroxidyme-catalyzed oxidation of AR into RSF via intermediate production of H_2O_2. In the presence of green light, the RSF forms the photoexcited state ^{3}(RSF)*. Reduction by NADH produces ground-state RSF, NAD^+, and H_2O_2. This reaction dominates until all NADH is consumed, comprising a "lag phase" of slow signal growth. In the absence of NADH, ^{3}(RSF)* interacts with AR, producing $RSF^{\bullet-}$ and the $AR^{\bullet+}$. $RSF^{\bullet-}$ is oxidized by molecular oxygen to return to ground-state RSF while $AR^{\bullet+}$ spontaneously deacetylates to form a second molecule of RSF. $O_2^{\bullet-}$ or H_2O_2 produced during this process further drives the peroxidyme-catalyzed oxidation of AR to RSF, thus the system achieves positive feedback and exhibits exponential fluorescent signal generation ("exponential phase"). The reaction accelerates until little AR remains in solution, at which point RSF fluorescence decays exponentially ("quenching phase"); this quenching is likely a combination of photodegredation and slight acidification of the solution (Figure **17**).

The optimized PARCR system allows for sensitive detection of peroxidymes across a wide range of concentrations. We achieved reliable visible detection of peroxidyme DNA at concentrations across five orders of magnitude ranging from 1 μM down to 100 pM (Figure 10). The concentration of peroxidyme in solution can be correlated with the characteristic time t_C of this sigmoid in a log-linear fashion. The duration, sensitivity, and dynamic range of this reaction can be tuned via several parameters (Figure 14, Figure **15**, Figure **18**, and Figure **19**).

A major advantage of PARCR is its capacity to generate an easily visible signal, both fluorescent and colorimetric. Unlike typical systems for fluorescent analyte detection that require complex optics and sophisticated detection instrumentation, PARCR requires only simple LEDs and an inexpensive camera (or the naked eye). As shown in Figure 20, we used an unaltered cell phone camera to quantify the PARCR-generated fluorescent signal. By quantifying the change in color (Equation 3) between images taken every 30 seconds over the course of the reaction, we constructed reaction plots displaying the same characteristic lag, exponential, and quenching phases of the fluorescent signal as observed with the sophisticated plate reader.

While the above results imply potential for the PARCR assay to provide direct detection of a target via labeling with peroxidymes (Li et al., 2008; Wang et al., 2011; Yuan et al., 2012), an advantage of PARCR over traditional continuous signal-generation systems (such as horseradish peroxidase or alkaline phosphatase) lies in the ability to produce the peroxidyme sequences *in situ* through nucleic acid amplification techniques. Such colorimetric peroxidyme-mediated detection of specific DNA sequences has been explored previously, but in all prior reports detection requires manual addition of concentrated H_2O_2 following nucleic acid amplification (Kosman and Juskowiak, 2011). PARCR, on the other hand, removes the necessity of these manual steps by relying on NADH for signal generation (unlike H_2O_2, NADH does not interfere with enzyme activity). To demonstrate this utility and flexibility of PARCR, we employed it as a readout for two classical nucleic acid amplification techniques. By engineering primers to contain an antisense-peroxidyme sequence at the 5' end of a target-recognition sequence (Table 1 and Figure **21**), we performed the ubiquitous

polymerase chain reaction (PCR) as well as the isothermal technique strand-displacement amplification (SDA) to generate peroxidyme sequences from an arbitrary DNA target in one-pot reactions. Assays contained both amplification and PARCR components: illuminating the PCR solution immediately following thermocycling enabled visible detection of as little as ten initial copies of target DNA, and illumination of the SDA mixture during amplification allowed real-time discernment of positive and negative samples (**Figure 11**).

3.5 Conclusion

The PARCR assay enables sensitive, visible detection of peroxidyme sequences at concentrations spanning five orders of magnitude down to picomolar levels. A positive-feedback loop within the system, created by illumination with green light and metered by consumption of NADH, provides exponential fluorescent and colorimetric signal growth, allowing for detection with a simple camera or by eye across its entire dynamic range. By relying on catalytic nucleic acids for signal generation, PARCR will prove to be more flexible and stable to heat, organic solvents, and desiccation than similar protein-based colorimetric assays which utilize horseradish peroxidase or alkaline phosphatase.[32–34] Furthermore, to the best of our knowledge, PARCR is the first peroxidyme-based system which enables truly one-pot visible detection of nucleic acid amplification by eliminating the manual hydrogen peroxide-addition steps common to other peroxidyme assays. PARCR can be used to directly detect peroxidymes in solution, suggesting application in a sandwich-assay format, but can also be used in tandem with thermocycled or isothermal nucleic acid amplification strategies, accommodating a wide range of potential analytes. These numerous advantages will

facilitate assay automation and dry storage of the complete reaction mixture, which we will explore in future works. The ease of operation and inexpensive optical instrumentation involved make PARCR particularly well suited for sensitive point-of-care detection strategies that require low cost, high portability, and a minimum of manual interventions.

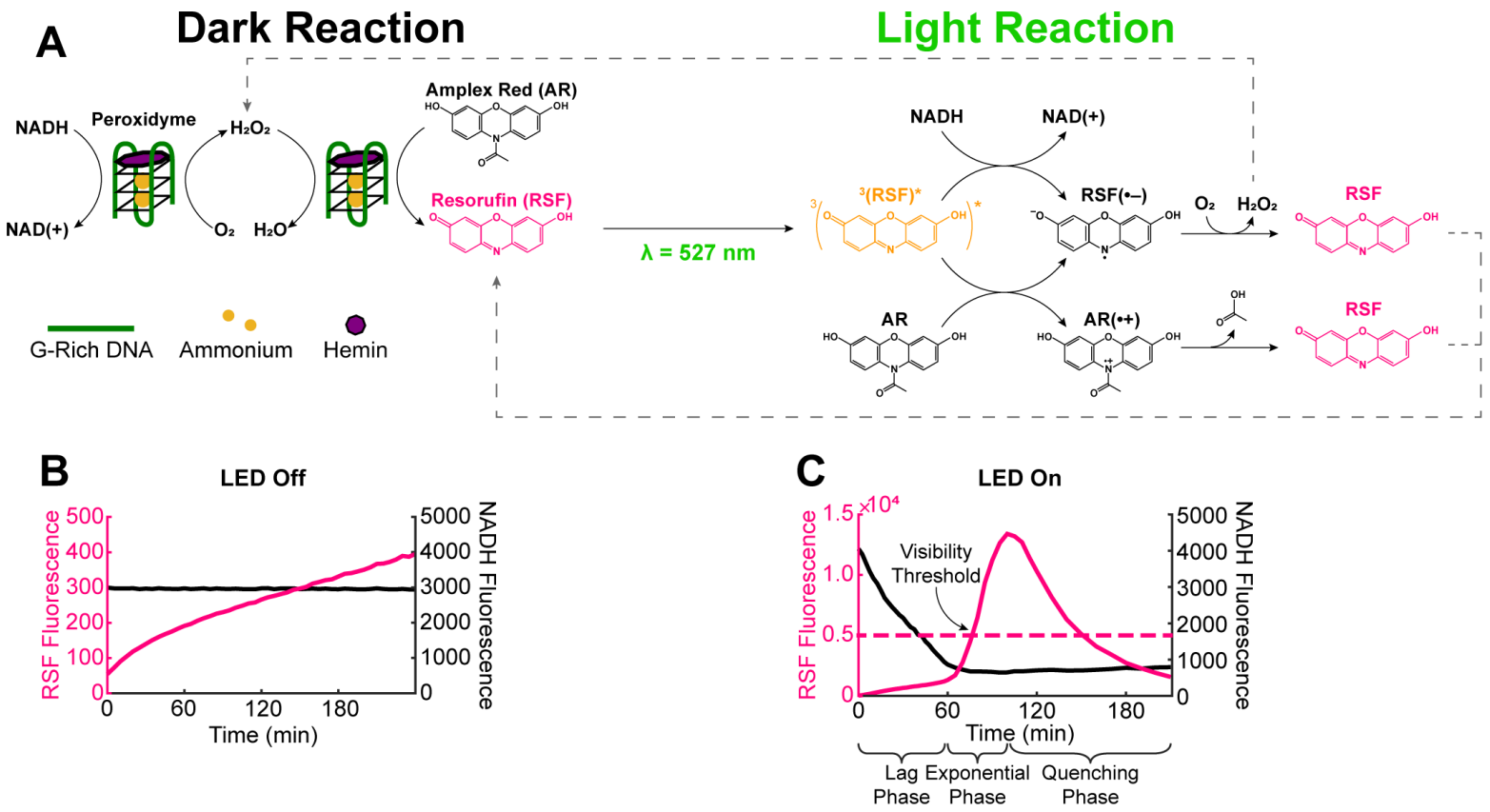

Figure 6. The PARCR reaction. **A** PARCR consists of light-independent (or "dark") and light-dependent (or "light") reactions occurring in tandem and feeding into each other. **B** On its own, the dark reaction slowly generates a weak fluorescent signal in an approximately linear manner. C During the light reaction, the NADH reduction of photoexcited dominates, yielding a "lag phase" of slow signal growth until all NADH is consumed. After depletion of NADH, the positive feedback resulting from photoexcited resorufin interacting with Amplex Red gives rise to an "exponential phase" of rapid, visible fluorescence growth. Finally, resorufin fluorescence displays exponential decay during the "quenching phase" of the reaction.

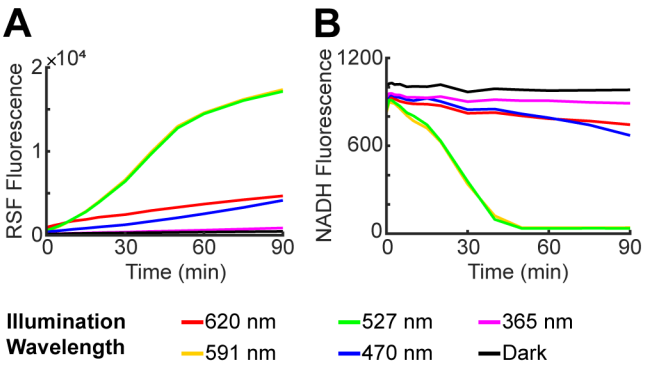

Figure 7. Green light photocatalyzes peroxidyme-mediate resorufin formation. 300 nM EAD, 1 µM hemin, 100 µM AR, 100 µM NADH in standard clear-walled microplates.

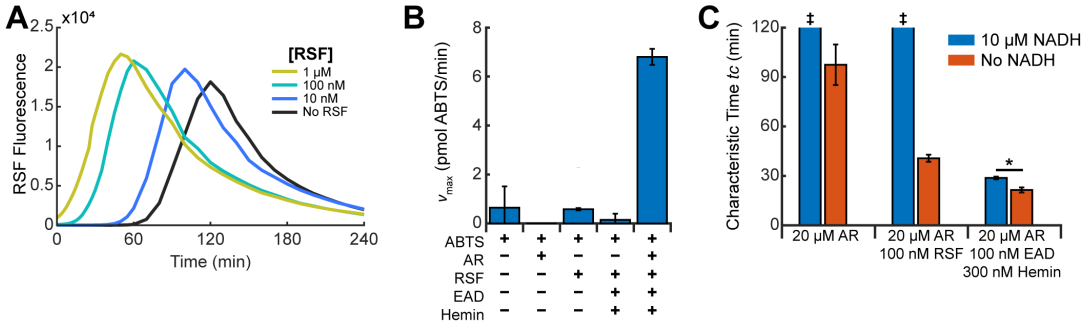

Figure 8. Investigations into the PARCR mechanism. **A** Spiking RSF into AR accelerates exponential signal generation in a concentration-dependent manner. 1.5 W/cm^2 527 nm illumination. **B** ABTS was included in various mixtures of PARCR reactants to aid in elucidating the photocatalyzed mechanism. Under illumination, ABTS was only oxidized when AR, RSF, and peroxidyme were all present, suggesting that H_2O_2 is produced during following the interaction of AR with photoexcited RSF and this drives further peroxidyme-mediated oxidation of AR. **C** NADH significantly delays onset of exponential-phase in all reaction mixtures tested. Note that the indicated reactions (‡) displayed no exponential signal growth within two hours. Trace RSF may be present in AR stocks and likely initiates reactions without added RSF or NADH.

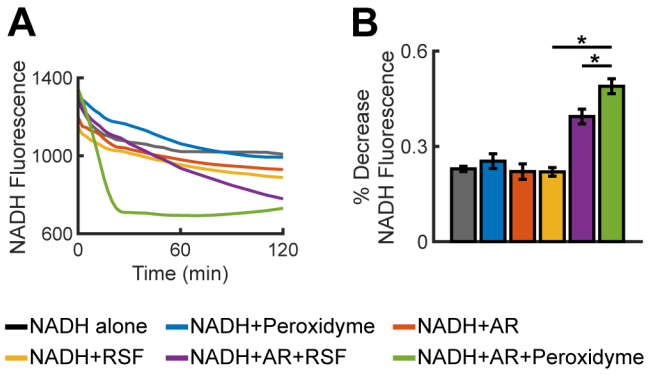

Figure 9. A NADH consumption is accelerated by the light-dependent interaction of resorufin and amplex red. **B** NADH consumption after two hours is significantly higher than baseline in solutions of Amplex Red and resorufin or in solutions of Amplex Red, 100 nM EAD, and 300 nM hemin.

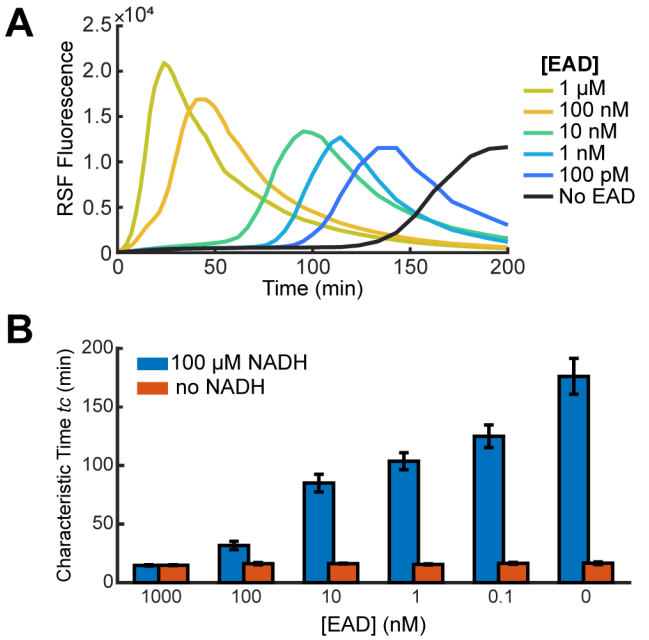

Figure 10. The PARCR system enables sensitive detection of G-quadruplex DNA. **A** Averaged fluorescence traces and **B** characteristic times for four replicates of PARCR reactions consisting of 300 nM hemin, 100 μM NADH as indicated, 3.0 mW/cm^2 illumination intensity.

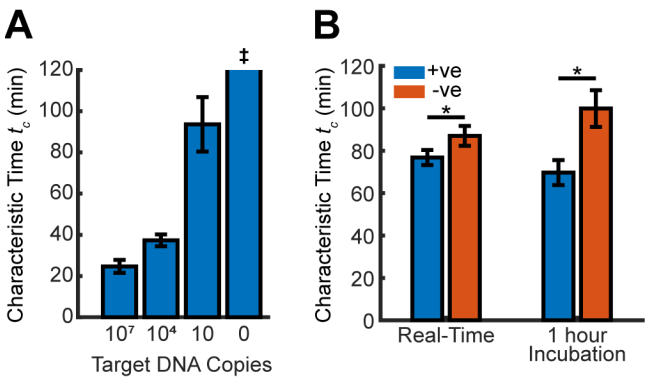

Figure 11. PARCR is a convenient readout compatible with classical nucleic acid amplification, enabling sensitive detection of arbitrary DNA sequences and monitoring of real-time reactions. **A** Illumination of PCR reactions following thermocycling allowed visible detection of 10 initial copies of target DNA in a *one-pot* reaction. ‡ The no-target control did not reach the visibility threshold in the two hours monitored. **B** Linear SDA reactions could be distinguished from background at room temperature with or without a 1 hour incubation prior to illumination.

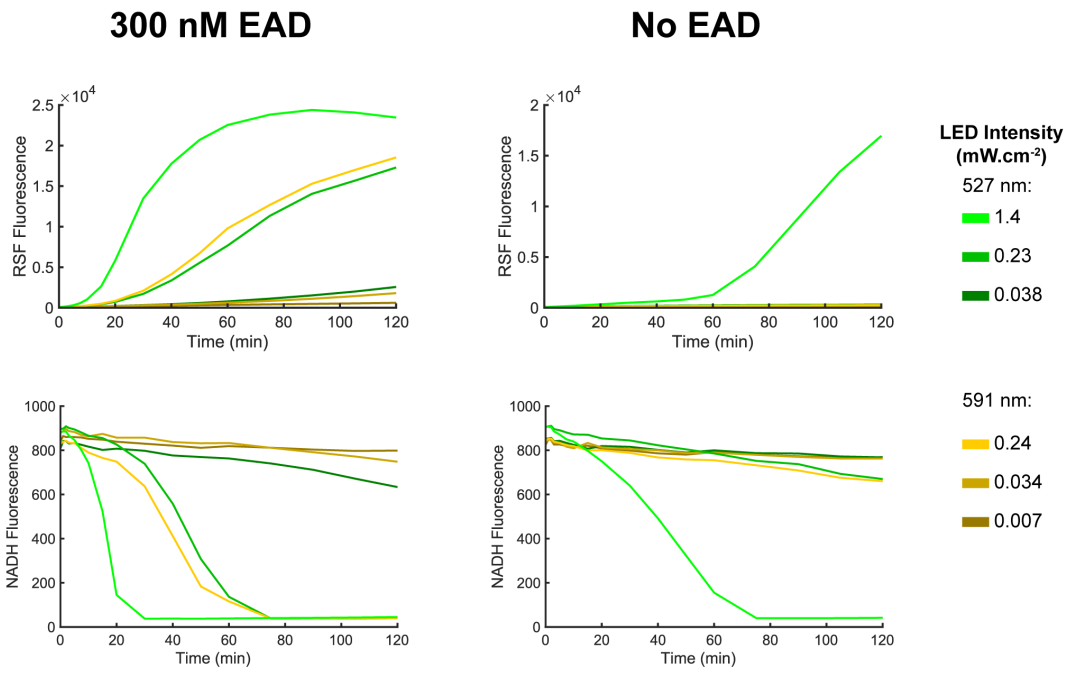

Figure 12. RSF production and NADH consumption rates increased with higher LED intensity. All reactions contained 100 µM NADH, 100 µM AR, 1 µM hemin in black-walled clear-bottom microplates.

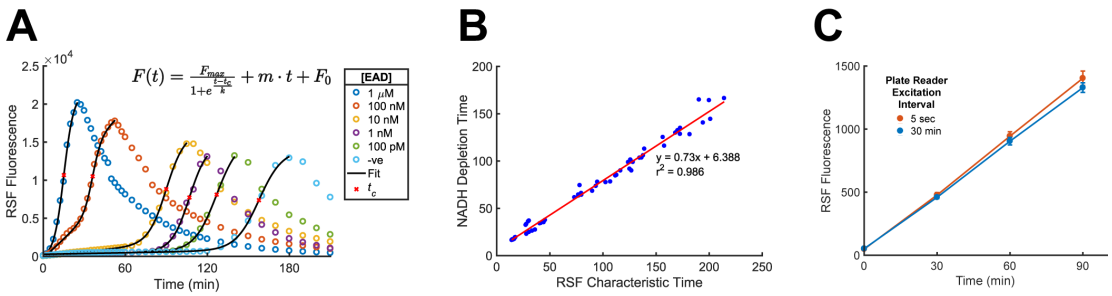

Figure 13. A Sigmoidal curve fits overlaid on raw data for a representative set of experiments (300 nM hemin, 100 μM NADH, 3.0 mW/cm^2, clear PCR plates). Data from the lag and exponential phases of amplification were fit to the displayed equation (Equation 1), a sigmoidal curve with a linear offset. Characteristic times t_c are noted by red x's. **B** Comparison of characteristic times of amplification onset and duration of NADH presence in solution. "Depletion times" were estimated by finding the length of time necessary to reach 110% of the minimum NADH fluorescence for each experiment. A strong linear relationship between NADH depletion time and exponential phase onset was observed, suggesting that the presence of NADH inhibits exponential RSF production. Data shown represent aggregated data from **Figure 14**B. **C** Using the Spectramax M5 plate reader to excite the sample with 570 nm light every five seconds (orange line) had no impact on reaction progression compared to taking fluorescence readings every 30 minutes using 530 nm light (blue line).

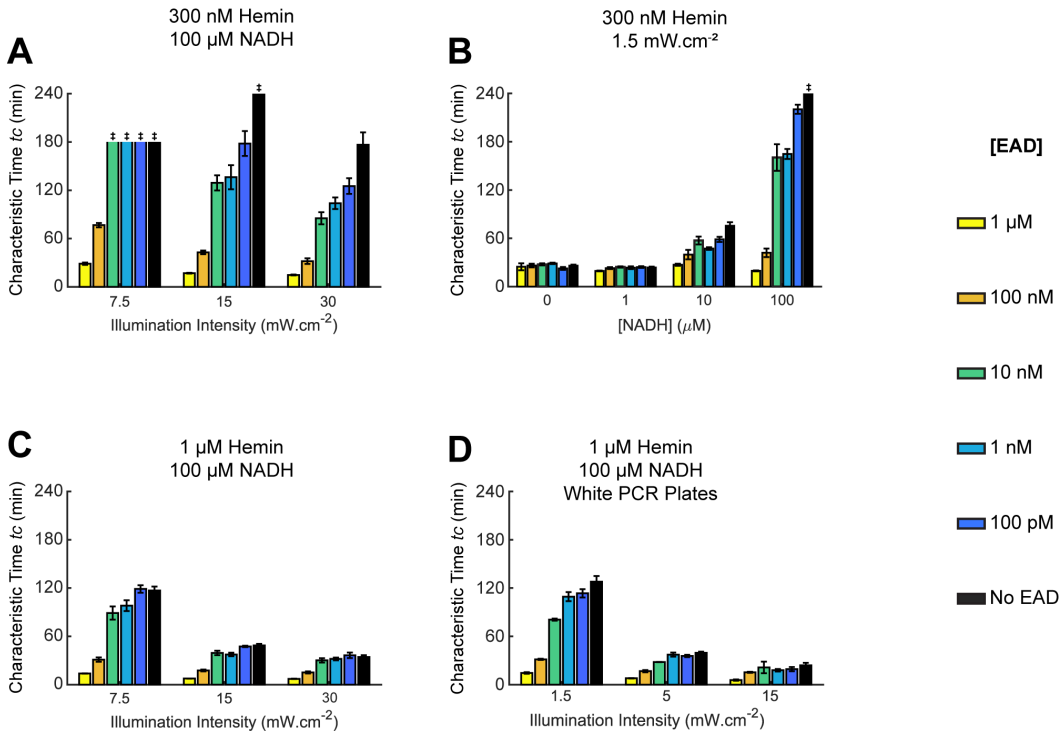

Figure 14. PARCR parameter tuning in clear- (A-C) and white-walled (D) PCR plates. **A** Increasing illumination intensity accelerates the reaction. **B** Higher concentrations of NADH prolong the reaction but yield better sensitivity. **C** A larger hemin concentration leads to faster reactions with worse sensitivity at all illumination intensities. **D** White-walled PCR plates require lower illumination intensities to achieve similar performance as clear-walled PCR plates.

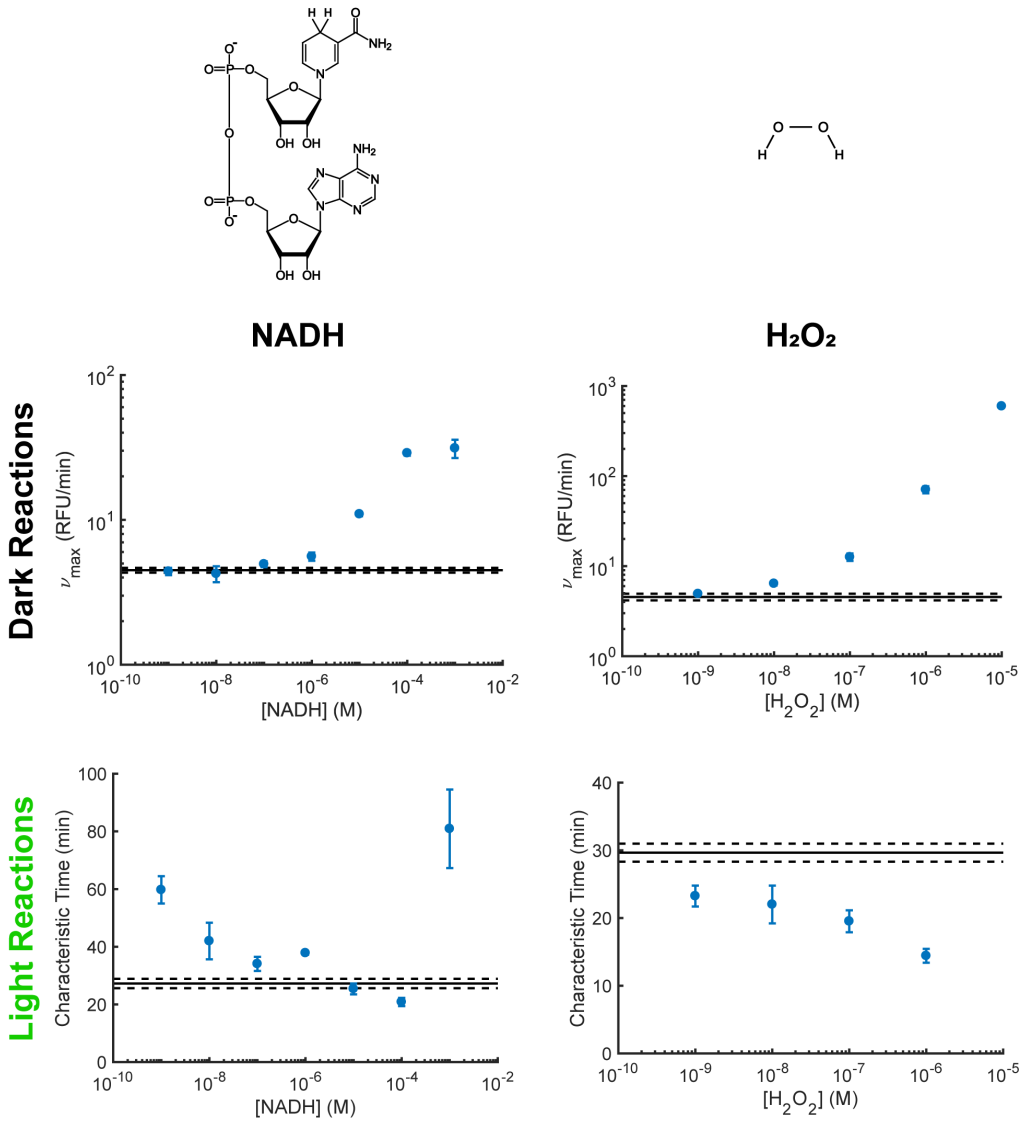

Figure 15. Effect of varying NADH (left panels) and H2O2 (right panels) concentration on the dark (top panels) and illuminated (bottom reactions). Reaction rate ν_{max} determined from RSF fluorescence. Solid lines represent negative reactions lacking the respective component and dashed lines represent one standard deviation from the negative controls. Note that while a higher [NADH] uniformly accelerates the dark reaction, a more complex relationship exists for the photocatalyzed reaction.

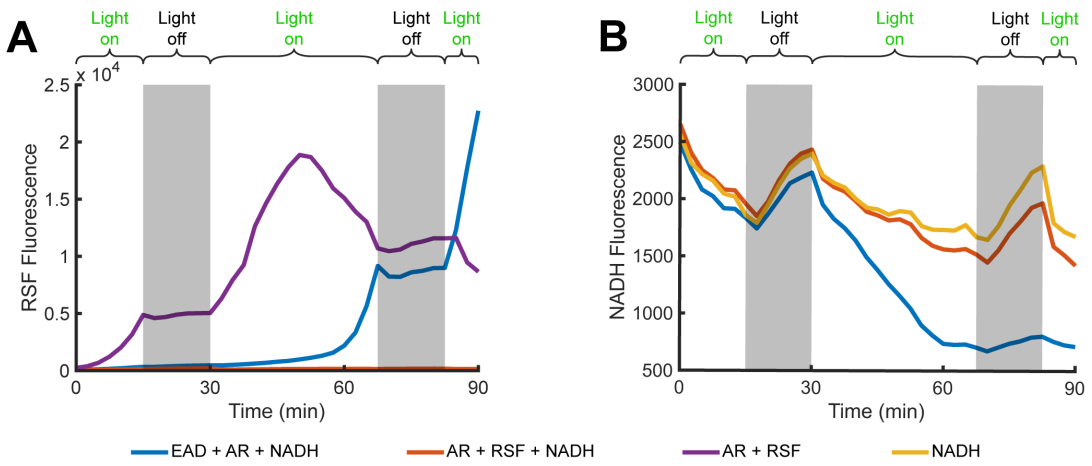

Figure 16. RSF fluorescence (**A**) and NADH fluorescence (**B**) behavior for various reaction mixtures in the sequential presence or absence of illumination, as indicated. Where applicable, reaction conditions are 100 nM EAD, 20 µM AR, 100 nM RSF, 100 µM NADH, 3.0 mW/cm^2 illumination, clear-wall PCR plates. RSF fluorescence approximately resumes dark-reaction behavior (very slow signal growth) when illumination is removed mid-reaction. Curiously, NADH fluorescence initially continues to fall before steadily increasing once illumition ceases, a effect less pronounced at the lower NADH levels found late in the reaction (blue line). The cause of this phenomenon is unknown, but is beyond the scope of this manuscript to be investigated further. Typical photocatalyzed behavior resumes when illumination is re-applied.

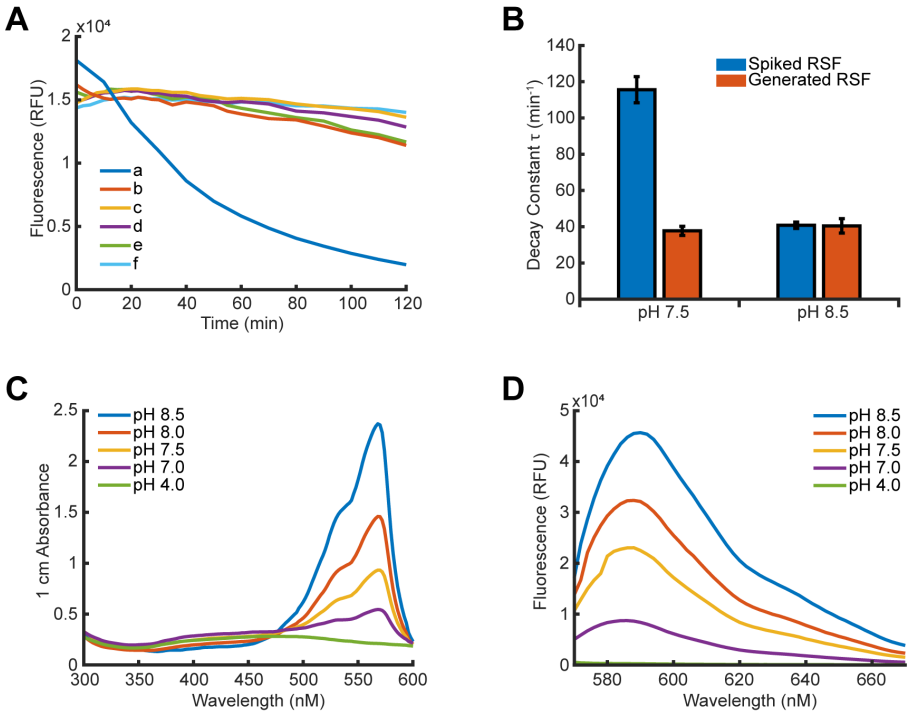

Figure 17. RSF quenching and photodegradation. **A** (a) RSF generated from AR in situ exhibits rapid quenching ("quenching phase" data (120 min to 240 min) from Main Text Figure 3A, AR alone), while spiked RSF alone (b) or with 100 mM NADH (c), 1 µM H_2O_2 (d), 300 nM hemin and 100 nM EAD (e), or H_2O_2 and hemin and EAD (f) decays slowly under illumination. **B** Fluorescence loss during the quenching phase of RSF generation or from RSF alone can be fit with an exponential decay curve $F = F_0 e^{-\frac{t}{\tau}}$ with decay constant τ. In a buffer containing 500 mM Tris and 500 mM NH_4OAc at pH 7.5, generated RSF decays much faster than spiked RSF, suggesting photodegradation alone cannot fully account for the former. In the same buffer at pH 8.5 the two rates are equivalent. The faster rate of photodegradation in alkaline solution above RSF's pK_a of 7.9 is to be expected given the strong impact of pH on resorufin absorbance (**C**) and fluorescence (**D**) (10 µg/mL). This suggests that acidification of the PARCR solution due to de-acetylation of AR may contribute to rapid fluorescence decay during the quenching phase.

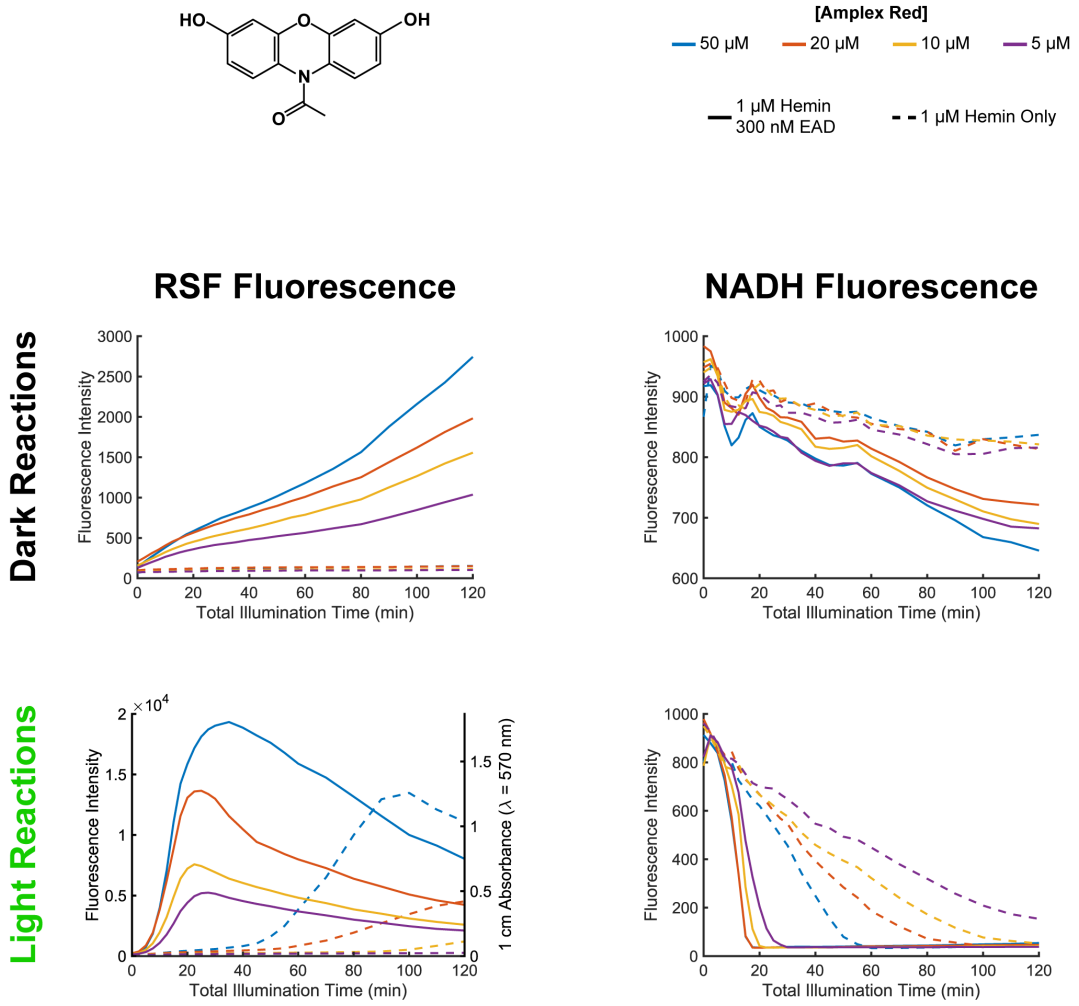

Figure 18. Effect of varying Amplex Red concentration of dark (top panels) and illuminated (bottom panels) peroxidyme reactions (1 µM hemin, 100 µM NADH, 1.4 mW/cm^2, black-walled clear-bottom microplates). EAD-containing reactions are shown by solid lines while EAD-negative reactions are denoted by dashed lines. Threshold of visibility in these microplates is approximately 2000 RFU. The strong dependence of amplification behavior on Amplex Red concentration suggests that trace amounts of RSF in AR stock solutions is a significant factor in nonspecific amplification.

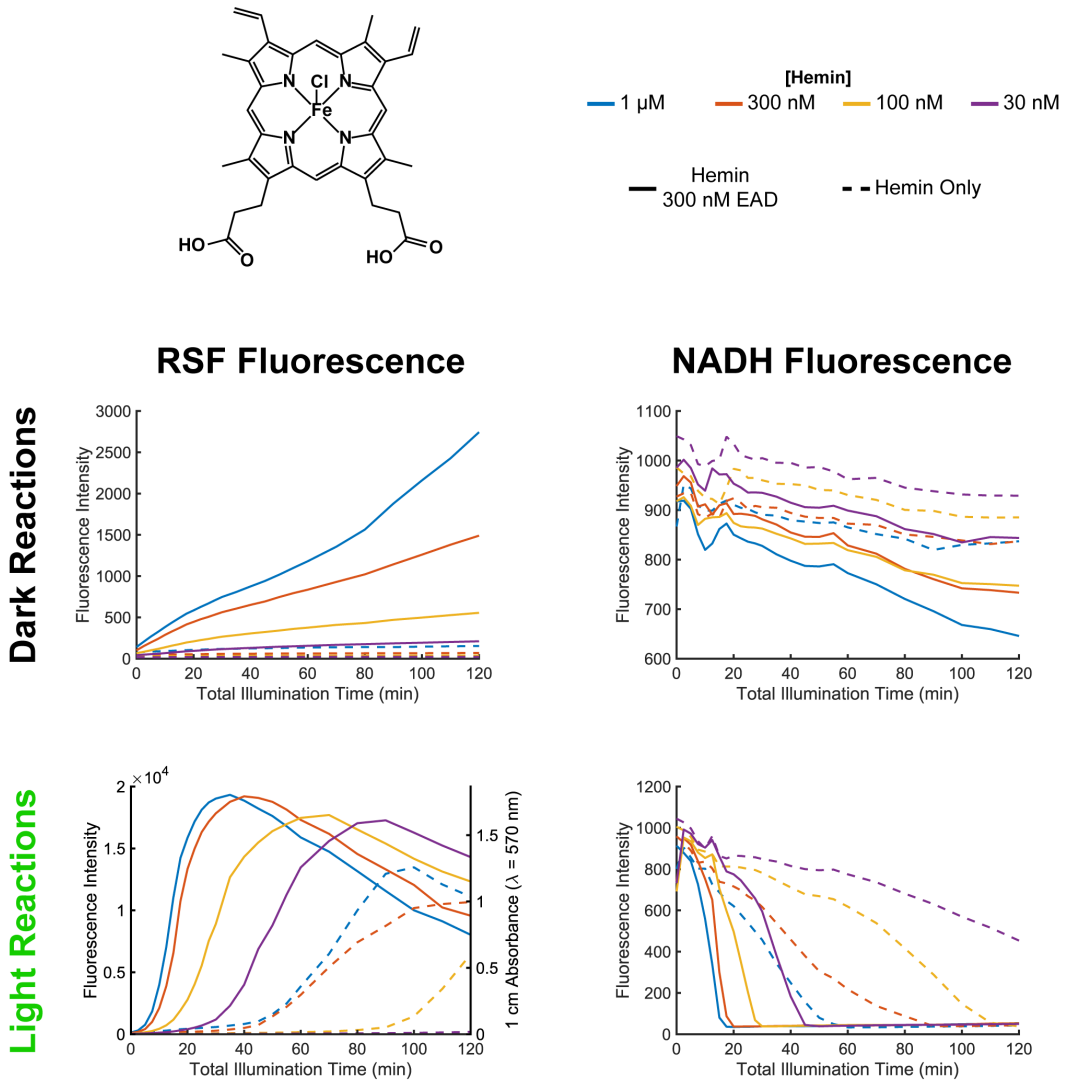

Figure 19. Effect of varying hemin concentration of dark (top panels) and illuminated (bottom panels) peroxidyme reactions (50 μM Amplex Red, 100 μM NADH, 1.4 mW/cm^2, black-walled clear-bottom microplates). EAD-containing reactions are shown by solid lines while EAD-negative reactions are denoted by dashed lines. Threshold of visibility in these microplates is approximately 2000 RFU.

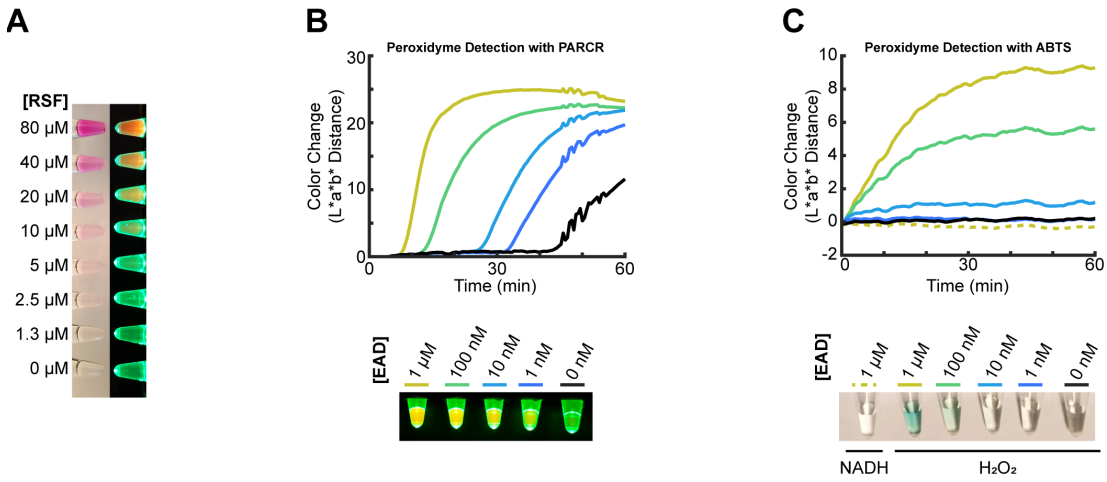

Figure 20. The PARCR assay can be monitored with the naked eye or a simple camera. **A** RSF under ambient light or illuminated with 527 nm LED light becomes visible above 2.5 µM. **B** Quantifying the change in color between images allows for monitoring of the PARCR assay using only a cell phone camera and LED light. Inset: fluorescence is clearly visible in all tubes containing EAD after 40 minutes. 1 µM hemin, 100 µM NADH, 1.5 mW/cm^2 light. **C** The same approach can used to quantify the color change resulting from the less efficient ABTS-oxidation method. Note that NADH is incompatible with this technique as the chromogen $ABTS^{\cdot+}$ is readily reduced back to ABTS. Inset: after 40 minutes of oxidation driven by 1 mM H_2O_2, only 1 µM and 100 nM EAD samples are readily visible and 10 nM EAD is barely visible.

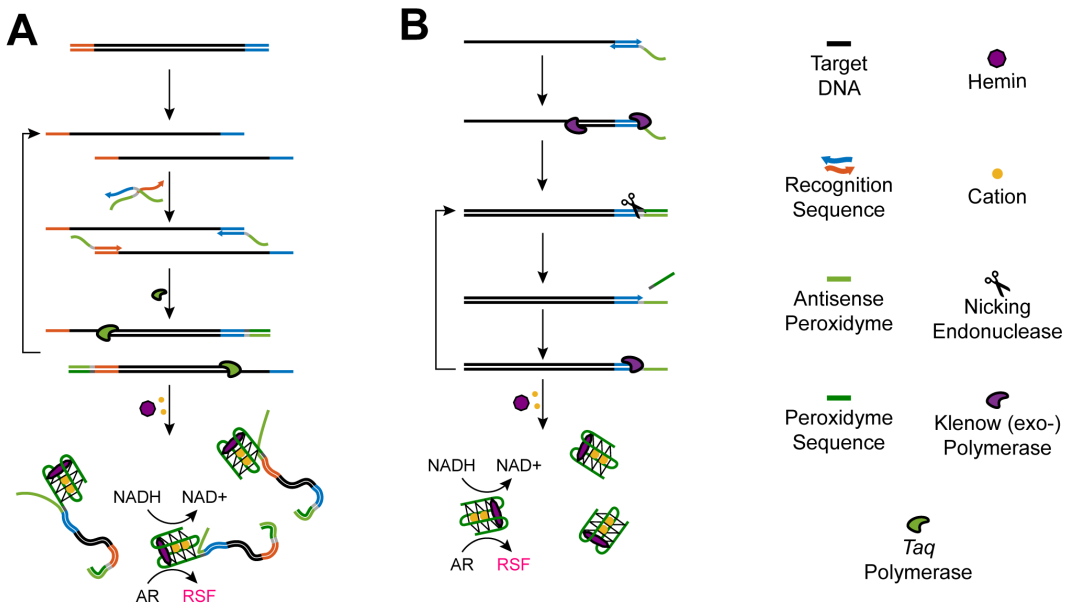

Figure 21. One-pot visible detection of arbitrary DNA sequences with PARCR-PCR and PARCR-SDA. **A** In PARCR-PCR, primers are designed to contain an antisense peroxidyme sequence at the 5' end of the target-recognition sequence. As PCR proceeds through melt, anneal, and extension steps, peroxidyme sequences are generated in tandem to the amplicon sequence. These G-rich sequences exhibit low affinity for their complement and ready adopt quadruplex conformation in the presence of hemins and ammonium. **B** In PARCR-SDA, one-sided strand-displacement amplification continuously produces free peroxidymes in a solution containing a single-stranded DNA sequence. In this system, we designed primers similar to those described above for peroxidyme-producing PCR. For PARCR-SDA primers, a recognition sequence for a nicking endonuclease (NEase) was placed between the target-recognition sequence and an antisense-peroxidyme sequence. A low-temperature polymerase extended the target sequence along the primer, generating the complete NEase recognition sequence in tandem with a peroxidyme sequence. The NEase then cleaved the nascent strand which was subsequently released by the strand-displacement activity of the polymerase as it re-replicated the primer sequence. This continuous production of free peroxidyme at room-temperature was successfully detected with the PARCR assay.

4 Phase-change partitions for thermal automation of multi-step reactions[3]

The peroxidyme-amplification strategy described in the previous chapter presents a capable system for sensitive, visible detection of analytes, and it does so without the need for manual addition of hydrogen peroxide. This chapter describes a system capable of automating any other necessary assay steps, providing a simple, low-cost manner to achieve thermal automation of complex reactions.

4.1 Abstract

Medical diagnostics and basic research in low-resource settings require automated reactions controlled in a simple, portable manner. Here, we present a novel platform that enables simple automation of multi-step reactions to facilitate robust, hands-free assay operation without complex microfluidics or paperfluidics. We separate reagent zones in a conventional PCR tube via solid layers of purified higher alkanes. Reagents can be mixed on demand by simply raising the temperature above the melting point of the alkane partition that separates the two zones. We partitioned various reagents to enable hands-free thermally automated isothermal nucleic acid amplification, heavy metal ion detection, as well as β-lactamase detection with tandem antibiotic specificity characterization. We anticipate this phase-change partition platform will find broad application in clinical diagnostics at the point-of-care and in low-resource settings.

4.2 Introduction

The advent of microfluidics promised biochemical assays that were portable because they were small and comprehensive because they were intricate (Whitesides, 2006). However, while the devices are small, their complex fluidic networks typically

[3] This work was published in *Analytical Chemistry* 90 (6) 2018, 3708-3713

require training and bulky syringe pumps to operate (Hu et al., 2014; Martinez et al., 2010), limiting their portability and demanding a certain finesse. Paper microfluidics achieve greater portability and ease-of-use, yet most such devices are constrained to reactions which require only one or two steps (Fu et al., 2011; Martinez et al., 2007). While more complex reactions can be achieved, control of reaction timing in these devices requires either intricate paper networks vulnerable to environmental variations or dissolvable barriers that intrinsically alter reaction composition (Fu et al., 2010; Lutz et al., 2013; Martinez et al., 2007). Furthermore, reaction timing is fixed by the manufacturer, preventing on-site optimization. The strengths and weaknesses of these two systems, microfluidic or paperfluidic, have resulted in one reaction platform suitable only for centralized labs and one only for field use, both with limited efficacy (Chin et al., 2012; Gubala et al., 2012). Here we introduce a novel platform with the potential to bridge this gap, offering equal utility to both lab and field setting while enabling greater ease-of-use than pump-driven microfluidics and greater complexity than paper microfluidics.

Our platform consists of partitioning aqueous or lyophilized reagent zones in a vertical tube format via thermally actuated alkane partitions (Figure **22**). An aqueous sample solution placed on top of this reagent/partition stack can be incrementally mixed with successive reaction zones

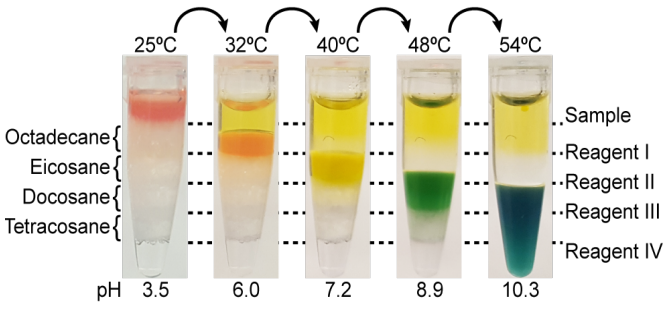

Figure 22. Layers of purified alkanes serve as phase-change partitions, segregating reagents into compartments which can be mixed on demand. Here, a “sample” of universal pH indicator solution is sequentially mixed with various buffers by incrementally raising the temperature of the tube.

by melting the respective organic layer. The aqueous sample is more dense than the liquid organic layer, causing the sample to "sink" through the melted partition and mix with the reaction compartment beneath; this process can be iterated to step the sample through multiple reactants. A related approach has employed paraffin wax for hot-start PCR but was restricted to one such barrier (Chou et al., 1992). Paraffin wax is a heterogenous mixture, displaying poorly-defined phase transitions inherently problematic for use as a phase-change partition. Accordingly, integration of multiple paraffin barriers into paper (Phillips et al., 2016) and centrifugal (Abi-Samra et al., 2011; Kong et al., 2015) microfluidic devices required high spatial or temporal control over temperature. The phase-change partitions we present here are comprised of purified long-chain alkanes with distinct melting profiles, permitting low-resolution thermal instrumentation. The technical requirement for operating these thermally actuated reactions consists only of coarse-grained temperature control, available in a common laboratory thermocycler or water bath. This flexibility positions phase-change partitions as well-suited for low-resource settings, portable devices, and central laboratories alike.

To demonstrate the flexibility and utility of this radically simple approach, we investigated the partitioning of three different classes of analyte detection. First, we partitioned the necessary reagents for isothermal nucleic acid amplification via rolling circle amplification (RCA). Second, we used this platform to detect heavy metal ions in a gold nanoparticle aggregation assay. Finally, we achieved detection and characterization of β-lactamase enzymes via a colorimetric antibiotic-resistance reaction. These proofs-of-concept demonstrate the potential of the phase-change

partition platform to be uniquely suited to automation of many multi-step reactions in both central laboratory and field settings.

4.3 Materials and Methods

Materials. Alkanes and palmitic acid were purchased from Alfa Aesar (Haverhill, MA); DNA sequences from Integrated DNA Technologies (Coralville, IA); Bst 3.0, T4 DNA Ligase, and their corresponding buffers from New England Biolabs (Ipswitch, MA); β-lactamase, broad spectrum (ESBL) from AG Scientific (San Diego, CA); calcein from Cayman Chemical (Ann Arbor, MI); hydrogen tetrachloroaurate (III) hydrate from Strem Chemicals (Newburyport, MA); AccuGel 29:1 from National Diagnostics (Atlanta, GA); 0.2 mL high-profile PCR tube strips from USA Scientific (Ocala, FL); SYBR Gold from Thermo Fisher Scientific (Waltham, MA); and all remaining chemicals and materials from Millipore Sigma (St. Louis, MO). A Bio-Rad (Hercules, CA) Mini-Protean Tetra Cell was used for electrophoresis. A Bio-Rad MiniOpticon Real-Time PCR Thermocycler was used for temperature control except where noted otherwise. A Spectramax M5 plate reader (Molecular Devices, Sunnyvale, CA) was used to collect spectroscopic data. The following DNA sequences were used:

Trigger: 5’-TAG TCG AGA CAT CCG AGA CA -3’

Target: 5’-Phos-GTC TCG ACT AAA AAC CCA ACC CGC CCT ACC CAA AAG AGA CAT CCG TTT TGT CTC GGA T-3’

The system shown in Figure 22 was assembled as follows, from top-to-bottom: 40 µL 1 mM H_2SO_4, 1% Triton, 60% Universal pH Indicator (pH 3.5); 50 µL octadecane; 10 µL 800 mM NH_4OAc, 250 mM Tris (pH 6.0); 40 µL eicosane; 10 µL

5 M NH_4OAc, 500 mM Tris (pH 8); 30 µL docosane; 10 µL 1.4 M NH_4OH; 25 µL tetracosane; 20 µL 14 M NH_4OH. The system was incubated at the indicated temperature for twenty minutes prior to imaging; the indicated pH is the resulting pH of the aqueous colored solution at that step. It is important to note that these alkane volumes should be considered approximate minimums in a practical sense. At their respective positions in the PCR tube, these volumes correspond to layer heights of roughly 3 mm; thinner layers occasionally lead to cracks and pores that penetrate through the barrier. Furthermore, the interface of the alkane and the tube wall is naturally a structural weak point: rough handling may dislodge the barrier and ruin the assay. Future work will seek to remedy this drawback.

Note that the conical shape of the PCR tubes introduced a particular constraint to the positioning of the final partition. In the absence of surfactant, the surface tension of the aqueous droplet within the oil phase resulted in the droplet remaining suspended above the narrow bottom of the tube (Figure 23). It was occasionally necessary to place palmitic acid beneath the final reactant layer. Palmitic acid remained solid under

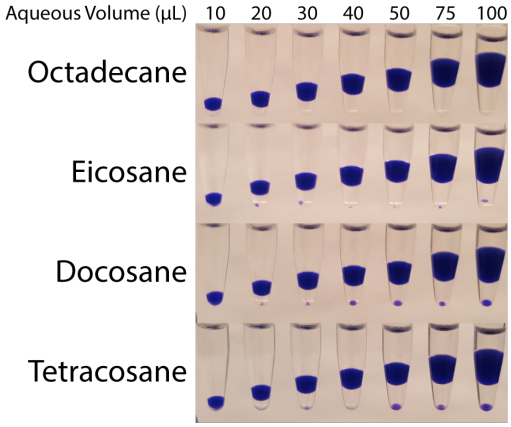

Figure 23. Equilibrium position of aqueous droplets (containing bromophenol blue) after incubation at 60°C for 25 minutes. The droplets remain suspended within liquid alkanes due to surface tension and the conical geometry of the PCR tubes.

experimental conditions and ensured merging of the mobile reaction solution with the final reagent mixture.

Dispersity of the AuNP was then quantified from the UV-vis spectra of the resulting solution via the indicated absorbance ratio. AuNPs were synthesized via kinetically controlled seeded growth (Bastús et al., 2011); diameter and concentration of AuNPs were characterized by UV-vis spectroscopy (Haiss et al., 2007).

Manual antibiotic resistance characterization with nitrocefin competition was performed with the same reactant volumes and quantities as the partitioned assay, albeit with manual addition of reagents.

Alkane characterization. We examined the melting rate profiles of alkanes used in this study by placing 50 µL of the respective melted alkane above 50 µL 3 µM 5-carboxytetramethylrhodamine (TAMRA) in 18 MΩ deionized (DI) H_2O. After the alkane solidified, fluorescence intensity was monitored while the temperature was increased at a constant rate of 2.3 °C/min. Breakthrough confirmation experiments, presented in Figure 24B, were assembled as follows, from top-to-bottom: 50 µL 6 µM calcein with 200 µM $FeCl_3$, 50 µL alkane, 50 µL 5 µM EDTA (both aqueous solutions in 150 mM KOAc, 50 mM Tris, pH 7.8).

Phase-change partition assembly. To assemble multi-layer reactions for thermal automation, alkanes were melted and then placed above the respective aqueous reactant mixture. After this alkane solidified, the subsequent reactant mixture was placed above this partition, followed by another alkane layer. All reactions were carried out in a thermocycler except where noted.

Rolling circle amplification. From top-to-bottom: 20 µL target solution (100 nM Target DNA in DI H_2O); 50 µL octadecane; 20 µL ligase solution (145 U T4 DNA Ligase, 1.8X Ligase Buffer with ATP); 50 µL eicosane; 20 µL polymerase solution (30 U Bst 3.0 DNA polymerase, 2.4X Isothermal Amplification Buffer II, 0.72X SYBR Gold, 360 nM Trigger DNA, 2.4 mM dNTPs); 25 µL palmitic acid. The full reaction was incubated at 32 °C for 1 hour then 55 °C for 1 hour. Reaction solutions were concentrated by evaporation then analyzed via 15% denaturing PAGE (500V, 15 minutes) and stained with SYBR Gold.

Heavy metal ion detection. From top-to-bottom: 10 µL $AgNO_3$ in DI H_2O; 50 µL octadecane; 90 µL 10 pM 60 nm gold nanoparticles (AuNPs) in 5 mM glycine-NaOH (pH 10); 20 µL docosane; 10 µL 1 mM β-mercaptoethanol. Reactions were incubated in a water bath at 32 °C for thirty minutes then at 48 °C for two hours.

Antibiotic resistance profiling. From top-to-bottom: 25 µL phosphate-buffered saline (PBS) (pH 7.0) with 50 µU ESBL and 5 µg bovine serum albumin (BSA); 50 µL octadecane; 25 µL PBS with 10 nmol nitrocefin and 50 pmol fluorescein (FAM); 30 µL eicosane; 25 µL DI H_2O with 500 nmol ampicillin, benzylpenicillin, or chloramphenicol. The reaction was incubated at 32 °C for fifteen minutes followed by 42 °C for twenty minutes. Nitrocefin hydrolysis was observed by measuring the resulting decrease in FAM fluorescence (the emission spectrum of FAM and the absorption spectrum of hydrolyzed nitrocefin overlap). The hydrolysis rate was determined by the final FAM fluorescence intensity as a fraction of the maximum in each stage. The negative control ("-ve") contained no β-lactamase in the sample while

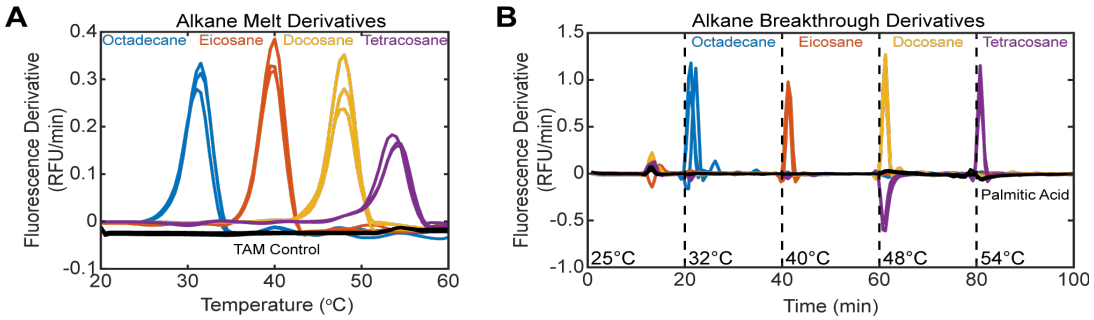

Figure 24. Purified alkanes exhibit sharp melting transitions. **A)** Melting rate profiles were obtained by observing TAM fluorescence of an aqueous solution beneath a layer of the respective alkane. As the alkane melted it became optically clear, leading to an increase in fluorescence intensity. **B)** Rate of partitioned reagent mixing following barrier melting was observed by partitioning a calcein-Fe^{2+} solution above an EDTA solution with a single phase-change material. Upon mixing, EDTA competitively chelated the iron, leading to an increase in calcein fluorescence. Complete mixing was observed within a few minutes for all alkane partition systems. Palmitic acid, with a melting point of 63°C, served as a negative control for barrier breakthrough.

the positive control ("+ve") contained β-lactamase in the sample but no antibiotic in the second stage.

4.4 Results and Discussion

We employed the purified higher alkanes octadecane ($C_{18}H_{38}$, m.p. 28 °C), eicosane ($C_{20}H_{42}$, m.p. 37 °C), docosane ($C_{22}H_{46}$, m.p. 42 °C), and tetracosane ($C_{24}H_{50}$, m.p. 52 °C) as phase-changing partitions, which displayed sharp melting transitions (Figure **24**A). We demonstrated the tight control over reagent zone mixing afforded by these alkane partitions by placing a mixture of calcein and iron chloride above an EDTA solution, separated by an alkane layer. Calcein fluorescence was quenched while bound to Fe^{3+}; mixing of the two solutions allowed EDTA to competitively chelate the iron cation and increased the solution fluorescence. Each alkane layer remained intact until its respective melting temperature was reached, at which point the two solutions mixed rapidly (Figure 24B).

We employed multiple phase-change partitions in tandem to separate several discrete reaction compartments in this manner. We partitioned buffers of various pHs

and incrementally increased the temperature, allowing pH indicator solution to mix with each (Figure **22**). The corresponding step-wise color change indicated that these alkane caps can stably partition reagent zones, isolating reactants until the appropriate temperature is reached. Thus, this strategy will be useful to automate reactions which require reagent addition at specified intervals, replacing manual interaction with pre-determined temperature changes. We proceeded to investigate the compatibility of this platform with three distinct reaction classes: nucleic acid amplification, heavy metal ion detection, and profiling of enzyme-mediated antibiotic resistance.

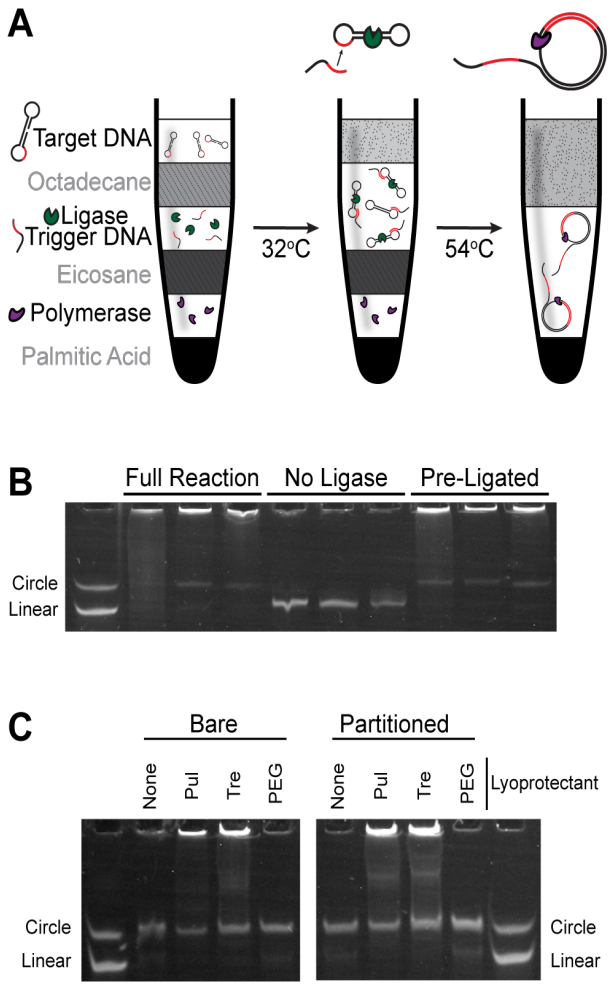

Figure 25. Isothermal nucleic acid amplification was successfully partitioned. **A)** Melting the initial barrier allowed ligase to circularize a dumbbell-forming target oligonucleotide and melting the second barrier allowed continuous replication of the nascent circle in rolling circle amplification (RCA), **B)** verified by denaturing PAGE. **C)** Denaturing PAGE of lyophilized polymerization reagents with pre-ligated DNA indicated successful RCA with or without an alkane cap when pullulan ("Pul") or trehalose ("Tre") were employed as lyoprotectants, but not PEG-200.

4.4.1 Partitioned Nucleic Acid Amplification

We constructed a multi-layered assembly for isothermal nucleic acid amplification (Figure **25**A). Rolling circle amplification (RCA) requires initial ligation to produce a circular oligonucleotide followed by continuous replication to

generate long single-stranded DNA (Ness et al., 2003; Yan et al., 2014). These steps are mutually exclusive, since polymerization is dependent on and inhibits ligation. Incubation at 32 °C in a thermocycler melted an octadecane layer and allowed the target solution to mix with the ligase, resulting in circularization of a dumbbell-forming target sequence. Subsequently raising the temperature to 65 °C melted an eicosane layer and allowed polymerase to replicate the newly-formed circle. Successful performance of the ligation and polymerization steps of this reaction was confirmed by the presence of a large, slowly-migrating DNA product observed via denaturing gel electrophoresis (Figure **25**B). Typically, these steps are performed separately with manual addition of the required reagents, yet here we leverage alkane phase-change partitions to reduce user intervention down to simply adding the target; all intervening steps are accomplished sequentially by incrementally increasing the temperature of the tube.

Isothermal nucleic acid amplification assays are particularly useful at the point-of-care. For this purpose, enzymes are typically lyophilized with their reagents to facilitate transport and ensure stability. We investigated the compatibility of lyophilized polymerase with alkane partitions and found that polymerase activity was unaltered by addition of an alkane cap following lyophilization (Figure 25C).

4.4.2 Partitioned Heavy Metal Detection

Gold nanoparticles exhibit unique aggregation-dependent optical properties that are commonly leveraged for detecting a variety of analytes, including DNA, proteins, small molecules, and ions. Typically 10-100 nm in diameter, gold nanoparticles (AuNP) dispersed in solution exhibit a vibrant red color but become dark gray when aggregated. We partitioned one such assay for detection of heavy metal ions (Figure 26A) (Hung

et al., 2010), an application critical to environmental monitoring. After addition of sample, we placed this reaction platform in a temperature-controlled water bath to melt the first barrier, at which point metallic cations (Ag+) in the sample reduced onto the surface of AuNPs (forming Ag^0). Raising the temperature of the bath melted the second partition and introduced β-mercaptoethanol to the solution, which complexed with the AuNPs via Au-S bonds. Atomic heavy metals sufficiently passivated the surface charge of the AuNPs, allowing interactions between β-mercaptoethanol groups to drive aggregation of the AuNPs. In the absence of heavy metal ions, citrate caps provided

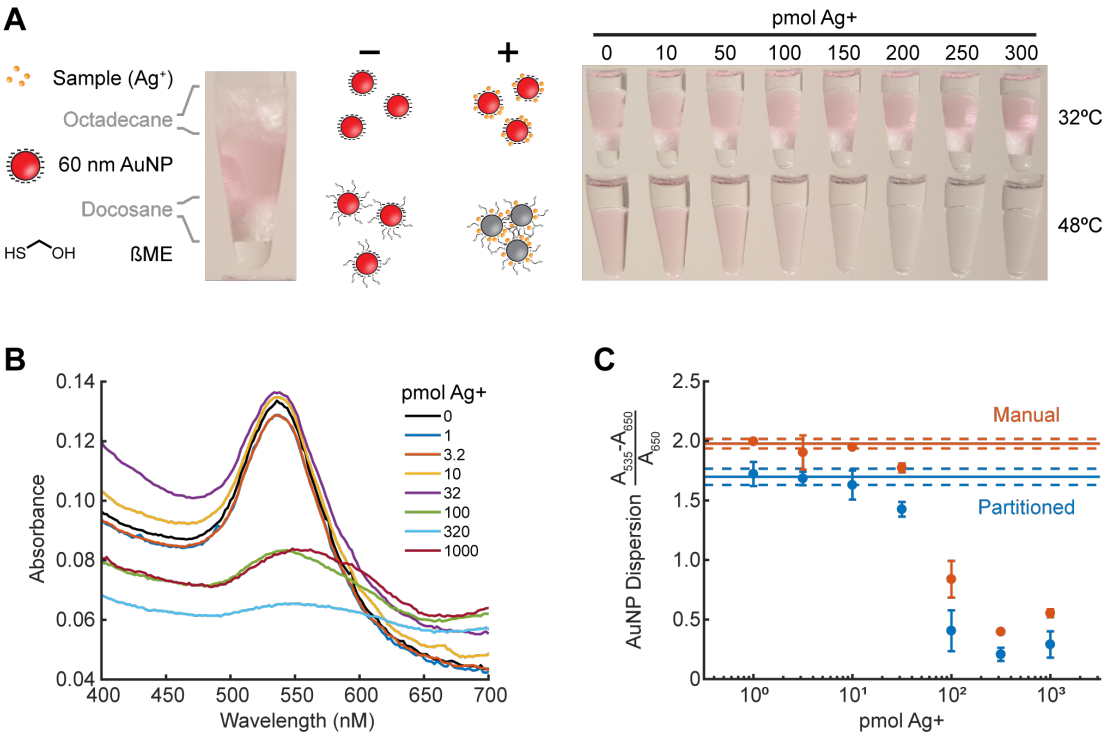

Figure 26. Phase-changed partitions enabled automation of a gold nanoparticle aggregation assay for detection of heavy metals utilizing a simple water bath for reaction control. **A)** After the first barrier is melted, target ions adsorb to the surface of AuNP in a basic solution, displacing citrate ligands. Melting the second barrier introduces β-mercaptoethanol, which forms S-Au bonds with the nanoparticle surface. AuNP passivated by atomic heavy metals aggregate, yielding a gray solution, but in the absence of target cations citrate surface ligands confer sufficient electrostatic repulsion to prevent AuNP aggregation, which retain a pink color. **B)** AuNP aggregation can be monitored spectroscopically as the characteristic surface plasmon peak broadens and red-shifts from its initial maximum at 535 nm. **C)** Quantifying nanoparticle aggregation via absorbance readings demonstrates comparable performance between the partitioned and manual reactions.

sufficient electrostatic repulsion to prevent AuNP aggregation. The presence of Ag^{+} could thus be detected by an easily-visible color change (Figure **26**B); similar strategies have been reported for detection of Cu^{2+}, Pb^{2+}, Hg^{2+}, and other heavy metal ions (Chen et al., 2015; Hung et al., 2010; Sener et al., 2014). Our partitioned system achieved comparable performance to the manual, room-temperature assay (Figure **26**) while synchronizing and automating addition of reagents. The use of a water bath also demonstrates the need for only simple instrumentation to control reaction progression.

4.4.3 Partitioned Antibiotic Susceptibility Testing

Determination of pathogen antibiotic susceptibility is crucial in infectious disease medicine. Epidemic antibiotic resistance renders many early-generation antimicrobials

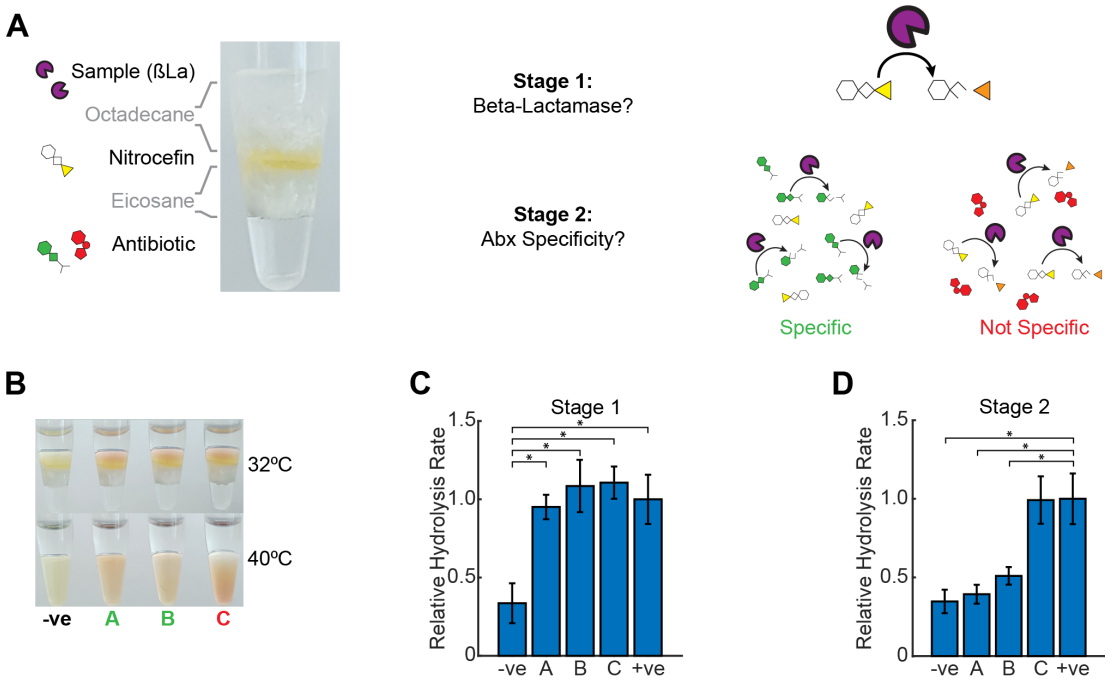

Figure 27. Phase-change partitions allow creation of a novel two-step reaction for detection of β-lactamase-mediated antibiotic resistance and subsequent characterization of the enzyme's antibiotic specificity. **A,B)** In the first stage, hydrolysis of nitrocefin, a cephalosporin derivative, yields an orange-colored solution indicative of β-lactamase presence. In the second stage the presence of an antibiotic susceptible to the enzyme competes with nitrocefin, slowing color change. **C)** All samples containing β-lactamase displayed a greater rate of nitrocefin hydrolysis than the negative control ($p<0.01$, $n=6$). **D)** Nitrocefin hydrolysis was arrested by presence of **A**mpicillin or **B**enzylpenicillin while undeterred by the presence of **C**hloramphenicol ($p<0.01$, $n=6$).

ineffective and, accordingly, conservative use of later-generation antibiotics is necessary to avoid proliferation of “superbugs” immune to all available treatments. Traditional techniques for determining antibiotic susceptibility are low-throughput and require several sequential culture steps (Jarlier et al., 1988). Shown in Figure **27**A, we have devised a two-stage partitioned assay for rapid detection and characterization of β-lactamases, the primary class of enzyme responsible for resistance to penicillins and cephalosporins. In the first stage of the assay the sample mixed with the colorimetric β-lactamase substrate nitrocefin (Boehle et al., 2017), at which point hydrolysis of nitrocefin produced a color change indicative of the presence of the enzyme. However, activity towards nitrocefin does not guarantee resistance to all cephalosporins and penicillins. The specificity of such resistance is commonly assessed via additional plate culture on a “double-disk diffusion test”, wherein the synergistic activity of the antibiotic of interest and a β-lactamase inhibitor reveals antibiotic specificity (Jarlier et al., 1988). The second stage of our assay was designed to assess competition of various antibiotics with nitrocefin for enzymatic hydrolysis (Papanicolaou and Medeiros,

1990), rapidly confirming β-lactamase activity towards those antibiotics without extensive culture. Melting the second partition introduced individual antibiotics to the sample-nitrocefin mixture, at which point ampicillin and benzylpenicillin arrested further hydrolysis of nitrocefin while signal change was unaffected by the presence of chloramphenicol (Figure **27**B). This partitioned assay enabled both detection of the antibiotic resistance enzyme (Figure **27**C) and rapid confirmation of its activity towards ampicillin and benzylpenicillin but not chloramphenicol (Figure **27**D), with a total assay time of approximately thirty minutes. While we observed similar behavior following manual addition of the required reagents (Figure 28), manual performance of this assay at scale would be impractical due to the short incubation times and need for simultaneous introduction of reagents across all samples. This proof-of-concept illustrates the utility of phase-change partitions to enable simple automation of high-throughput clinical assays.

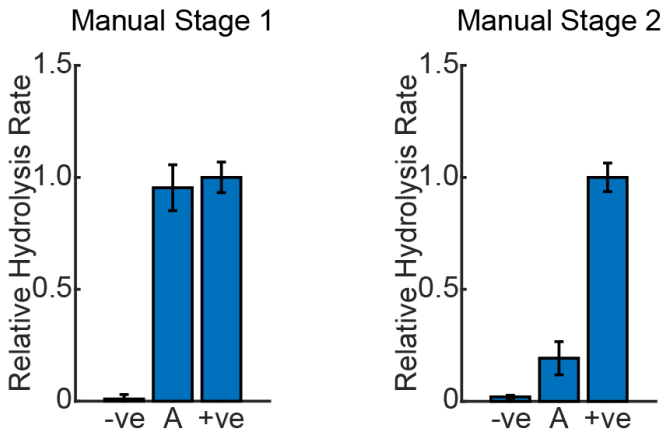

Figure 28. Manual addition of reagents for antibiotic resistance characterization demonstrates similar behavior to the partitioned reaction. In the first stage, all samples containing beta-lactamase hydrolyze nitrocefin rapidly, but addition of lactamase-sensitive **A**mpicillin in the second stage dramatically reduces the rate of nitrocefin hydrolysis.

4.5 Conclusion

We have demonstrated phase-change partitions as a novel, radically simple reaction-automation platform for thermal actuation of multiple reagent additions. These partitions, consisting of purified long-chain alkanes, create stable storage compartments that allow on-demand reagent mixing through simple heating. The melting points of the four alkanes used here are separated by six or more degrees Celsius, thus accommodating lenient specifications for operation. Such broad tolerance makes this phase-change partition platform suitable for both laboratory and field instrumentation. A key advantage of this system is its compatibility with equipment already ubiquitous in diagnostic laboratories. While most microfluidic devices require additional pumps and training to operate, the platform we introduce here can be operated with a common thermocycler or water bath. Similarly, the planar paper format is incompatible with most laboratory instrumentation (i.e., plate readers and thermocyclers), complicating quantification, and recovery of the sample and reaction mixture from the platform for further analysis is difficult; phase-change partitions enable automation within form factors already familiar to many laboratory personnel. For field settings, this platform allows hands-free operation while isolating reactants from the user and the environment, potentially improving assay reliability and improving safety if dangerous reagents are required. Furthermore, reaction timing is tunable by the end-user, allowing optimization towards site- or sample-specific considerations.

We have illustrated the flexibility and utility of this novel system through three distinct, common assay types: two-step isothermal nucleic acid amplification, heavy

metal ion detection through gold nanoparticle aggregation, and antibiotic susceptibility characterization via a colorimetric reaction. We expect this phase-change partition platform will spur new innovation in a variety of form factors and applications, enabling automation of many labor-intensive assays and facilitating translation of many assays to the point-of-care which were previously unfeasible.

5 Thermally-triggered effervescent mixing for assay automation[4]

The phase-change partitions described in the previous chapter enable thermal reaction automation, but most temperature-control systems (e.g., water bath, thermocycler) do not allow the manual or mechanical agitation necessary to achieve efficient reaction kinetics. Furthermore, we observed during the experiments in that chapter that if a lower solution was more dense than the upper solution, mixing of the two was severely impaired. This chapter describes the design of a system of thermally-automated convective mixing to extend the capabilities of the phase-change partition system.

5.1 Abstract

Meltable barriers are an attractive means to achieve controlled delivery of reagents in a variety of settings, enabling assays to be performed through thermal automation instead of manual addition of reactants. However, mixing kinetics in such systems can be slow due to the lack of active flow or mechanical shaking. We demonstrate a new strategy for hands-free, thermally-automated agitation of biochemical reactions. Reagents for binary effervescent reactions are lyophilized then capped with a phase-change partition, eicosane. This barrier can be melted at moderate temperatures, at which point an aqueous solution dissolves the reactants, generating bubbles that mix the solution through convection. We explore reactions that generate bubbles of carbon dioxide and oxygen gasses, characterizing the induced mixing rate of two aqueous solutions with dissimilar densities. This strategy affords control over the initiation and

[4] This work was done in collaboration with Andrew B. Lippe and has been submitted for publication to *Biosensors and Bioelectronics.*

duration of convective mixing, providing a tool for thermal automation of biochemical reactions with efficient reaction kinetics.

5.2 Introduction

Thermal automation has the potential to improve the usability and accessibility of diverse biochemical reactions with applications that include biomedical diagnostics. The wide range of potential heating systems available make such an approach amenable to a variety of form-factors and settings. Recently, we reported phase-change partitions as a means of achieving modular, thermal control over multi-step reactions (Goertz and White, 2018). Separating reactants by layers of purified alkanes in a common PCR tube kept them isolated from one another, interacting only when the melting temperature of the appropriate barrier was reached. The discrete, well-defined melting transitions of the alkanes used enabled such partitions to be actuated through such diverse means as an expensive thermocycler, a simple heated water-bath, or electricity-free chemical heating (Goertz et al., submitted).

However, the drawback of designing reactions for this platform is the lack of possible manual agitation. In many biochemical reactions, the manual addition of a reagent is typically accompanied by vigorous mixing to ensure solution homogeneity. Similarly, assays involving the use of microbeads are often agitated for the duration of incubation to maintain bead dispersion and promote rapid catalysis or binding kinetics (Chen et al., 2008; Dunbar et al., 2003; Kourilov and Steinitz, 2002). Microfluidic platforms employ various strategies to achieve hands-free mixing, such as post arrays, serpentine channels, and acoustic waves (Lee et al., 2011). Portable platforms have been developed that allow hands-free mixing through the use of small, magnetically-

actuated beads included in the reaction mixture (S. H. Lee et al., 2009; Lillis et al., 2016; Rida and Gijs, 2004). Both microfluidic and magnetic strategies, however, are highly device-specific, offering little flexibility in form-factor and instrumentation.

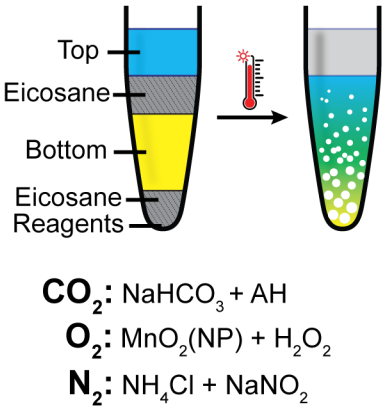

Figure 29. Effervescent mixing schematic. Reagents for binary effervescent reactions were dried at the bottom of PCR tubes, then capped with eicosane to allow thermally-triggered reaction initiation. On top of this was placed a lower yellow solution and an upper blue solution separated by a second eicosane partition. When the eicosane melted, the two solutions began to mix and form a green solution. At the same time, the effervescent reagents were reconstituted, reacting together to generate bubbles and induce convective mixing.

Here, we employ effervescent reactions to create gas bubbles in situ and induce convective mixing. We leverage phase-change partitions to isolated dried reactants from an aqueous solution, allowing the reaction to be triggered on-demand by mild heating. We explore the interaction of sodium bicarbonate with various organic acids (citric, tartaric, and benzoic) to generate CO_2 and the interaction of manganese dioxide nanoparticles with hydrogen peroxide to generate O_2. Bubble generation has been utilized previously to achieve pumping in microfluidic systems but has not been characterized for its ability to promote mixing (Choi et al., 2004; Eddings and Gale, 2006; Good et al., 2006), although manually-pumped gas has achieved mixing in specially-designed microfluidic channels (Garstecki et al., 2006). We first demonstrate the need for convective mixing by observing the exceedingly slow mixing kinetics of solutions that differ even slightly in density. Next, we demonstrate the rapid mixing promoted by in situ bubble generation and characterize the time scales involved. Our results provide tunable

mixing kinetics and a range of chemical systems adaptable to the particular constraints of various biochemical reactions.

5.3 Materials and Methods

Materials. Eicosane was purchased from Alfa Aesar; thioflavin T, methylene blue, sodium bicarbonate, citric acid, benzoic acid, potassium permanganate, 100kDa-180kDa poly(allylamine hydrochloride) (PAH), sodium percarbonate, sodium nitrite, and ammonium chloride from Sigma; high-profile 0.2 mL PCR tubes from USA Scientific; thermal epoxy from JB Weld; 2 megapixel Arducam camera sensor and Arducam Arduino UNO from Arducam; temperature probe; aluminum block; nylon mesh sieves from Component Supply Company.

MnO_2 nanoparticle synthesis. 416 mg of PAH was added under magnetic mixing at room temperature to a 100 mL solution of 20 mM $KMnO_4$, for an approximately 4:1 molar ratio of PAH repeat unit to $KMnO_4$ (Luo, 2007). The solution was mixed for five minutes, during which it underwent a characteristic color change from pink to brown (**Figure 30**A) accompanied by an increase in UV-vis absorbance in the 300-400 nm region and a loss of absorbance peaks in the 500-600 nm region (**Figure 30**D). DLS confirmed a tight size distribution of nanoparticles (NPs) approximately 50 nm in diameter (**Figure 30**E). Addition of H_2O_2 either in liquid or solid (percarbonate) form led to vigorous bubbling, which did not occur in a solution of $KMnO_4$ (**Figure 30**B,C). The nanoparticle suspension was stored at room temperature until further use.

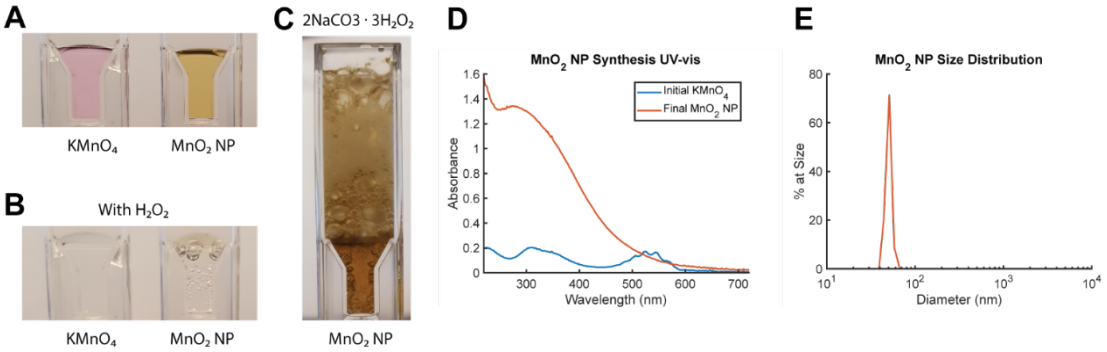

Figure 30. MnO_2 nanoparticle synthesis. **A)** Prepared MnO_2 NPs were a brownish color, compared to the pink of the starting solution of $KMnO_4$. **B)** In the presence of H_2O_2, MnO_2 NPs generated bubbles, whereas $KMnO_4$ did not. **C)** Addition of a ~1.5 mm granule of sodium percarbonate to MnO_2 NPs led to vigorous bubbling. **D)** Change in UV-vis absorbance corresponding to NP formation. **E)** NP diameters exhibited a tight distribution around 50 nm.

Static mixing reactions. 50 µL of molten eicosane was placed in the bottom of a PCR tube and allowed to solidify. A 2 mg/mL solution of (yellow) thioflavin T containing 1% Triton X-100 was prepared with varying amounts of glycerol. Note that 25% glycerol has a density of 1.070 g/cm^3 at room temperature and pure water 0.997 g/cm^3; at 48 °C these decrease to 1.060 and 0.989 g/cm^3, respectively, implying that the density ratio is roughly constant with temperature in the ranges investigated (Cheng, 2008; Volk and Kähler, 2018). This solution was placed in the tube above the eicosane, followed by a second 50 µL layer of eicosane. After this second alkane barrier solidified, a 50 µL solution of 15 mg/mL methylene blue with an appropriate amount of glycerol was placed on top.

CO_2 generation. Sodium bicarbonate was dissolved in de-ionized water (DI), deposited in a PCR tube, then dried at room temperature under vacuum. Citric, tartaric, or benzoic acid was dissolved in methanol, deposited on top of the dried bicarbonate in an equimolar amount, then dried similarly. A 50 µL layer of molten eicosane was placed above the dried effervescent reactants and allowed to solidify, after which the

system was assembled as above with a 25% glycerol lower solution and a 0% glycerol upper solution.

O_2 generation. 7.5 µL of MnO_2 nanoparticle solution was placed in the bottom of a PCR tube and dried under vacuum at room temperature. Sodium percarbonate was sieved to obtain granules of the indicated size and placed with the dried MnO_2, after which the system was assembled as above.

N_2 generation. Effervescent generation of nitrogen gas was performed similar to reported protocols (Flinn Scientific; Kaushick et al., 1986). 4 M NH_4Cl was prepared in 0.2 M H_2SO_4 and added to an equal volume of 4 M $NaNO_2$.

Temperature control. Wells were milled into an aluminum block to hold a PCR tube strip with windows for viewing. A polycarbonate sheet was glued to this block with thermal epoxy, then the wells were filled with water to facilitate heat transfer. A high-density cartridge heater (MCH1-96W-005, ComstatInc.com) powered by a 12V/3A DC power supply was actuated with PID control from an Arduino Uno to melt the eicosane barriers at 48 °C.

Image analysis. Time-lapse images were taken approximately 1-3 seconds apart with an Arducam-equipped Arduino Uno and analyzed in Matlab. Images were converted from the RGB to the CIE L*a*b* colorspace, which enables analysis of green (negative a* coordinates) separately from cyan and yellow (negative and positive b* coordinates, respectively) and luminance (L* coordinate), with greater fidelity than RGB (**Figure 31**). Rectangular, equally-sized Regions of Interest (ROI) no wider than the bottom of the tube were drawn by hand over each tube in the image, then the average

a* value was taken across rows of pixels within each ROI. Green regions of the image manifested as negative peaks in this vertical profile and so extent of mixing was quantified by taking the full-width-at-half-max (FWHM) of these peaks, normalized to the height of the aqueous layer. Complete mixing corresponded to a FWHM value of 0.8-0.9 or greater.

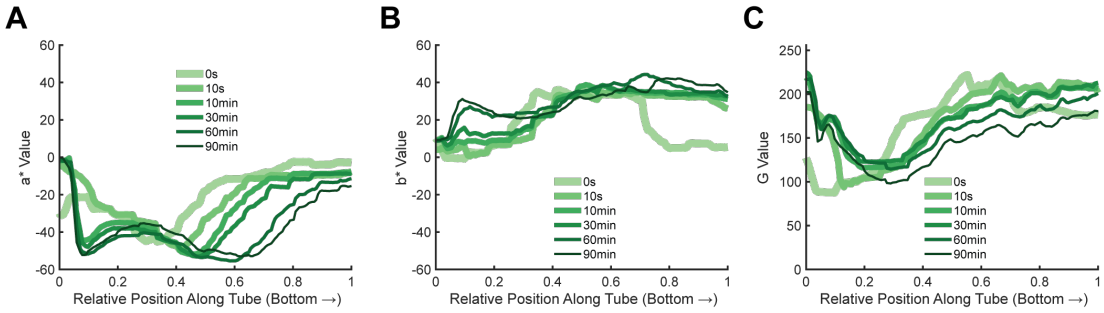

Figure 31. Image Analysis of 0%/25% glycerol static mixing. **A)** The -a* coordinate of the CIE L*a*b* colorspace correlates well with the visual progression of the green area in Figure **32** (main text), more so than **B)** the blue-yellow b* coordinate or **C)** the RGB colorspace G coordinate.

5.4 Results and Discussion

To demonstrate the mixing characteristics of solutions of various densities, we separated glycerol-doped yellow and blue solutions with an eicosane phase-change partition (Figure 29). When the eicosane barrier melted, the two solutions combined to produce a green color. If the top and bottom solutions had the same density they mixed rapidly, reaching homogeneity within seconds, independent of the particular density (Figure 32A). However, if the lower solution had a higher density than the upper solution, even slightly, mixing was severely impaired (Figure 32B). To quantify the effects of various conditions on the mixing rate, we analyzed the corresponding images in the CIE L*a*b* colorspace. As the green region grew, it produced a peak in the *-a** color coordinate; the full-width-at-half-max of this peak was used as a quantitative

indicator of the extent of mixing (Figure 32C). We observed that difference in density of approximately 1% (0%:3% glycerol layers) was sufficient to delay homogeneity by an hour and a half (Figure 32D). While here we demonstrate this phenomenon with solutions of varying glycerol content, the same behavior was observed with bottom

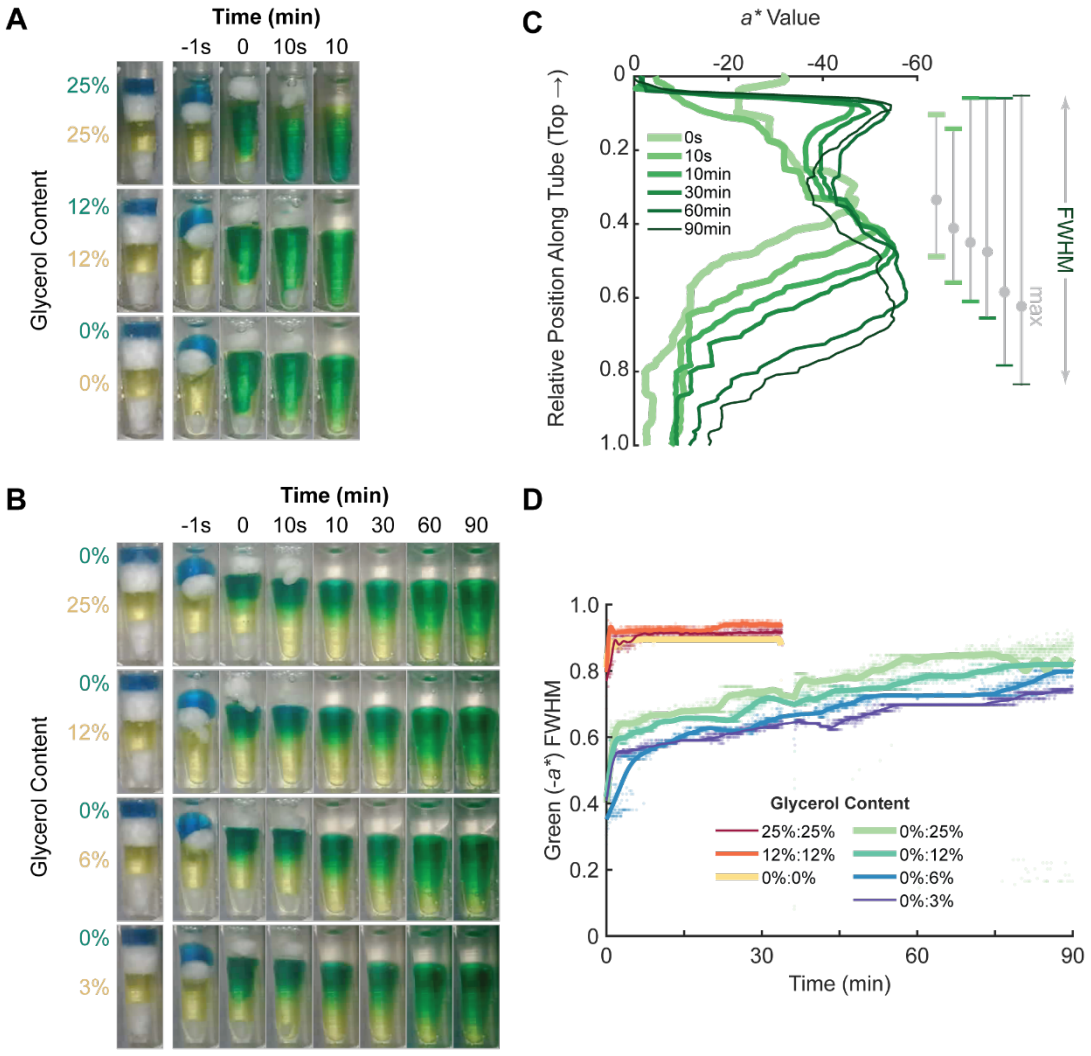

Figure 32. Static mixing. **A)** When two solutions of equal density encounter one another, mixing is rapid regardless of the actual density. **B)** If an upper solution of low density encounters a solution of higher density below, mixing is considerably impaired, taking well over an hour to reach equilibrium even for a 1% difference. **C)** The extent of mixing exhibited by each image (here, the 0%:25% glycerol combination) can be quantified by taking the full-width-at-half-max (FWHM) of the -a* color coordinate. **D)** Image analysis demonstrates that similar solutions reach equilibrium with a single, rapid burst phase, while dissimilar solutions exhibit an initial burst followed by steady diffusion.

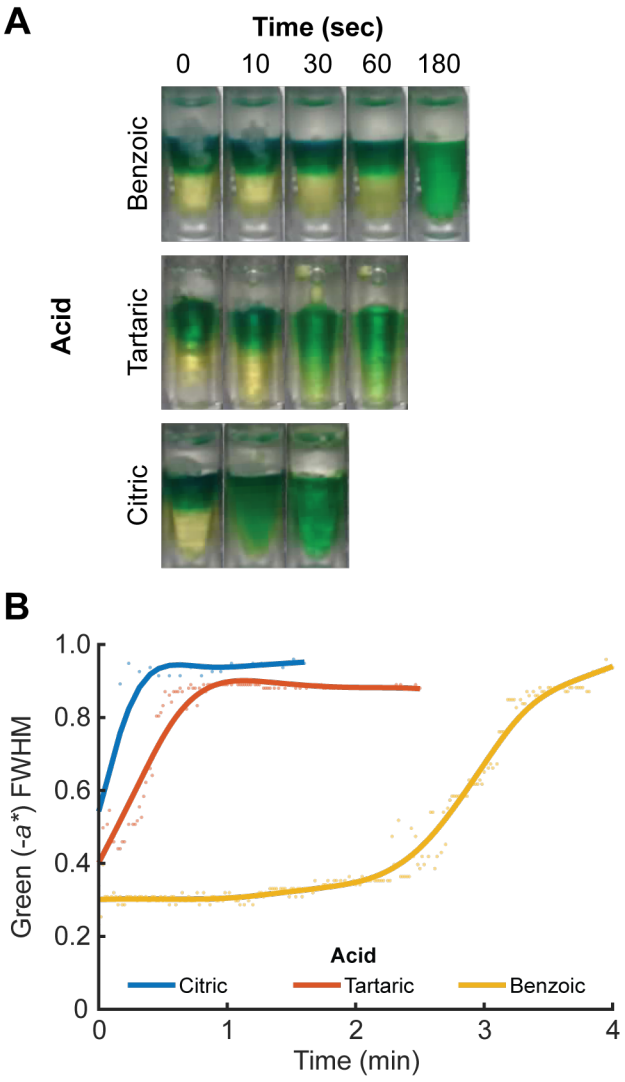

Figure 33. CO_2-mediated mixing of 0%:25% upper and lower glycerol layers, respectively. **A)** 4 µg sodium bicarbonate reacting with equimolar citric, tartaric, or benzoic acid generates CO_2 bubbles, rapidly mixing the two solutions. **B)** The three acids produce mixing rates proportional to their solubility (citric > tartaric > benzoic).

solutions containing sodium hydroxide (2.13 g/cm³) or sulfuric acid (1.84 g/cm^3) (not shown).

We attempted to accelerate the rate of homogenization through *in situ* generation of CO_2 gas bubbles from the classic reaction between sodium bicarbonate and acid. We dried an aqueous solution of bicarbonate at the bottom of PCR tubes. We then dissolved various organic acids in methanol and dried them on top of the bicarbonate. Using methanol as a solvent prevented premature reaction with the bicarbonate. The dried reagents were covered by a layer of eicosane (m.p. 36 °C) to isolate them from the colored solutions used above. We characterized the behavior of bubble-induced mixing in the worst-case combination shown in Figure 32B, a ~6% density difference between pure water above and 25% glycerol below. Upon melting of the eicosane barrier, the effervescent reactions reconstituted and reacted rapidly, drastically accelerating equilibration over the static

case (Figure 33). The time-to-homogeneity correlated with the hydrophobicity of the organic acid used: the most hydrophilic (citric) completely mixed the solutions within seconds, while the most hydrophobic (benzoic) took roughly three minutes. This demonstrates tuning the mixing rate from rapid to more gradual can be achieved by selecting an acid with appropriate solubility in water.

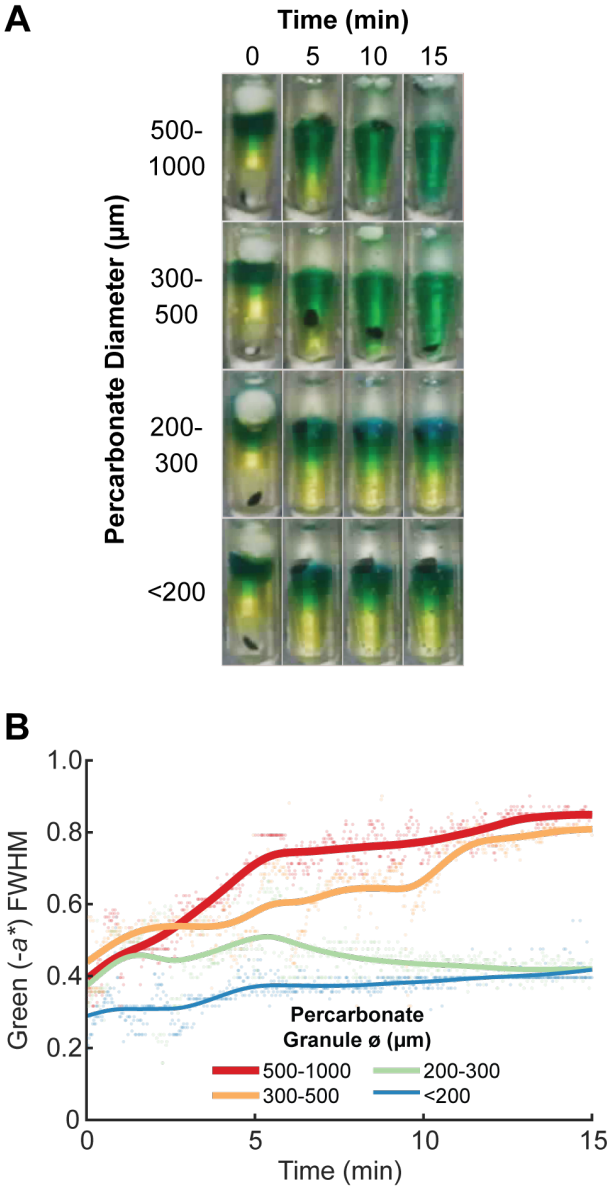

Figure 34. O_2-mediated mixing of 0%:25% upper and lower glycerol layers, respectively. **A)** 7.5 µL MnO_2 nanoparticles catalyze the decomposition of H_2O_2 (from sodium percarbonate) to generate O_2 bubbles. **B)** Mixing kinetics are slower than via CO_2 generation, but still much faster than static mixing for large percarbonate granules.

While *in situ* CO_2 generation achieved very rapid mixing kinetics, it will naturally lead to acidification of the mixed solution, even if the effervescent reaction occurs in a separate chamber. To achieve bubble-mediated convection without an accompanying pH change, we leveraged the catalyzed decomposition of H_2O_2 into O_2 gas. We employed MnO_2 nanoparticles as stable, easily-prepared catalysts and sodium percarbonate as a solid-state source of H_2O_2. MnO_2 NPs

were dried in the bottom of PCR tubes, while percarbonate granules were sieved to obtain various sizes and placed in the same tubes. This system was analyzed in the same manner as the CO_2-generating reactions. When the eicosane barrier melted, the two reagents interacted to produce O_2 bubbles. Reactions with percarbonate granules larger than 300 µm achieved homogeneous solutions within 5-10 minutes, while smaller granules did not noticeably accelerate mixing compared to the static case (Figure 34). The MnO_2 layer did not appear to dissolve completely, instead remaining a cohesive mass that floated about the tube, buoyed by generated gas. Future investigations should consider the use of excipients to promote dispersion of the NPs.

The two effervescence systems discussed so far are compatible with reaction constraints: O_2 bubbles may be suitable for pH-sensitive systems because they avoid acidifying the mixed solutions, unlike CO_2, yet they have the potential to interfere with redox-sensitive systems. However, should a system be intolerant to both acidification and oxidation, an inert gas such as N_2 would be an ideal source for bubble-mediated convection. We were able to generate visible bubbles by mixing acidified ammonium chloride with an aqueous solution of sodium nitrite (not shown). However, the high concentrations required and the necessity of sulfuric acid made it difficult to dry the reagents together without premature reaction. A capsular, wet-storage approach may be necessary for this system.

5.5 Conclusion

Mechanical agitation is a nearly universal component of many biochemical reactions. For many reactions used as medical diagnostics, this necessity complicates ease-of-use and impairs portability and adaptation to low-resource settings. Thermal

automation, through systems such as our phase-change partitions, are particularly vulnerable to this drawback: the lack of active mixing can lead to slow equilibration between reactant solutions. Here, we present a system for thermally-automated in situ generation of gas bubbles that promote convective mixing. Through a variety of phase-change partitioned effervescent reactions, we demonstrate that the very slow mixing rate between solutions of even slightly dissimilar densities can be greatly accelerated to achieve rapid homogenization. We dried effervescent components at the bottom of PCR tubes and then sequestered them from an aqueous solution through an eicosane phase-change partition. Melting this barrier led to reconstitution of the reagents and initiation of effervescence, producing CO_2 or O_2 bubbles.

It should be noted that there has been much debate over the relative impact of viscosity and density differences on mixing rate, and there have been vastly more studies on this relationship in chaotic- or laminar-flow systems than in comparably static or pulsed systems like the one examined here (Bouwmans et al., 1997; Burmester et al., 1992; Chien et al., 1986; Mohr et al., 1957). Here, all solution combinations investigated displayed an initial burst-mixing phase driven by the inertia of the upper solution. If the upper and lower solutions were of the same density and viscosity, this inertia was sufficient to overcome viscous resistance and homogeneity was achieved rapidly with no dependence on the magnitude of those properties. If there was even a slight mismatch, however, the initial burst phase was only incomplete, and achieving equilibrium was viscosity-limited. The mixing rate achieved by the effervescent systems, on the other hand, was largely limited by the solubility of the reactants. The CO_2-generating reactions produced almost instantaneous mixing, proportional to the

solubility of the acid used. The O_2-generating reactions produced slower mixing, albeit still faster than the static case, in large part due to the poor solubility of the MnO_2 catalyst.

In the investigations presented here, the effervescent reagents were directly dissolved by the solution to be mixed. This has obvious drawbacks, which we envision to be solved in future studies through the use of semi-permeable membranes that allow gas diffusion but isolate the effervescent and working solutions from one another. Even in that scenario, however, the dissolution of evolved gasses into the working solution may still be a concern; to that end, we described systems for generation of CO_2, O_2, and N_2, so that the mixing system can be tailored to the constraints of the desired biochemical reaction. In our hands, the CO_2 system produced very rapid equilibration, within a few seconds in the case of the bicarbonate-citric acid reaction. The O_2 system exhibited more gradual mixing kinetics, but this may be preferable if, for example, a bead-based reaction needs to be agitated for a prolonged period. Leveraging both systems in parallel may also be advantageous: the burst-mixing accompanying CO_2 generation could be used to rapidly disperse a bead bed while the gradual mixing provided by O_2 generation could prevent re-settling.

The effervescent mixing strategy described here expands the capabilities of thermally-automated systems leveraging phase-change partitions, improving their portability by eliminating yet another common element of manual intervention. This approach may also be useful in other platforms, such as microfluidics, in which diffusive mixing is a limiting consideration. Ultimately, effervescent mixing provides

one more tool for point-of-care diagnostics, a low-cost option to automate medical tests and help alleviate access-to-care deficiencies in rural, poor settings.

6 Multi-stage chemical heating for instrument-free biosensing[5]

The earlier chapter describing phase-change partitions demonstrated barrier actuation through temperature control with a thermocycler and a water bath, alluding to the possibility of chemical temperature control. A truly electricity-free actuation system would be ideal for portable, point-of-care diagnostics. While passively-regulated chemical heating had been described previously, none had achieved the multiple temperature stages necessary to actuate multiple phase-change partitions. This chapter describes the development of a system that does.

6.1 Abstract

Improving the portability of diagnostic medicine is crucial to alleviating global access-to-care deficiencies. This requires not only designing devices that are small and lightweight but also autonomous and independent of electricity. Here, we present a strategy for conducting automated multi-step diagnostic assays using chemically generated, passively regulated heat. Ligation and polymerization reagents for Rolling Circle Amplification of nucleic acids are separated by melt-able phase-change partitions, thus replacing precise manual reagent additions with automated partition melting. To actuate these barriers and individually initiate the various steps of the reaction, field ration heaters exothermically generate heat in a thermos while fatty acids embedded in a carbonaceous matrix passively buffer the temperature around their melting points. Achieving multi-stage temperature profiles extends the capability of instrument-free diagnostic devices and improves the portability of reaction automation systems built around phase-change partitions.

[5] This work was done in collaboration with Kenya M. Colvin, Andrew B. Lippe, John L. Daristotle, and Peter Kofinas. It has been submitted for publication.

6.2 Introduction

Access to healthcare remains one of the primary challenges of modern medicine. Technological advances often remain concentrated in wealthy urban centers, out of reach to rural and poor populations in developing and developed nations alike. Alleviating this disparity is not simply a matter of making existing techniques affordable: many traditional assay platforms are incompatible with field-use at any cost. Instead, alternative technologies must be designed for high portability (small, lightweight, not reliant on electricity) and ease-of-use (simple and autonomous, with minimal hands-on steps).

Two primary approaches have emerged to answer this need: chip- and paper-based microfluidics (Martinez et al., 2010; Whitesides, 2006). Traditional microfluidic devices that utilize micro-fabricated fluidic networks are capable of housing numerous reactions with myriad components that proceed in a well-orchestrated pattern, yet the requisite pumps and other peripheral equipment severely impair portability (Foudeh et al., 2012). While paper devices significantly improve the portability of biosensing reactions, the simplicity that makes them easy to use limits the throughput and complexity of assays they can support (Hu et al., 2014). To address this gap between miniaturized assays suitable only for laboratory use and those restricted to field use, we recently described the novel approach of employing thermally-removable barriers to sequester reagents within a common PCR tube (Goertz and White, 2018). This approach demonstrated the potential to offer the tight reaction control of microfluidics with portability and ease-of-use that parallels paper devices.

These “phase-change partitions” consist of ordinarily-solid purified hydrocarbon waxes that exhibit sharply-defined melting transitions at distinct temperatures. Reagents for each step of a multi-part reaction remain isolated from one another until the respective barrier is melted, at which point a sample solution sinks through the now-molten alkane and mixes with the reagent beneath. This approach allows arbitrarily long reaction stages and at least five distinct reagent zones within a single 200 µL PCR tube. While the temperature range spanned by the alkanes we employed is narrow enough to remain accessible to simple heating devices, the melting transitions are discrete enough to avoid the need for tightly-calibrated temperature control. Indeed, we demonstrated actuation of these phase-change partitions in a simple water-bath as well as a commercial thermocycler.

However, even a temperature-regulated water-bath requires a consistent source of electricity, unavailable in field settings or low-resource clinics. A similar challenge is faced by many isothermal nucleic acid amplification techniques such as LAMP (loop-mediated isothermal amplification, Notomi et al., 2000; Sema et al., 2015) and RPA (recombinase-polymerase amplification, Piepenburg et al., 2006; Wahed et al., 2015), which require elevated temperatures to achieve highly-sensitive detection of pathogens. Numerous groups have employed chemically-generated heat with thermal buffers to reach the incubation temperature for these reactions (Buser et al., 2015; Curtis et al., 2012; LaBarre et al., 2011). This is typically achieved using the exothermic hydration of calcium oxide or the galvanic corrosion of MgFe alloys in the presence of saline (Buser et al., 2015; Singleton et al., 2013). This latter reaction is extensively employed in military Meal-Ready-to-Eat (MRE) field ration heaters and thus has been

thoroughly optimized to rapidly reach boiling temperatures while remaining compact and lightweight.

To achieve prolonged incubation at temperatures amenable to biochemical reactions rather than a brief burst of excessive heat, researchers have employed phase-change materials (PCMs) as thermal buffers in these exothermic systems (Buser et al., 2015; Curtis et al., 2012; Kubota et al., 2013; LaBarre et al., 2011; Liao et al., 2016; Singleton et al., 2013; Song et al., 2016). These materials surround the reaction compartment so that, as they melt, the temperature of the reaction remains near that of the compound's melting point (Farid et al., 2004). Phase-change materials with specified thermal characteristics are commercially available (PureTemp) but can also be inexpensively fashioned from materials such as fatty acids and hydrated salts with high latent heats of fusion and desirable melting temperatures (Ryu et al., 1992b; Yuan et al., 2014). Previous reports have described systems which are designed for only a single operating temperature; here, we present the use of MRE heaters with blended PCMs to achieve multi-stage temperature profiles. We leveraged this platform to sequentially actuate two phase-change partitions in a PCR tube, at the same time providing ideal operating temperatures for the respective ligation and polymerization stages of Rolling Circle Amplification (RCA). Our results demonstrate the potential for platforms based on phase-change partitions to automate the field use of complex, multi-stage biosensing reactions without the need for electricity.

6.3 Materials and Methods

Materials. Carbon black (CB) (99.9%), lauric (dodecanoic) acid (LA) (98%), and palmitic (hexadecanoic) acid (PA) (95%) were purchased from Alfa Aesar (Haverhill,

MA). Sodium thiosulfate pentahydrate, sodium acetate trihydrate, and carboxymethyl cellulose (CMC) were purchase from Sigma. 0.2 mL high-profile PCR tubes were purchased from USA Scientific (Ocala, FL). RCA reagents were purchased from New England Biolabs (Ipswitch, MA), and DNA sequences were purchased from Integrated DNA Technologies (Coralville, IA). DNA Sequences used are:

Trigger: 5'-TAG TCG AGA CAT CCG AGA CA -3'

Template: 5'-Phos-GTC TCG ACT AAA AAC CCA ACC CGC CCT ACC CAA AAG AGA CAT CCG TTT TGT CTC GGA T-3'

MRE Heaters were provided by Luxfer Magtech Inc. Tahoe Trails 10 oz vacuum insulated double wall stainless steel travel tumblers, 4 x 5 inch sealable tea bags, Kayose natural tea filter bags, and the iTouchless handheld heat bag sealer were purchased from Amazon. 1 mm nylon mesh sieves were purchased from Component Supply Company. The custom-designed thermos insert was 3D printed in ABS with a Zortrax M200. All remaining materials were purchased from MilliporeSigma (Burlington, MA).

Preparation of Encapsulated PCMs. Fatty acids and hydrated salts were melted on a hot plate under magnetic stirring. Carbon black or activated carbon was mixed with melted fatty acids at specified weight ratios. The hydrated salts were mixed first with 5 wt% CB and subsequently with 10 wt% CMC; a small amount of methanol was added to allow CB to mix with the molten salt hydrate. The resulting pastes were spread on aluminum foil to cool, ground in a mortar and pestle, and sieved to obtain granules <1 mm in diameter. To produce systems with multiple temperature stages, multiple PCMs

were encapsulated separately then mixed after cooling so as not to impact their individual melting points.

Form-Stability of Encapsulated PCMs. To assess the stability of the encapsulated PCMs against melt leakage, ~4 g composite was placed in Kayose tea bags, sandwiched between paper towels and then aluminum foil, and placed on an 80 °C hotplate. Mass of the composite was taken before and after one hour of incubation.

Differential Scanning Calorimetry (DSC). Approximately 10 mg samples were sealed in aluminum hermetic pans (TA Instruments) using a sample encapsulation press. DSC measurements were made on a TA Instruments DSC Q100. Samples were held isothermal at 0 °C for 5 min, then heated to 100 °C and cooled to 0 °C at a rate of 3 °C min^{-1}, ± 0.20 °C amplitude, with a modulation period of 60 s for two continuous cycles.

Chemical Heating. MRE heaters were used as is to determine the temperature profile of the exothermic reaction between saline and the MgFe alloy in the MREs. A single packet of the MgFe alloy was added to a thermos followed by 100 mL of saline. The reaction was examined using NaCl concentrations of 0, 0.1, 0.3, 0.5, 1.0, and 1.5 wt%. Temperature was recorded using a Sparkfun waterproof temperature sensor (DS18B20) and an Arduino Uno.

Passively Regulated Temperature. MRE heaters were repackaged using heat-sealable tea bags, as described previously. MgFe alloy granules from MREs were distributed into each tea bag in 3.70 g allotments, sealed, then placed in the bottom of the vacuum thermos. The exothermic reaction was initiated by adding 100 mL of 0.1%

saline, after which a 3D-printed insert made of ABS was placed in the container and covered with aluminum foil, suspending the PCM above the saline level. A Styrofoam lid provided insulation at the top of the thermos, while a small hole allowed hydrogen gas produced in the chemical reaction to vent. The temperature within the PCM was recorded using a Vernier Labquest Mini and a stainless steel temperature probe.

Phase-Change Partitioned Assays. The pH indicator demonstration was constructed in a PCR tube, from top to bottom, with 40 µL indicator solution (1 mM H_2SO_4, 1% Triton, 60% Indicator), 50 µL octadecane, 10 µL each buffer A (800 mM

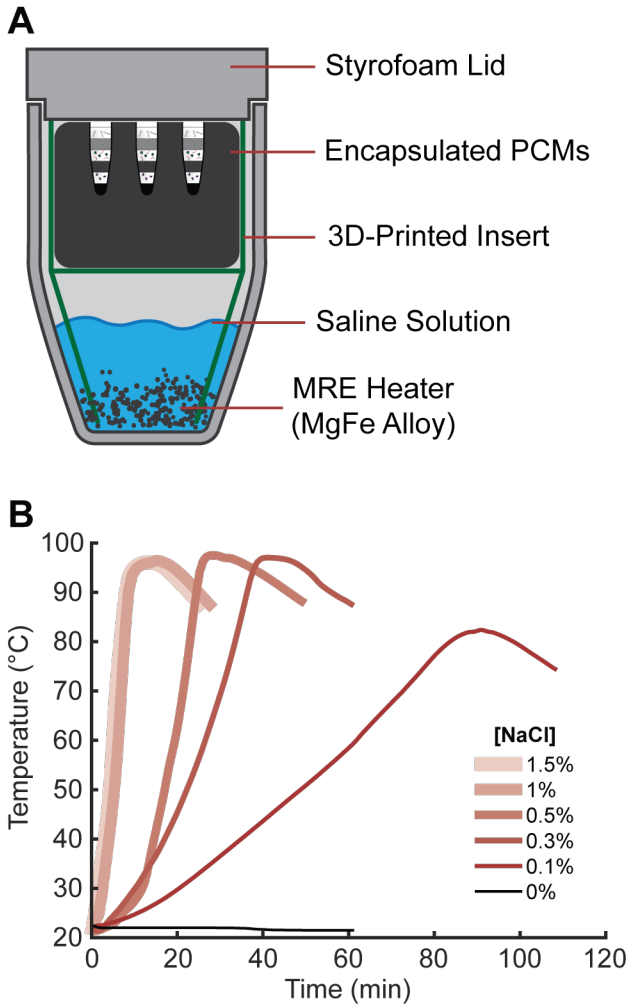

Figure 35. Chemical heating. **A)** A 10 oz thermos provides the housing for PCM-MRE actuation of phase-change partitioned assays. **B)** Decreasing the saline concentration used to initiate the exothermic reaction provides a more gradual temperature profile, facilitating passive thermal regulation with PCMs.

NH_4OAc, 250 mM Tris, pH 6.0) and B (5 M NH_4OAc, 500 mM Tris, pH 8.0), 40 µL tetracosane, and 30 µL 9.8 M NH_4OH. The RCA reaction was constructed, from top to bottom, with 20 µL 1.36 µM Template DNA in DI water, 50 µL octadecane, 20 µL ligase solution (18 U/µL T4 DNA Ligase, 1.8x Ligase Buffer with ATP), 50 µL tetracosane, 20 µL polymerase solution (1.1 U/µL Bst 3.0 DNA Polymerase, 2.7x Isothermal Amplification Buffer, 2.7 mM dNTPs, 1.36 µM Trigger DNA). Tubes were embedded into a mixture of 20 g encapsulated LA and 20g encapsulated PA, then heated as described above with an MRE heater initiated by 0.1% saline. Reactions marked *L* in Figure 38 were removed once the vessel temperature reached 40 °C, and reactions marked *F* were removed one hour after the vessel temperature exceeded 55 °C.

Gel Electrophoresis. Denaturing polyacrylamide was used to analyze RCA products. Reactions were removed at the respective time and halted by immersion in ice water. Reaction solutions were extracted, mixed with two parts 12 M urea, heated to 95 °C for five minutes, then run on a 15% gel at 500 V for 15 minutes in a BioRad mini PROTEAN.

6.4 Results and Discussion

The usability of phase-change partitions for diagnostic reactions in low resource settings heavily depends on being able to easily manipulate the heat source without the use of electricity or additional equipment. Our multi-stage heating device consisted of an off-the-shelf vacuum thermos separated by a 3D-printed insert: a lower chamber contained the MRE alloy packet while the encapsulated PCMs and reaction tubes were housed in an upper chamber above the saline level (Figure 35A). We were able to easily

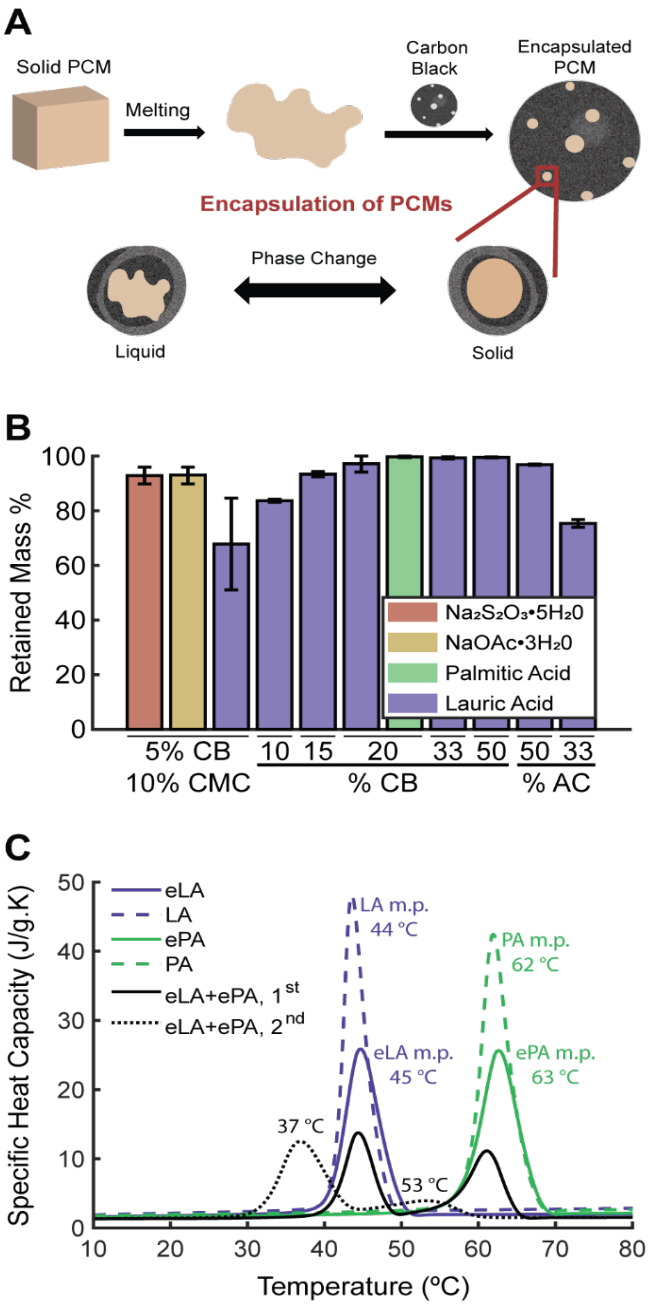

Figure 36. PCM Encapsulation. **A)** Fatty acids are melted then mixed with carbon black, causing the molten PCM to impregnate the pores of the carbon matrix. Upon re-melting, capillary tension prevents the PCM from leaking out of the encapsulation. **B)** Form-stability of encapsulations was evaluated by measuring the mass lost after one hour of heating at 80 °C. **C)** DSC analysis demonstrates the tight melting profile of fatty acids. LA, PA: pure fatty acid alone. eLA, ePA: fatty acid with 20% CB. eLA+ePA: 1:1 mixture of each fatty acid individually encapsulated in 20% CB, first and second run. Black text labels refer to eLA+ePA, 2nd peaks.

fine tune the temperature profile of the saline-activated MgFe alloy by changing the concentration of salt in the solution (Figure 35B). The saline pack included with the MREs contained 1.5 wt% salt and caused a rapid increase in temperature up to 97°C. Reducing the salt concentration increased the time it took for the MgFe alloy to reach its maximum temperature while lowering that maximum, reducing the thermal burden needed to be buffered by PCMs.

We investigated two fatty acids (LA, m.p. ~43 °C, and PA, m.p. ~63 °C) and two hydrated salts (sodium thiosulfate pentahydrate, $Na_2S_2O_3 \cdot 5H_2O$, m.p. ~48 °C; and sodium acetate trihydrate, $NaOAc \cdot 3H_2O$, m.p. ~58 °C) for use as PCMs. Ideally, PCMs must be encapsulated to prevent leakage of the melted material during operation and, in the case of hydrated salts, to prevent phase-separation in the molten state; doing so also has the advantage of improving the thermal conductivity of the material. There is an extensive body of literature devoted to such encapsulation techniques for the purposes of solar heating as well as "smart" construction and textile materials, most of which entail either formation of core-shell microparticles or distribution of the PCM within a porous matrix (Aftab et al., 2018). Here, we chose carbon black (CB) as an encapsulant for fatty acids due to its affordability, ease of encapsulation, and thermal-conduction properties. The fatty acid was melted, mixed rapidly with CB to penetrate the porous matrix, cooled, ground, and sieved (Figure 36A). Upon subsequent re-melting, surface tension caused the molten fatty acid to remain entrapped within CB pores. This composite exhibited bulk minimal leakage at elevated temperatures when the CB mass fraction was 20% or greater (Figure 36B); curiously, CB provided greater form-stability than activated carbon, despite the latter's nominally higher surface area

to volume ratio and prominent position in the PCM literature (Shin et al., 2015; Yuan et al., 2014). For hydrated salts, 5% CB with 10% CMC achieved adequate form-stability (Shin et al., 2015).

We used differential scanning calorimetry to investigate the thermal properties of our encapsulated PCMs. As shown in Figure 36C, encapsulation resulted in minimal change in PCM melting point (defined as the temperature at maximal specific heat capacity), implying no chemical interaction between core and matrix materials. However, upon re-melting a mixture of LA and PA encapsulated separately, the two melting points were significantly lower. This suggests that the molten fatty acids migrate between the carbon black particles, mixing with one another and mutually depressing their respective melting points.

This mixture of encapsulated fatty acids provided an adequate thermal buffer for to produce multi-stage temperature profile from an MRE heater. By combining 20 g encapsulated PA with 20 g encapsulated LA, the temperature profile generated by an MRE heater with 0.1% saline was successfully modulated to exhibit an approximately 1 hour hold between 30 and 40 °C and a greater than 1 hour hold between 55 and 65 °C (Figure 37A). This temperature profile allowed well-controlled actuation of phase-change partitions, demonstrated by stepping a pH indicator solution through sequential eicosane and tetracosane barriers to mix with various buffers (Figure 37B). Combinations of encapsulated hydrated salt also produced multiple temperature stages (not shown).

The lowered melting points of the encapsulated fatty acid mixture provided ideal temperature regimes to achieve Rolling Circle Amplification. RCA is a two-step method for DNA detection: a template sequence is first ligated into a circle, then a complementary trigger sequence is extended by a polymerase to continuously replicate the template.(Lizardi et al., 1998; Yan et al., 2014) While each stage requires 30-60 minutes at only a single temperature, the ligase enzyme is most active between 30 and 40 °C and the fastest polymerase enzymes are active between 55 and 65 °C; furthermore, the two steps must be performed separately, since premature extension of

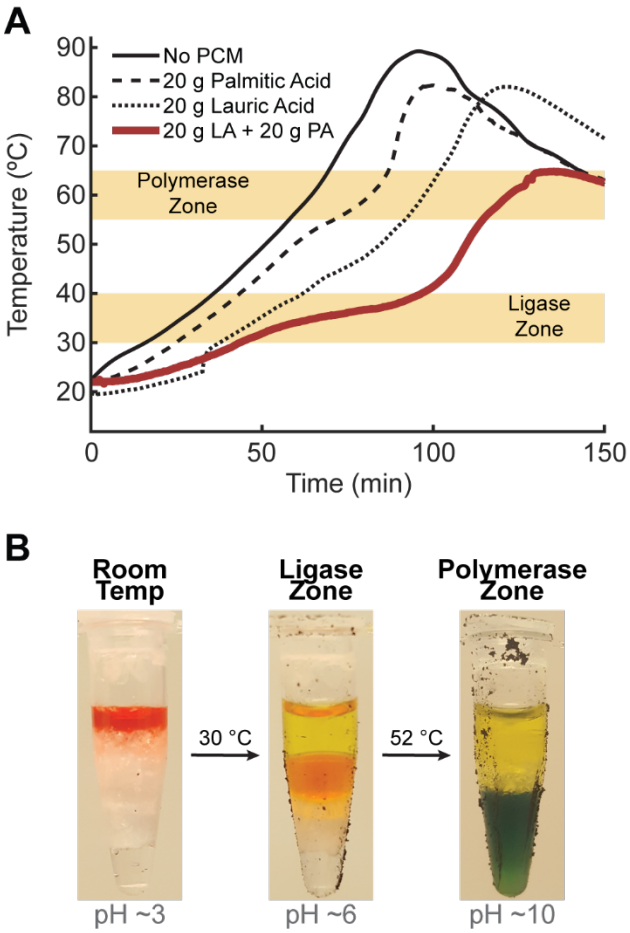

Figure 37. Multi-stage chemical heating. **A)** An MRE heater activated with 0.1% saline and buffered with a mixture of 20 g encapsulated lauric acid and 20 g encapsulated palmitic acid produces two distinct temperature zones amenable to different biochemical processes. **B)** This two-stage heating can be used to actuate phase-change partitions. Here, pH Indicator is stepped through different buffers sequestered by eicosane and tetracosane barriers.

the trigger sequence along an un-circularized template prevents ligation and continuous amplification.

We constructed a partitioned RCA reaction by placing a dumbbell-forming template DNA sequence above a layer of octadecane (m.p. 30 °C), followed by a buffer containing ligase, a layer of tetracosane (m.p. 52 °C), and finally a buffer containing trigger DNA and polymerase (Figure 38A). Six such reactions were run in parallel in the MRE-PCM system described above. Three were removed once the thermos reached 40 °C and the remaining three were incubated further until the thermos had spent an hour above 55 °C, during which time the temperature never exceeded 65 °C. As demonstrated by gel electrophoresis (Figure 38B), both ligation and polymerization proceeded efficiently; furthermore, the trigger sequence is not present in the reactions incubated only until 40 °C, indicating that the phase-change partitions completely sequestered the various reaction components.

6.5 Conclusion

We have demonstrated the electricity-free automation of a multi-step biosensing reaction. The phase-change partition platform reported previously enabled stable separation of reactants with thermally-reversible alkane barriers; the current work provides a system capable of actuating these partitions in an automated, field-compatible manner. Tempering the saline concentration added to MRE heater granules metered the rate of the accompanying exothermic reaction, while phase-change materials buffered the reaction temperature within multiple sequential ranges amenable to biochemical reactions. Encapsulating the PCMs within porous matrices prevented bulk leakage, enabling re-use. When used alone, encapsulated LA produced a

temperature hold of approximately 45 °C, but when combined with encapsulated PA, the first temperature hold occurred at a temperature regime more amenable to T4 DNA Ligase, between 30 and 40 °C. The melting point of PA was similarly depressed, remaining within an optimal region for *Bst* polymerase. Additionally, future investigations should explore numerical approaches to quantitatively model PCM-

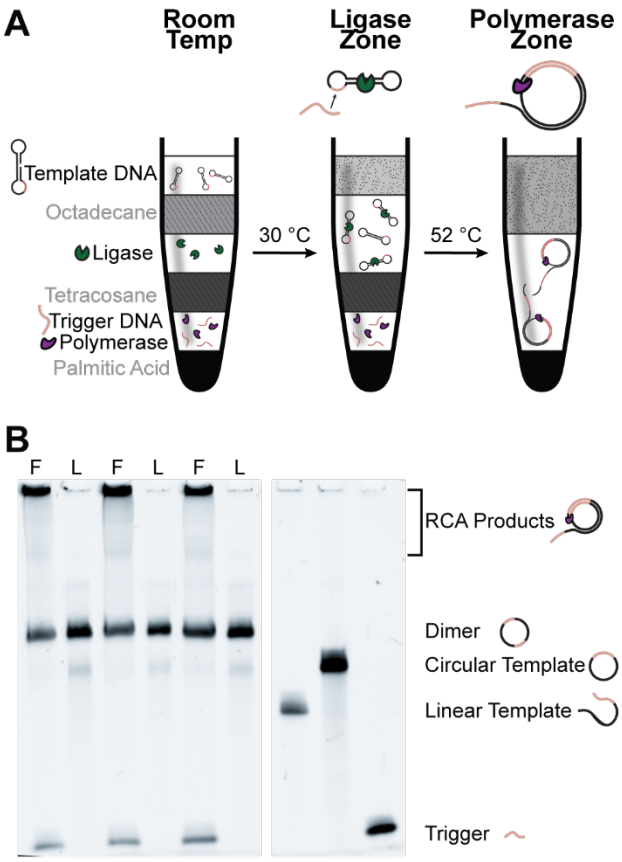

Figure 38. Portable biosensing with multi-stage chemical heating. **A)** The phase-change partitioned RCA assay is initiated by melting of an octadecane layer once the tube exceeds 30 °C, causing ligase enzyme to ligate the template DNA into a circle. The amplification stage is initiated by melting of a tetracosane layer once the tube exceeds 52 °C, at which point the polymerase extends a trigger sequence to continuously replicate the template. **B)** Denaturing acrylamide gel electrophoresis reveals successful ligation in all reactions, and successful generation of amplicon in those incubated for the full duration (F). The absence of trigger DNA in reactions incubated only for the ligase portion (L) confirms the integrity of the tetracosane barrier below its melting point. Note that the apparent difference in circular template band intensity between Ligase-only and Full reactions is due to the further dilution by the polymerase solution in the latter.

MRE temperature profiles and accelerate the development cycle of non-instrumented diagnostic assays.

We successfully actuated a phase-change partition system with passively-buffered chemical heating to demonstrate the capacity of this system to automate nucleic acid amplification. This report extends the compatibility of the phase-change partition platform to include not only well-equipped laboratories (via thermocyclers) and generic clinics (via water baths), but also resource-poor settings and field operation (via multi-stage PCM-MRE heaters). The key advantage of such broad compatibility is that it enables a common form factor to be employed in diverse settings: the same assay can be given to a central lab technician and a field nurse. Our results demonstrate that phase-change partitions have the potential to bridge the current gap between centralized and remote diagnostic platforms. Now further developments are necessary to adapt a wide range of clinical assays to this system and support efforts to close the urban-rural divide that persists in 21st century medicine.

7 Highly stable encapsulation of diverse mesoscale materials with thermally-controlled burst-release[6]

This final experimental chapter improves upon two drawbacks of the phase-change system described in Chapter 4. In that system, the partitions and reagents are stacked in a tube as layers, one after the next. That strategy makes manufacture of the system difficult, as each component must be added in a specific order. Additionally, not only is quality control of the individual assay components difficult, if any component fails quality control then the entire device fails. Furthermore, the interface between the hydrophobic layers and the polymer tube walls is a natural weak point. The work described in this chapter involves the engineering of the phase-change partitions in a self-contained, capsular structure.

7.1 Abstract

Controlled encapsulation and release of reagents has the potential to facilitate automation in a variety of integrated systems, yet many existing approaches are highly specific to a given platform or core material. Here, we present a generic encapsulation strategy, adaptable to a range of geometries and cargos, that enables thermal control over reagent release. We use 3D printing to cast hollow "phase-change" capsules out of purified waxy materials (alkanes and fatty acids), which can then be loaded with any desired material and sealed. When submerged, the resulting capsules are stable against leakage for at least five days, and in air they are stable against evaporation for at least

Figure 39. Phase-change capsule graphical abstract.

[6] This work was done in collaboration with Srini R. Raghavan and has been submitted for publication.

four weeks. Mild thermal stimulus leads to immediate release of the core, presenting a highly modular platform for thermally-regulated reaction systems. We demonstrate the utility of these capsules for controlled release of a common unstable biochemical reagent, hydrogen peroxide. Furthermore, we illustrate the ability of these capsules to enable safe, semi-automated field operation of environmental-surveillance assays (nitrate detection) requiring hazardous chemicals (pure sulfuric acid). These phase-change capsules provide a modular, mass-producible platform for stable, stimuli-responsive encapsulation.

7.2 Introduction

Engineering complex, autonomous materials systems requires tight control over interactions between the myriad components. The ideal platform perfectly isolates each node from its environment, rapidly releasing the cargo in entirety on demand. Many current approaches for encapsulation, however, are leaky in their "closed" state or respond poorly to an "opening" stimulus (Duncanson et al., 2012; Keen et al., 2014; Ma et al., 2013; Reinhold E. Samuel et al., 2012; Sun et al., 2010; Zieringer et al., 2015). Furthermore, most current approaches are suitable only for solids or liquids or hydrogels; few are compatible with all three classes of materials. Here, we present a general-purpose approach that offers equal utility to reversible encapsulation of mesoscale solids, hydrogels, and liquids.

Traditional bulk encapsulation techniques have the potential to rapidly produce large quantities, yet most require extensive optimization for each new core phase and are typically only compatible with a single class of material. Emulsion strategies, for instance, are conducive only towards encapsulation of liquids or nanoscale solids

(Elkharraz et al., 2011; Morita et al., 2000; O'Donnell and McGinity, 1997; Taguchi et al., 2014). Industrial techniques such as spray-coating, rolling-drum encapsulation, or spinning-disk encapsulation are largely suitable only for solids and rely on a degree of interaction between core and shell material (Jenjob et al., 2012; Jozwiakowski et al., 1990; Knezevic et al., 1998; Mackaplow et al., 2006). Furthermore, these approaches are often prohibitively expensive for exploratory, laboratory-scale preparation.

Previously, microfluidic devices have been used to produce core-shell microstructures from waxy materials, encapsulating one or more aqueous reagents within such thermally-reversible materials (Sun et al., 2010). However, capillary microfluidic device fabrication and operation requires sophisticated instrumentation and careful optimization while remaining largely incompatible with solid or even semi-solid core materials. Indeed, the literature is virtually devoid of reports on microfluidic manipulation of mesoscale (100 μm – 1 mm) solids or hydrogels prepared off-line (Duncanson et al., 2012; Lee et al., 2016; Pan et al., 2018; Sakai et al., 2008; Seiffert et al., 2010; Vladisavljević et al., 2017). Even encapsulation of liquids in this manner presents severe limitations: core volumes on the scale of microliters or larger are difficult or impossible to prepare, and high salt concentrations are required to prevent leakage in an aqueous environment (Keen et al., 2014; Y. Zhao et al., 2011; Zieringer et al., 2015). Finally, strategies relying on capillary microfluidics are likely present difficulties in scaling-up to industrial production scales.

Thermal control over reaction systems is particularly attractive for applications such as point-of-care biomedical diagnostics, for which portability and ease of

automation are paramount. Recently, we described phase-change partitions as an approach to sequester reagents that mix only in response to a mild thermal stimulus (Goertz and White, 2018). Separating aqueous or lyophilized reagents in a common PCR tube with layers of purified alkanes provided a platform for multi-step reactions where each stage could be triggered by incrementally raising the temperature. However, the layered nature of the system meant each component had to be added sequentially, potentially complicating mass-manufacture of assays leveraging this platform. Furthermore, the interface between each wax layer and the polymer tube wall created a natural weak point: rough handling of the assembled reaction could dislodge the barriers, potentially leading to premature mixing of reagents and ruining the assay. Formation of these phase-change partitions into self-contained capsules would improve the robustness of the platform while enabling asynchronous production of various complementary reaction components at industrial scales.

Here, we leverage phase-change partitions as encapsulants of a variety of core materials, creating self-contained reagent capsules amenable to modular system assembly. We melt-cast alkanes and fatty acids into a cup shape using 3D-printed molds. Any core material can be placed within these cups, which are capped with more shell material and subsequently sealed. The final capsules are stable against leakage and evaporation, enabling storage of hazardous assay components with easily controlled release. These phase-change capsules have the potential to provide an ideal stimulus-responsive platform for diverse applications, including biomedical diagnostics, environmental surveillance, and chemical synthesis.

7.3 Materials and Methods

Materials. Alkanes and fatty acids were purchased from Alfa Aesar; Sylgard 184 polydimethylsiloxane (PDMS) monomer and crosslinker from Ellsworth Adhesives; dichlorofluorescein diacetate (DCF-DA), resorufin, sodium percarbonate (20-30% avail. H_2O_2), diphenylamine from Sigma; and well plates from Greiner. A Formlabs Form2 printer was used for stereolithographic 3D printing with ≤0.05 mm layer height.

Capsule molds. Capsules were designed to have a 10 µL hemispherical core with a 15 µL cylindrical headspace. Molds for phase-change capsules were made by 3D printing, either directly or via a master template. The master was printed with Formlabs High Temp Resin and coated in mold-release (Ease Release 200, Mann Release Technologies). An elastomer mold was made by filling the master with PDMS (prepared at a 10:1 ratio), curing in an 80 °C oven for 30 minutes, removing the partially-cured mold, and replacing it in the oven for an additional 30 minutes. Molds were also directly 3D-printed in Formlabs Flexible Resin. A stamp, used to produce the hollow core of the phase-change cups during casting, was 3D-printed in High Temp Resin. Molds and stamps were coated with mold-release prior to each use.

Capsule fabrication. Shell material was melted and held at 200 °C, then poured into a mold placed atop a thin metal plate. This high of a temperature was found to be necessary to delay solidification of the poured material allow for positioning of mold components. A stamp was then inserted and secured with heavy-duty binder clips. Air was allowed to circulate underneath the casting assembly during cooling. Once cooled, the mold was peeled away. Often, the resulting capsules remained lightly trapped to stamp posts and were removed with a razor blade. After filling with the desired core

material, capsules were capped with additional 200 °C shell material. First, 15 µL was deposited and allowed to solidify, followed by an additional 5 µL. As indicated, some capsules were further sealed by immersion for 10 or 30 seconds in mineral oil or 34 °C octadecane then removed with a sieved and agitated lightly as they cooled. No difference was observed between capsules immersed for 10 or 30 seconds, so the two groups were pooled for analysis.

Stability tests. Eicosane (m.p. 36 °C) capsules were prepared as above, filled with 10 µL 100 µM resorufin in 50 mM Tris-HCl, 320 mM NH_4OAc, pH 8.7. They were then immersed in individual wells of a 96-well plate containing 200 µL de-ionized water (DI). At the indicated time points, 50 µL was removed from each and placed in a black-walled half-area plate for fluorescent analysis in a Spectramax m5 plate reader. A reading ten-fold above the noise floor of the instrument (corresponding to ~0.1% leakage) was considered a failure. The solutions were then replaced with the capsules in their original wells. After five days, the wells were left uncovered to dry. Four weeks after the capsules were fabricated, they were placed in new wells of a 96-well plate with 100 µL DI, melted by incubation at 42 °C, allowed to re-solidify, then analyzed in bottom-read mode. Release of resorufin was compared with a freshly-prepared dilution of core solution in DI, with a comparable layer of eicosane melt-cooled on top.

Controlled-release of H_2O_2. Sodium percarbonate was sieved to obtain granules approximately 1-2 mm in diameter, placed in prepared eicosane capsules (0.5 mm wall, two per capsule), and capped. 1-2 mm Alginate beads were prepared by extrusion of a 1.5% sodium alginate solution into 1 M CaCl through a blunt 25G needle. Beads were allowed to crosslink for one hour, vacuum-drained, immersed in 30% H_2O_2 for one

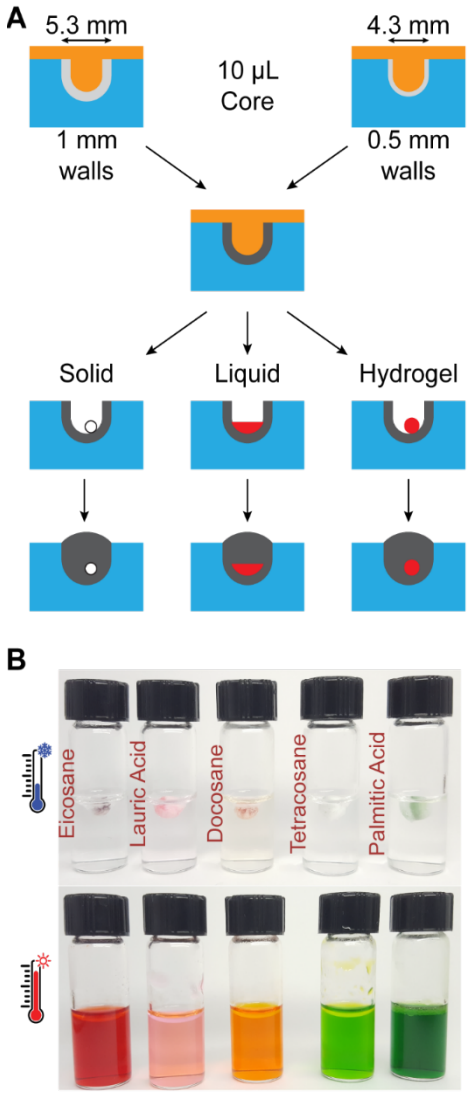

Figure 40. Phase-change capsule fabrication. **A)** Molten wax is poured into molds (blue) then a stamp (orange) is inserted to form hollow cavities. After the shell hardens, capsules can be loaded with solid granules, liquids, or hydrogel beads, then capped with more shell material. **B)** Capsules can be fabricated from a variety of materials, isolating the cargo until melted.

hour, vacuum-drained again, placed in prepared eicosane capsules (0.5 mm wall, two per capsule), and capped. Capsules with no core material were also prepared. Capsules were placed in 200 µL PCR tubes with 100 µL 10 µM DCF-DA, then analyzed with a BioRad MiniOpticon thermocyclers for 30 minutes at 25 °C followed by 30 minutes at 45 °C.

Blue-violet test for nitrate (Grotz, 1973). Test reagent was prepared by mixing 6 mg diphenylamine into 1.2 mL 3 M H_2SO_4, then adding 300 µL 18 M H_2SO_4 (this two-step process is necessary: the heat evolved during the addition of pure sulfuric acid allows the diphenylamine to fully dissolve). The traditional test is performed by mixing

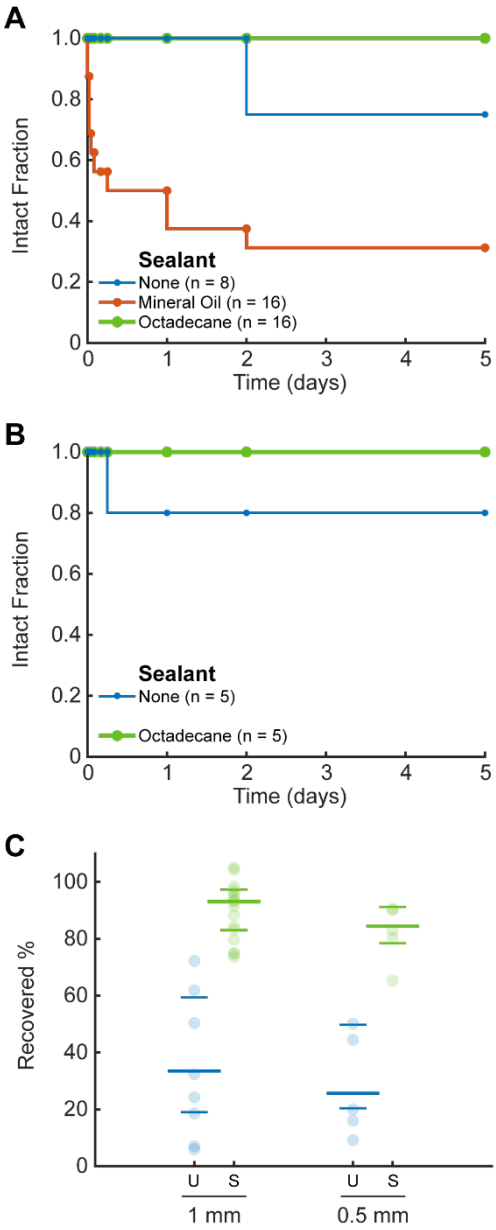

Figure 41. Capsule stability. Leakage of cargo into an aqueous solution from eicosane capsules with walls **A)** 1 mm or **B)** 0.5 mm thick. **C)** Cargo release four weeks after encapsulation. Low release indicates core solution had evaporated. Sealed capsules (S) exhibited good stability against evaporation, while unsealed capsules (U) did not. Large and small bars represent median and quartiles, respectively.

sample solution, test reagent, and pure sulfuric acid sequentially at a 3:3:10 ratio, producing a deep blue color in the presence of nitrate (improper order slows color development). We prepared eicosane capsules with 0.5 mm walls containing 10 µL test reagent or 18 M H_2SO_4. 10 µL sample solution was placed in a 0.6 mL centrifuge tube with one test reagent capsule and three pure sulfuric acid capsules then immersed in near-boiling water.

7.4 Results and Discussion

We fabricated phase-change capsules with 0.5 or 1 mm walls in a manner analogous to manual injection molding (Figure **40**A). Arrays of capsule molds were either directly 3D-printed in a flexible material or, alternatively, cast in PDMS cured in a rigid 3D-printed master 3D-printed. Molten shell material was poured into the cup-shaped molds, then a 3D-printed stamp consisting of an array of posts was inserted into the molten material to form cup-shaped hollow cavities. PDMS molds were cheaper and easier to produce in quantity than directly-printed molds, but slight (~1%) deformation during curing led to mis-alignment of the post array and produced many failed capsules with discontinuous walls. Despite a previous report (Madsen et al., 2014), room-temperature curing of the PDMS did not provide higher fidelity. The directly-printed mold gave a higher yield, particularly of 0.5 mm capsules, but imprecisions in the printing process still led to some failures. Even in intact capsules, slight misalignment produced inconsistencies in wall thickness, so the nominal thickness should be taken as approximate. Careful optimization of print design and the printing process should be able to alleviate these drawbacks.

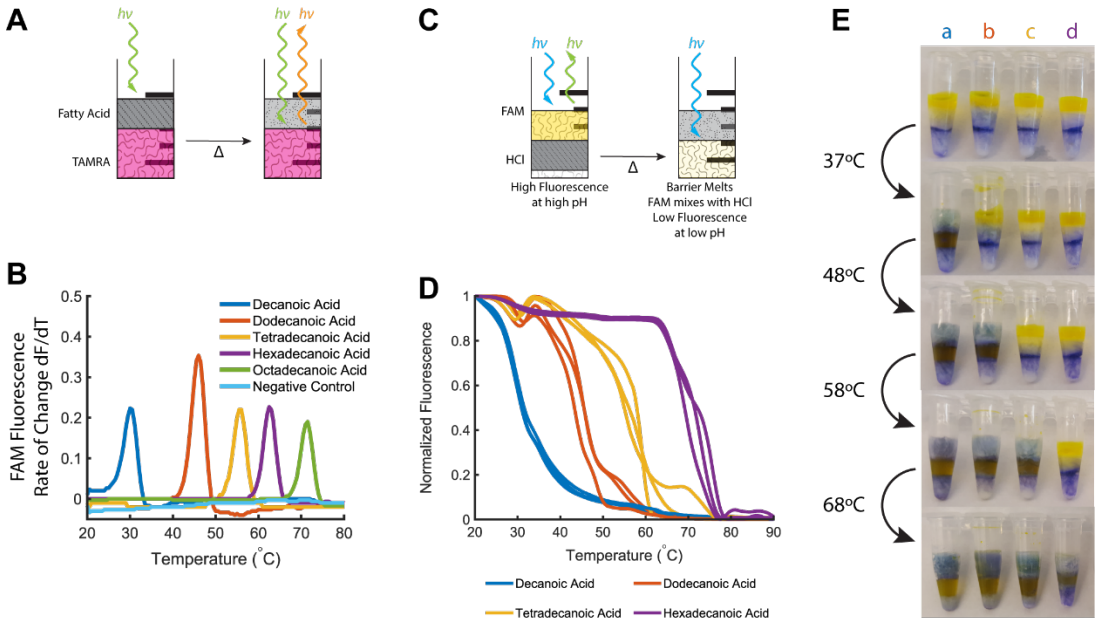

Figure 42. Characterization of fatty acids as phase-change partitions. **A)** Fatty acids were layered on top of a solution of tetramethylrhodamine (TAMRA) for fluorescent observation of melting point. **B)** Fatty acids display well-defined melting points separated by approximately 10 °C to 15 °C, as observed by a transition from opaque to transparent. **C)** Fatty acids were used to partition a solution of fluorescein (FAM) from HCl. D) As the fatty acids melted, they were displaced by the more-dense aqueous FAM solution, which mixed with the HCl. FAM is quenched at acidic pH, so the corresponding drop in fluorescence could be used to observe partition actuation. E) Fatty acids (a, decanoic; b, dodecanoic; c, tetradecanoic; d, hexadecenoic) stably isolate aqueous reagents until the appropriate actuation temperature is reached.

We successfully fabricated capsules from eicosane (m.p. 36 °C), docosane (m.p. 44 °C), tetracosane (m.p. 54 °C), lauric acid (m.p. 43 °C), and palmitic acid (m.p. 63 °C) (Figure **40**B). Fatty acids act as suitable phase-change partitions (Figure **42**), similar to the higher alkanes characterized previously. We attempted to make capsules from low-melting octadecane (m.p. 30 °C) and capric acid (m.p. 32 °C), but they lacked sufficient rigidity to be removed from the mold and manipulated without deforming. Myristic acid also failed to produce sufficiently intact capsules. After filling with 10 µL of core material, capsules were capped with molten shell material in two stages: an initial 15 µL followed by an additional 5 µL after the first had solidified. This was necessary because the high thermal gradients experienced by

the small amount of wax often led to formation of a visible pore through the center of the solidified layer; the second shell addition adequately sealed this pore. In fact, it was the formation of such a pore that limited the minimum thickness of the previously-reported layered phase-change partitions,(Goertz and White, 2018) and this staged-addition strategy may allow for thinner layers. This is in contrast to the gradual thermal gradients experienced by the capsules during casting: the large volume of molten shell material poured into the molds led to slower, more homogeneous cooling, and no such pores were observed.

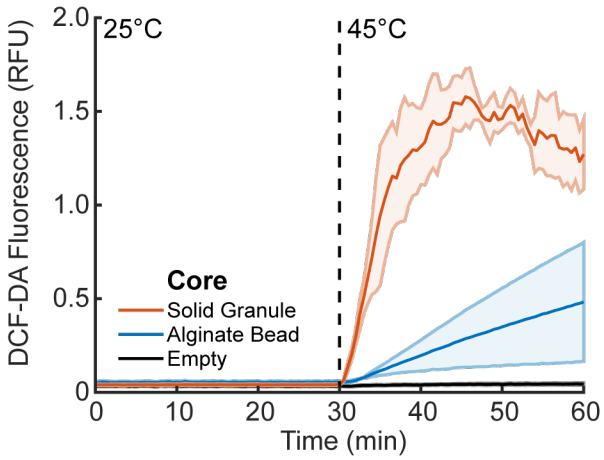

Figure 43. Capsules facilitate controlled release of diverse cargo materials. Eicosane capsules successfully sequestered both solid percarbonate granules and alginate hydrogel bea*F*ds until melting, at which point released H_2O_2 activated DCF-DA to turn-on fluorescence.

However, while the capsule walls were visibly intact, initial tests suggested that miniscule pores and cracks may be present. Previous reports have addressed this issue by preparing “self-sealing” microcapsules (Keen et al., 2014; Y. Zhao et al., 2011). In this strategy, sodium carbonate is included (at 1%) in the aqueous core, and the prepared capsules are immersed in a solution of calcium chloride. As the two salt solutions interact, calcium chloride precipitates and effectively blocks any gaps in the wall. While this approach would likely be adaptable to our capsules, we sought a sealing method less potentially harmful to encapsulated biochemical reagents and more amenable to diverse core materials. Briefly dipping the capped capsules in additional molten shell material, as reported elsewhere (Sather et al., 2015), added excessive

thickness to the capsule and risked bursting thin capsule walls during the sealing process.

Instead, we chose to immerse the capsules in a phase-change material with a lower melting point, sealing microscopic gaps while maintaining wall integrity without greatly increasing the capsule volume. Eicosane capsules were filled with the fluorophore resorufin, capped, then briefly dipped in 34 °C octadecane (below eicosane's melting point of 36 °C). For comparison, other capsules were dipped in mineral oil. We assessed stability against leakage by immersing filled capsules in DI and periodically measuring the fluorescence of this bulk solution. The minimum fluorescence we could confidently detect corresponded to leakage of approximately 0.1% of the core volume, so this constituted our threshold for "failed" encapsulation. Capsules with 1 mm walls that had been treated with mineral oil failed rapidly, nearly half leaking within a few hours (Figure **41**A). This is to be expected, since higher alkanes are slightly soluble within mineral oil. Unsealed capsules with either 0.5 or 1 mm walls led to some failures, but all octadecane-sealed capsules displayed perfect encapsulation for the entire five days (Figure **41**B).

To assess stability against evaporation, capsules were left exposed to air for an additional three weeks, then placed in fresh DI and melted. Resorufin is poorly soluble at neutral pH, so evaporated cores led to low fluorescence intensity; in contrast, cores which retained their aqueous content produced comparable fluorescence to freshly-diluted resorufin. Capsules sealed with octadecane exhibited excellent cargo release, while unsealed capsules had permitted significant evaporation of their cores (Figure **41**B).

A particularly attractive application of these phase-change capsules as a thermally-releasable reagent storage platform lies in portable assays for biological or chemical detection. To address inequities in quality of care between rural and urban areas, or between low-resource and well-funded settings, there is a great need to make biomedical diagnostic assays lightweight, portable, and easy-to-use (Chin et al., 2011; Chin et al., 2012; Ozcan, 2014; Sia and Kricka, 2008; Vashist et al., 2015; World Health Organization, 2018, 2013). Simple thermal automation via phase-change partitions offers a promising alternative to microfluidic and paper-based strategies.(Goertz and White, 2018) To this end, we investigated strategies for thermally-controlled release of H_2O_2 via phase-change capsules. Hydrogen peroxide is used to drive signal generation in a vast array of in vitro diagnostic assays (Rackus et al., 2015; Hu and Yuan, 2018; Kosman and Juskowiak, 2011; Roda et al., 2016; X. Wang et al., 2014), yet typically must be manually added after all other reaction steps have completed due to its potential to interfere with biochemical reagents. Additionally, to demonstrate the flexibility of our capsules to diverse core materials, we employed H_2O_2 both in solid state (sodium percarbonate granules) and loaded into a hydrogel (alginate beads). Granules and beads were placed into prepared capsules, capped, and immersed in a solution of DCF-DA, an oxidation-sensitive probe that reacts with H_2O_2 to yield intense fluorescence. Capsules successfully isolated their cargo until melting, at which point the solid or hydrogel cores were liberated to interact with the bulk solution (Figure **43**). This presents a convenient approach to storage and controlled-release of hydrogen peroxide for in vitro assays.

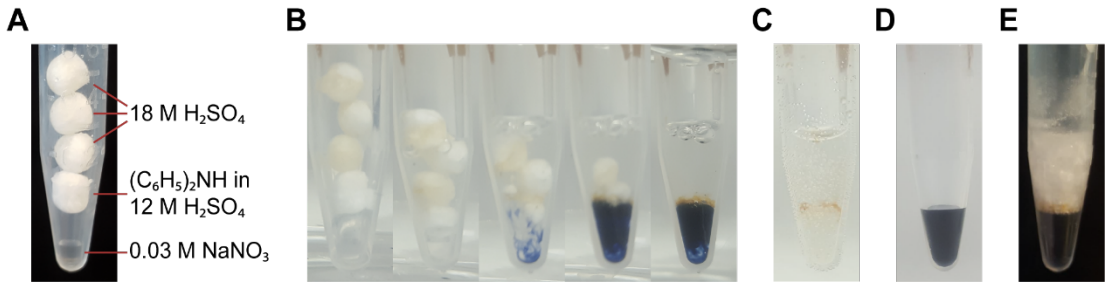

Figure 44. Encapsulation of hazardous assay reagents. **A)** Our capsule-based blue-violet test for nitrate consisted of three capsules of pure sulfuric acid and one capsule of diphenylamine in sulfuric acid. **B)** When the tube is placed in near-boiling water, the test reagent capsule melts first, mixing its cargo with the sample solution. Then, when the first sulfuric acid capsule bursts, a blue color starts to appear. Addition of more sulfuric acid from the other two capsules deepens the color. **C)** The capsule-based test run in the absence of nitrate produces no color change. **D)** Manual performance of the assay steps yields a deep blue color comparable to the capsule-based assay. **E)** After the capsule-based assay cools, the shell material re-solidifies in a layer on top of the reagent solution, isolating the hazardous chemicals.

The phase-change capsules presented here also serve the role of protecting the user from hazardous reagents, particularly important for assays intended for field-use. To demonstrate the utility, we encapsulated the reagents for the blue-violet test for nitrate (Grotz, 1973). Nitrates are pervasive groundwater contaminants that can cause severe health conditions (Bouchard et al., 1992; Power and Schepers, 1989); however, this classic assay relies on sequential addition of a test reagent and pure sulfuric acid. Naturally, the handling of such a potent oxidizing acid is extremely dangerous, and the exposure to the user and the environment should be minimized. We encapsulated these reaction components in eicosane, then placed one capsule of test reagent and three capsules of H_2SO_4 in a tube with the sample (Figure **44**A). The reaction was initiated by immersing the capped tube in near-boiling water, causing first the test-reagent capsule to burst (since it was closest to the tube walls), followed by the H_2SO_4 capsules (Figure **44**B). A blue color developed only when nitrate was present in the sample (Figure **44**C), comparable in intensity to the manually-prepared assay (Figure **44**D). After reagents were successfully released, the reaction was allowed to cool and the

eicosane re-solidified in a thick layer above the test solution, thus continuing to shield the user from exposure to the caustic components (Figure **44**E). It should be noted that this assay would have been difficult to construct with layered phase-change partitions: the high density of sulfuric acid relative to the aqueous test solution (~80% more dense) would have impaired passive mixing.

7.5 Conclusion

The phase-change capsules we present here enable encapsulation of diverse mesoscale liquids, hydrogels, and solids with thermally-stimulated burst-release. They protect core compounds from leakage and evaporation while fully releasing cargo upon mild thermal stimulation. Fabricated by a simple casting process with 3D-printed molds, capsules could be prepared from several different alkanes and fatty acids. Our approach parallels injection-molding closely, providing a modular strategy for mass-production of thermally-automated assays. We leveraged these capsules for sequestration and controlled release of hydrogen peroxide, potentially reducing the manual steps required in common biochemical reactions, and for isolation of hazardous sulfuric acid reagents from the user in an environmental-surveillance assay. Manually-molded paraffin wax capsules have previously been used to prepare aliquots of air- and moisture-sensitive reagents for chemical synthesis (Sather et al., 2015). The capsules we present here have the potential to provide similar benefits, albeit with greater flexibility in thermal characteristics and improved manufacturability. Further optimization is necessary to identify melting/cooling profiles which produce capsules of each material with the ideal crystallinity that provides maximal structural integrity. Future investigations should also attempt to fabricate smaller capsules that adequately

retain barrier functionality while minimizing the ratio of shell volume to core volume. While simple hemispherical capsules were presented here, 3D printing should allow arbitrary shapes. a range of core volumes, and an even greater diversity of shell materials than presented here. We envision the extension of our technique to the fabrication of multilayered systems and complex 3D fluidic networks actuated by heat. This system provides an ideal system for pre-packaged assays that require sequential release of reagents. The breadth of shell material melting points available should enable the design of such multi-stage assays in a thermally automated platform. These phase-change capsules provide a generic a controlled-release platform and may enable design of a broad range of portable, thermally-automated biomedical diagnostics.

8 Conclusion

The work presented here has created the potential for further development, but they have also produced many independent contributions to the field, both of which are summarized below.

8.1 Chapter 2: Literature Review: Amplified and Automated Strategies for Point-of-Care Assays

In this chapter, I collected many of the advancements made in thermal automation systems, from physical to biochemical strategies and approaches to portable temperature control. I highlighted the strengths and weaknesses of these techniques, and suggested ways in which they could be combined synergistically.

8.2 Chapter 3: Peroxidyme Amplified Radical Chain Reaction (PARCR): Visible Detection of a Catalytic Reporter

8.2.1 Summary

Here, I detailed a photochemically amplified reaction that requires no manual addition of hydrogen peroxide. In this approach, Peroxidyme-Amplified Radical Chain Reaction (PARCR), H_2O_2 is generated *in situ* from milder reagents, leading to the production of a fluorescent signaling molecule. This reaction achieves sensitive detection across a broad dynamic range due to numerous feedback loops that result from the presence of green light: positive feedback to give exponential amplification in response to the target and negative feedback to dampen the signal produced in the absence of the target. Key to its potential application at the point-of-care, quantitation of a prepared analyte with this assay requires only a cell phone camera and green LEDs.

8.2.2 Limitations and future work

Certain aspects of the reaction mechanism remain unclear, such as the nature of the observed quenching phenomenon. It also remains to be seen if the detection limit or

the assay time can be improved by identifying an optimal combination of hemin and NADH concentrations, which was observed to be a complex relationship. Furthermore, even the electrical power required for intense illumination by the green LEDs may render this system unsuitable for field settings; it would be exciting to develop a system for generating the green light chemically, *in situ*, perhaps through the chemiluminescence found in glow sticks.

8.2.3 Scientific Contributions

- A reaction driven by G-quadruplex DNA that does not require exogenous H_2O_2 but yields an intense signal across a broad dynamic range of reporter concentrations.
- Further understanding of the interaction between NADH, hemin, and G-quadruplexes aptamers.
- A mechanism for visible detection of biochemical targets through G-quadruplex DNA.
- A strategy for leveraging instability (here, photosensitivity of Amplex Red) as an asset for exponential amplification.
- The use of negative feedback to temper the nonspecific signal inherent to an amplification system driven by positive feedback.

8.3 Chapter 4: Phase-change partitions for thermal automation of multi-step reactions

8.3.1 Summary

While the assay developed in Chapter 3 provides a capable amplification strategy, it does little to improve the capabilities and accessibility of existing strategies. In

Chapter 4, I described a generic platform for achieving thermal automation of multi-part assays. Separating reagent layers with layers of purified alkanes in a common PCR tube allowed on-demand mixing through melting these barriers one-by-one. A key advantage of this system is its flexibility: the same assay in the same form-factor can be given to a researcher, a central-lab technician, and a field clinician. Several model applications were presented, but there is potential to adapt even more assays to this platform.

8.3.2 Limitations and future work

While this approach is ideal for partitioning of aqueous reagents, it is nonetheless incompatible with some oils as well as some organic solvents, such as chloroform, limiting its applicability to reactions requiring those. The thermoresponsive nature of the partitions may also complicate storage of platform, as shipping containers can readily reach temperatures in excess of 40 °C. Higher-melting alkanes could also be used but doing so would increase the materials cost of the platform and the power consumption required during operation. The platform can be improved by investigating strategies for minimizing the alkane layer thickness, thereby maximizing the number of steps available within a single PCR tube, as well as exploring techniques to improve the stability of the interface between the hydrocarbon layers and the polymer tube wall, increasing the robustness of the platform. Quantitative, theoretical analysis of the behavior of the aqueous layers within the phase-changing partitions will enable broader development of platforms based on this principle. For instance, an understanding of the forces at play leading to suspension of the aqueous solution above the bottom of the conical tube should enable construction of more complex geometries, perhaps through

3D printing. The marriage of this approach with passive microfluidic systems could greatly improve the usability of those devices. Furthermore, the range of materials capable of providing thermally-actuated partitioning of reaction solutions should be explored, perhaps with the goal of partitioning organic solvents incompatible with the alkanes used here.

8.3.3 Scientific Contributions

- A novel platform for reaction automation.
- Thermally-automated assays for isothermal nucleic acid amplification, heavy metal ion detection, and antibiotic resistance characterization.
- Insight into interplay of capillary forces in a system with non-negligible gravitational effects.
- A principle of leveraging buoyancy and density differences for reagent integration.

8.4 Chapter 5: Thermally-triggered effervescent mixing for assay automation

8.4.1 Summary

Chapter 5 showcased a potential drawback of the phase-change partition system, slow static mixing, and provided an approach to get around this problem through convective mixing from bubbles generated chemically *in situ.* Mixing of dissimilar solutions was greatly accelerated from effervescent production of CO_2 and O_2 bubbles, while a reaction for production of N_2 was also described.

8.4.2 Limitations and future work

The effervescent system should be expanded to include *in situ* generation of N_2, which exhibits the lowest reactivity of the three gases, while strategies for isolation of

the effervescent reagents from the bulk solution, perhaps through a semi-permeable membrane or capsule, would minimize their potentially detrimental impact on the main reaction system. Additionally, the tuning of this strategy to promote both burst and sustained mixing, for instance to maintain dispersion of microbeads, should be explored, as should integration of several sequential burst-mix steps. Integration of these thermally-triggered effervescent reactions into microfluidic devices could potentially simplify their design.

8.4.3 Scientific Contributions

- Demonstration of thermally-triggered reconstitution and reaction of co-dried reagents.
- An exploration of the semi-static mixing characteristics of similar and dissimilar solutions.

8.5 Chapter 6: Multi-stage chemical heating for instrument-free biosensing

8.5.1 Summary

This chapter described the actuation of these phase-change partitions in a portable manner unreliant on electricity. Encapsulated phase-change materials provided thermal buffers to a chemically-heated system, providing discrete temperature zones amenable to biochemical nucleic acid amplification.

8.5.2 Limitations and future work

Quantitative modeling of the thermodynamics of the system would provide a framework to accelerate future development of similar chemical-heating systems with bespoke, multi-phasic temperature profiles. To simplify assembly, non-eutectic

mixtures of phase change materials should be optimized and formed prior to encapsulation.

8.5.3 Scientific Contributions

- Examination of encapsulation methods for a variety of phase-change materials.
- A strategy for leveraging multiple phase-change materials and their mixed-melting thermal characteristics to achieve multi-stage temperature profiles.
- A portable heating platform for actuation of phase-change partitions.

8.6 Chapter 7: Highly stable encapsulation of diverse mesoscale materials with thermally-controlled burst-release

8.6.1 Summary

Chapter 7 detailed the re-engineering of the phase-change partition system into a self-contained, capsular format. 3D printing enabled casting of various phase-change materials to form hollow capsules that could be filled with a variety of core materials, including solid-state and hydrogel-loaded hydrogen peroxide. Sealing the capsules ensured their stability against leakage and evaporation for extensive periods of time. This platform enabled encapsulation of pure sulfuric acid for the purposes of an environmental-surveillance assay, but many more assays could be adapted to this system, which offers the benefits of high-throughput, modular, and asynchronous assembly.

8.6.2 Limitations and future work

The ideal casting conditions should be investigated further, in particular the heating/cooling profiles for each shell material which produce optimal crystallinity for capsule rigidity and minimize formation of miniscule pores and cracks. Different wall

materials could extend the capabilities of these capsules, while the adaptation of the 3D-printed casts to more complex geometries could also be explored further, as could the direct 3D printing of phase-change walls.

8.6.3 Scientific Contributions

- A method of encapsulation independent of the cargo's material characteristics, stable against leakage with thermally-controlled burst-release.
- A novel form-factor for thermal automation.
- A method for storage of air-sensitive reagents.
- A strategy for constructing dosage-controlled assays with hazardous components while protecting the user and the environment from accidental exposure.

8.7 Afterword

Thus concludes our story about hydrogen peroxide. I have described several strategies for circumventing the drawbacks of this essential reagent, from optically generating it in place to controlling biochemical reactions with thermal automation. These advances contribute to the development of point-of-care assays for detecting biological and chemical analytes in a portable, easy-to-use, low-cost manner and will hopefully one day find their way to facilitating hazardous chemical analysis, environmental surveillance, and human diagnostics.

9 References

Abe, H., Abe, N., Shibata, A., Ito, K., Tanaka, Y., Ito, M., Saneyoshi, H., Shuto, S., Ito, Y., 2012. Structure Formation and Catalytic Activity of DNA Dissolved in Organic Solvents. Angew. Chem. 124, 6581–6585. https://doi.org/10.1002/ange.201201111

Abi-Samra, K., Hanson, R., Madou, M., Gorkin, R.A., 2011. Infrared controlled waxes for liquid handling and storage on a CD-microfluidic platform. Lab. Chip 11, 723–726. https://doi.org/10.1039/C0LC00160K

Aftab, W., Huang, X., Wu, W., Liang, Z., Mahmood, A., Zou, R., 2018. Nanoconfined phase change materials for thermal energy applications. Energy Environ. Sci. 11, 1392–1424. https://doi.org/10.1039/C7EE03587J

Alivisatos, A.P., Johnsson, K.P., Peng, X., Wilson, T.E., Loweth, C.J., Bruchez, M.P., Jr, Schultz, P.G., 1996. Organization of "nanocrystal molecules" using DNA. Nature 382, 609–611. https://doi.org/10.1038/382609a0

Alva, G., Huang, X., Liu, L., Fang, G., 2017. Synthesis and characterization of microencapsulated myristic acid–palmitic acid eutectic mixture as phase change material for thermal energy storage. Appl. Energy 203, 677–685. https://doi.org/10.1016/j.apenergy.2017.06.082

Archibong, E., Konnaiyan, K.R., Kaplan, H., Pyayt, A., 2017. A mobile phone-based approach to detection of hemolysis. Biosens. Bioelectron., Special Issue Selected papers from the 26th Anniversary World Congress on Biosensors (Part I) 88, 204–209. https://doi.org/10.1016/j.bios.2016.08.030

Arnott, S., Chandrasekaran, R., Marttila, C.M., 1974. Structures for polyinosinic acid and polyguanylic acid. Biochem. J. 141, 537–543.

Baker, M.S., Phillips, S.T., 2012. A small molecule sensor for fluoride based on an autoinductive, colorimetric signal amplification reaction. Org. Biomol. Chem. 10, 3595–3599. https://doi.org/10.1039/C2OB25363A

Bastús, N.G., Comenge, J., Puntes, V., 2011. Kinetically Controlled Seeded Growth Synthesis of Citrate-Stabilized Gold Nanoparticles of up to 200 nm: Size Focusing versus Ostwald Ripening. Langmuir 27, 11098–11105. https://doi.org/10.1021/la201938u

Bhadra, S., Codrea, V., Ellington, A.D., 2014. G-quadruplex-generating PCR for visual colorimetric detection of amplicons. Anal. Biochem. 445, 38–40. https://doi.org/10.1016/j.ab.2013.10.010

Bi, S., Li, L., Zhang, S., 2010. Triggered Polycatenated DNA Scaffolds for DNA Sensors and Aptasensors by a Combination of Rolling Circle Amplification and DNAzyme Amplification. Anal. Chem. 82, 9447–9454. https://doi.org/10.1021/ac1021198

Binks, B.P., Murakami, R., Armes, S.P., Fujii, S., 2005. Temperature-Induced Inversion of Nanoparticle-Stabilized Emulsions. Angew. Chem. 117, 4873–4876. https://doi.org/10.1002/ange.200501073

Boehle, K.E., Gilliand, J., Wheeldon, C.R., Holder, A., Adkins, J.A., Geiss, B.J., Ryan, E.P., Henry, C.S., 2017. Utilizing Paper-Based Devices for Antimicrobial-Resistant Bacteria Detection. Angew. Chem. 129, 6990–6994. https://doi.org/10.1002/ange.201702776

Bouchard, D.C., Williams, M.K., Surampalli, R.Y., 1992. Nitrate Contamination of Groundwater: Sources and Potential Health Effects. J. Am. Water Works Assoc. 84, 85–90. https://doi.org/10.1002/j.1551-8833.1992.tb07430.x

Bouwmans, I., Bakker, A., Van Den Akker, H.E.A., 1997. Blending Liquids of Differing Viscosities and Densities in Stirred Vessels. Chem. Eng. Res. Des., Fluid Flow 75, 777–783. https://doi.org/10.1205/026387697524443

Buchholz, B.A., Doherty, E.A.S., Albarghouthi, M.N., Bogdan, F.M., Zahn, J.M., Barron, A.E., 2001. Microchannel DNA Sequencing Matrices with a Thermally Controlled "Viscosity Switch." Anal. Chem. 73, 157–164. https://doi.org/10.1021/ac001023z

Bueno, C., Villegas, M.L., Bertolotti, S.G., Previtali, C.M., Neumann, M.G., Encinas, M.V., 2002. The excited-state interaction of resazurin and resorufin with amines in aqueous solutions. Photophysics and photochemical reactions. Photochem. Photobiol. 76, 385–390.

Burge, S., Parkinson, G.N., Hazel, P., Todd, A.K., Neidle, S., 2006. Quadruplex DNA: sequence, topology and structure. Nucleic Acids Res. 34, 5402–5415. https://doi.org/10.1093/nar/gkl655

Burmester, S.S.H., Rielly, C.D., Edwards, M.F., 1992. The Mixing of Miscible Liquids with Large Differences in Density and Viscosity, in: Fluid Mechanics of Mixing, Fluid Mechanics and Its Applications. Springer, Dordrecht, pp. 83–90.

Buser, J.R., Diesburg, S., Singleton, J., Guelig, D., Bishop, J.D., Zentner, C., Burton, R., LaBarre, P., Yager, P., Weigl, B.H., 2015. Precision chemical heating for diagnostic devices. Lab. Chip 15, 4423–4432. https://doi.org/10.1039/C5LC01053E

Chang, D., Zakaria, S., Deng, M., Allen, N., Tram, K., Li, Y., 2016. Integrating Deoxyribozymes into Colorimetric Sensing Platforms. Sensors 16, 2061. https://doi.org/10.3390/s16122061

Chang, T., Gong, H., Ding, P., Liu, X., Li, W., Bing, T., Cao, Z., Shangguan, D., 2016. Activity Enhancement of G-Quadruplex/Hemin DNAzyme by Flanking d(CCC). Chem. – Eur. J. 22, 4015–4021. https://doi.org/10.1002/chem.201504797

Cheglakov, Z., Weizmann, Y., Beissenhirtz, M.K., Willner, I., 2006. Ultrasensitive detection of DNA by the PCR-Induced generation of DNAzymes: The DNAzyme primer approach. Chem. Commun. 3205. https://doi.org/10.1039/b605205c

Chemeris, D.A., Nikonorov, Y.M., Vakhitov, V.A., 2008. Real-time hybridization chain reaction. Dokl. Biochem. Biophys. 419, 53–55. https://doi.org/10.1134/S1607672908020014

Chen, X., Hou, Y., Wang, H., Cao, Y., He, J., 2008. Facile Deposition of Pd Nanoparticles on Carbon Nanotube Microparticles and Their Catalytic Activity for Suzuki Coupling Reactions. J. Phys. Chem. C 112, 8172–8176. https://doi.org/10.1021/jp800610q

Chen, Y., Yao, L., Deng, Y., Pan, D., Ogabiela, E., Cao, J., Adeloju, S.B., Chen, W., 2015. Rapid and ultrasensitive colorimetric detection of mercury(II) by

chemically initiated aggregation of gold nanoparticles. Microchim. Acta 182, 2147–2154. https://doi.org/10.1007/s00604-015-1538-0
Chen, Z., Cao, L., Shan, F., Fang, G., 2013. Preparation and characteristics of microencapsulated stearic acid as composite thermal energy storage material in buildings. Energy Build. 62, 469–474. https://doi.org/10.1016/j.enbuild.2013.03.025
Chen, Z., Wang, J., Qian, S., Bau, H.H., 2005. Thermally-actuated, phase change flow control for microfluidic systems. Lab. Chip 5, 1277–1285. https://doi.org/10.1039/B508275G
Cheng, N.-S., 2008. Formula for the Viscosity of a Glycerol−Water Mixture. Ind. Eng. Chem. Res. 47, 3285–3288. https://doi.org/10.1021/ie071349z
Cheng, X., Liu, X., Bing, T., Zhao, R., Xiong, S., Shangguan, D., 2009. Specific DNA G-quadruplexes bind to ethanolamines. Biopolymers 91, 874–883. https://doi.org/10.1002/bip.21272
Chevalier, Y., Bolzinger, M.-A., 2013. Emulsions stabilized with solid nanoparticles: Pickering emulsions. Colloids Surf. Physicochem. Eng. Asp., 439, 23–34. https://doi.org/10.1016/j.colsurfa.2013.02.054
Chien, W.-L., Rising, H., Ottino, J.M., 1986. Laminar mixing and chaotic mixing in several cavity flows. J. Fluid Mech. 170, 355–377. https://doi.org/10.1017/S0022112086000927
Chin, C.D., Laksanasopin, T., Cheung, Y.K., Steinmiller, D., Linder, V., Parsa, H., Wang, J., Moore, H., Rouse, R., Umviligihozo, G., Karita, E., Mwambarangwe, L., Braunstein, S.L., van de Wijgert, J., Sahabo, R., Justman, J.E., El-Sadr, W., Sia, S.K., 2011. Microfluidics-based diagnostics of infectious diseases in the developing world. Nat. Med. 17, 1015–1019. https://doi.org/10.1038/nm.2408
Chin, C.D., Linder, V., Sia, S.K., 2012. Commercialization of microfluidic point-of-care diagnostic devices. Lab. Chip 12, 2118–2134. https://doi.org/10.1039/C2LC21204H
Cho, Y.-K., Lee, J.-G., Park, J.-M., Lee, B.-S., Lee, Y., Ko, C., 2007. One-step pathogen specific DNA extraction from whole blood on a centrifugal microfluidic device. Lab. Chip 7, 565–573. https://doi.org/10.1039/B616115D
Choi, Y.H., Son, S.U., Lee, S.S., 2004. A micropump operating with chemically produced oxygen gas. Sens. Actuators Phys., Micromechanics section of Sensors and Actuators, based on contributions revised from the Technical Digest of the 16th IEEE International conference on Micro Electro mechanical Systems (MEMS 2003) 111, 8–13. https://doi.org/10.1016/j.sna.2003.10.005
Chou, Q., Russell, M., Birch, D.E., Raymond, J., Bloch, W., 1992. Prevention of pre-PCR mis-priming and primer dimerization improves low-copy-number amplifications. Nucleic Acids Res. 20, 1717–1723.
Chu, L.-Y., Utada, A.S., Shah, R.K., Kim, J.-W., Weitz, D.A., 2007. Controllable Monodisperse Multiple Emulsions. Angew. Chem. Int. Ed. 46, 8970–8974. https://doi.org/10.1002/anie.200701358
Curtis, K.A., Rudolph, D.L., Nejad, I., Singleton, J., Beddoe, A., Weigl, B., LaBarre, P., Owen, S.M., 2012. Isothermal Amplification Using a Chemical Heating

Device for Point-of-Care Detection of HIV-1. PLOS ONE 7, e31432. https://doi.org/10.1371/journal.pone.0031432
Darius, A.K.L., Ling, N.J., Mahesh, U., 2010. Visual detection of DNA from salmonella and mycobacterium using split DNAzymes. Mol. Biosyst. 6, 792. https://doi.org/10.1039/c001923b
De, P., Li, M., Gondi, S.R., Sumerlin, B.S., 2008. Temperature-Regulated Activity of Responsive Polymer−Protein Conjugates Prepared by Grafting-from via RAFT Polymerization. J. Am. Chem. Soc. 130, 11288–11289. https://doi.org/10.1021/ja804495v
Dehghan Esmatabadi, M.J., Bozorgmehr, A., Motalebzadeh, H., Bodaghabadi, N., Farhangi, B., Babashah, S., Sadeghizadeh, M., 2015. Techniques for Evaluation of LAMP Amplicons and their Applications in Molecular Biology. Asian Pac. J. Cancer Prev. APJCP 16, 7409–7414.
Deng, H., Gao, Z., 2015. Bioanalytical applications of isothermal nucleic acid amplification techniques. Anal. Chim. Acta 853, 30–45. https://doi.org/10.1016/j.aca.2014.09.037
Deng, M., Zhang, D., Zhou, Y., Zhou, X., 2008. Highly Effective Colorimetric and Visual Detection of Nucleic Acids Using an Asymmetrically Split Peroxidase DNAzyme. J. Am. Chem. Soc. 130, 13095–13102. https://doi.org/10.1021/ja803507d
Destribats, M., Lapeyre, V., Sellier, E., Leal-Calderon, F., Ravaine, V., Schmitt, V., 2012. Origin and Control of Adhesion between Emulsion Drops Stabilized by Thermally Sensitive Soft Colloidal Particles. Langmuir 28, 3744–3755. https://doi.org/10.1021/la2043763
Díaz-González, M., Fernández-Sánchez, C., Baldi, A., 2016. Multiple actuation microvalves in wax microfluidics. Lab. Chip 16, 3969–3976. https://doi.org/10.1039/C6LC00800C
Ding, Z., Fong, R.B., Long, C.J., Stayton, P.S., Hoffman, A.S., 2001. Size-dependent control of the binding of biotinylated proteins to streptavidin using a polymer shield. Nature 411, 59–62. https://doi.org/10.1038/35075028
Dirks, R.M., Pierce, N.A., 2004. Triggered amplification by hybridization chain reaction. Proc. Natl. Acad. Sci. U. S. A. 101, 15275–15278.
Dobosy, J.R., Rose, S.D., Beltz, K.R., Rupp, S.M., Powers, K.M., Behlke, M.A., Walder, J.A., 2011. RNase H-dependent PCR (rhPCR): improved specificity and single nucleotide polymorphism detection using blocked cleavable primers. BMC Biotechnol. 11, 80. https://doi.org/10.1186/1472-6750-11-80
Dong, J., Cui, X., Deng, Y., Tang, Z., 2012. Amplified detection of nucleic acid by G-quadruplex based hybridization chain reaction. Biosens. Bioelectron. 38, 258–263. https://doi.org/10.1016/j.bios.2012.05.042
Dou, M., Sanjay, S.T., Dominguez, D.C., Liu, P., Xu, F., Li, X., 2017. Multiplexed instrument-free meningitis diagnosis on a polymer/paper hybrid microfluidic biochip. Biosens. Bioelectron. 87, 865–873. https://doi.org/10.1016/j.bios.2016.09.033
Drain, P.K., Hyle, E.P., Noubary, F., Freedberg, K.A., Wilson, D., Bishai, W.R., Rodriguez, W., Bassett, I.V., 2014. Diagnostic point-of-care tests in resource-limited settings. Lancet Infect. Dis. 14, 239–249.

Dunbar, S.A., Vander Zee, C.A., Oliver, K.G., Karem, K.L., Jacobson, J.W., 2003. Quantitative, multiplexed detection of bacterial pathogens: DNA and protein applications of the Luminex LabMAP™ system. J. Microbiol. Methods, Detection of Microbial Pathogens using Molecular Methods 53, 245–252. https://doi.org/10.1016/S0167-7012(03)00028-9

Duncanson, W.J., Lin, T., Abate, A.R., Seiffert, S., Shah, R.K., Weitz, D.A., 2012. Microfluidic synthesis of advanced microparticles for encapsulation and controlled release. Lab. Chip 12, 2135–2145. https://doi.org/10.1039/C2LC21164E

Dungchai, W., Chailapakul, O., Henry, C.S., 2010. Use of multiple colorimetric indicators for paper-based microfluidic devices. Anal. Chim. Acta 674, 227–233. https://doi.org/10.1016/j.aca.2010.06.019

Du, Y., Li, B., Guo, S., Zhou, Z., Zhou, M., Wang, E., Dong, S., 2011. G-Quadruplex-based DNAzyme for colorimetric detection of cocaine: Using magnetic nanoparticles as the separation and amplification element. Analyst 136, 493–497. https://doi.org/10.1039/C0AN00557F

Eddings, M.A., Gale, B.K., 2006. A PDMS-based gas permeation pump for on-chip fluid handling in microfluidic devices. J. Micromechanics Microengineering 16, 2396. https://doi.org/10.1088/0960-1317/16/11/021

Elkharraz, K., Ahmed, A.R., Dashevsky, A., Bodmeier, R., 2011. Encapsulation of water-soluble drugs by an o/o/o-solvent extraction microencapsulation method. Int. J. Pharm. 409, 89–95. https://doi.org/10.1016/j.ijpharm.2011.02.029

Ellington, A.D., Szostak, J.W., 1990. In vitro selection of RNA molecules that bind specific ligands. Nature 346, 818–822. https://doi.org/10.1038/346818a0

Ereku, L.T., Mackay, R.E., Craw, P., Naveenathayalan, A., Stead, T., Branavan, M., Balachandran, W., 2018. RPA using a multiplexed cartridge for low cost point of care diagnostics in the field. Anal. Biochem. 547, 84–88. https://doi.org/10.1016/j.ab.2018.02.010

Fang, G., Chen, Z., Li, H., 2010a. Synthesis and properties of microencapsulated paraffin composites with SiO2 shell as thermal energy storage materials. Chem. Eng. J. 163, 154–159. https://doi.org/10.1016/j.cej.2010.07.054

Fang, G., Li, H., Chen, Z., Liu, X., 2011. Preparation and properties of palmitic acid/SiO2 composites with flame retardant as thermal energy storage materials. Sol. Energy Mater. Sol. Cells 95, 1875–1881. https://doi.org/10.1016/j.solmat.2011.02.010

Fang, G., Li, H., Liu, X., 2010b. Preparation and properties of lauric acid/silicon dioxide composites as form-stable phase change materials for thermal energy storage. Mater. Chem. Phys. 122, 533–536. https://doi.org/10.1016/j.matchemphys.2010.03.042

Fan, H., Chang, Z., Xing, R., Chen, M., Wang, Q., He, P., Fang, Y., 2008. An Electrochemical Aptasensor for Detection of Thrombin based on Target Protein-induced Strand Displacement. Electroanalysis 20, 2113–2117. https://doi.org/10.1002/elan.200804281

Farid, M.M., Khudhair, A.M., Razack, S.A.K., Al-Hallaj, S., 2004. A review on phase change energy storage: materials and applications. Energy Convers. Manag. 45, 1597–1615. https://doi.org/10.1016/j.enconman.2003.09.015

Flinn Scientific. The Effervescent Oscillator. Publ. No 74510. https://www.flinnsci.com/effervescent-oscillator/dc07451/

Foudeh, A.M., Didar, T.F., Veres, T., Tabrizian, M., 2012. Microfluidic designs and techniques using lab-on-a-chip devices for pathogen detection for point-of-care diagnostics. Lab. Chip 12, 3249–3266. https://doi.org/10.1039/C2LC40630F

Fu, E., Kauffman, P., Lutz, B., Yager, P., 2010. Chemical signal amplification in two-dimensional paper networks. Sens. Actuators B Chem. 149, 325–328. https://doi.org/10.1016/j.snb.2010.06.024

Fu, E., Liang, T., Houghtaling, J., Ramachandran, S., Ramsey, S.A., Lutz, B., Yager, P., 2011. Enhanced Sensitivity of Lateral Flow Tests Using a Two-Dimensional Paper Network Format. Anal. Chem. 83, 7941–7946. https://doi.org/10.1021/ac201950g

Gao, Z., Hou, L., Xu, M., Tang, D., 2014. Enhanced Colorimetric Immunoassay Accompanying with Enzyme Cascade Amplification Strategy for Ultrasensitive Detection of Low-Abundance Protein. Sci. Rep. 4, srep03966. https://doi.org/10.1038/srep03966

Garstecki, P., Fuerstman, M.J., A. Fischbach, M., K. Sia, S., M. Whitesides, G., 2006. Mixing with bubbles: a practical technology for use with portable microfluidic devices. Lab. Chip 6, 207–212. https://doi.org/10.1039/B510843H

Gellert, M., Lipsett, M.N., Davies, D.R., 1962. Helix formation by guanylic acid. Proc. Natl. Acad. Sci. U. S. A. 48, 2013–2018.

Ginardi, R.V.H., Saikhu, A., Sarno, R., Sunaryono, D., Kholimi, A.S., Shanty, R.N.T., 2014. Intelligent Method for Dipstick Urinalysis Using Smartphone Camera, in: Information and Communication Technology. Presented at the Information and Communication Technology - EurAsia Conference, Springer, Berlin, Heidelberg, pp. 66–77. https://doi.org/10.1007/978-3-642-55032-4_7

Glinel, K., Sukhorukov, G.B., Möhwald, H., Khrenov, V., Tauer, K., 2003. Thermosensitive Hollow Capsules Based on Thermoresponsive Polyelectrolytes. Macromol. Chem. Phys. 204, 1784–1790. https://doi.org/10.1002/macp.200350033

Goertz, J.P., Colvin, K.M., Lippe, A.B., Daristotle, J.L., Kofinas, P., White, I.M., submitted. Multi-stage chemical heating for instrument-free biosensing. Appl. Mater. Interfaces. https://doi.org/10.1101/367029

Goertz, J.P., Raghavan, S.R., White, I.M., submitted. Highly stable encapsulation of diverse mesoscale materials with thermally-controlled burst-release. Appl. Mater. Interfaces.

Goertz, J.P., White, I.M., 2018. Phase-Change Partitions for Thermal Automation of Multistep Reactions. Anal. Chem. 90, 3708–3713. https://doi.org/10.1021/acs.analchem.7b05400

Golden, A.L., Battrell, C.F., Pennell, S., Hoffman, A.S., J. Lai, J., Stayton, P.S., 2010. Simple Fluidic System for Purifying and Concentrating Diagnostic

Biomarkers Using Stimuli-Responsive Antibody Conjugates and Membranes. Bioconjug. Chem. 21, 1820–1826. https://doi.org/10.1021/bc100169y
Golub, E., Freeman, R., Willner, I., 2013. Hemin/G-Quadruplex-Catalyzed Aerobic Oxidation of Thiols to Disulfides: Application of the Process for the Development of Sensors and Aptasensors and for Probing Acetylcholine Esterase Activity. Anal. Chem. 85, 12126–12133. https://doi.org/10.1021/ac403305k
Golub, E., Freeman, R., Willner, I., 2011. A Hemin/G-Quadruplex Acts as an NADH Oxidase and NADH Peroxidase Mimicking DNAzyme. Angew. Chem. Int. Ed. 50, 11710–11714. https://doi.org/10.1002/anie.201103853
Gong, L., Zhao, Z., Lv, Y.-F., Huan, S.-Y., Fu, T., Zhang, X.-B., Shen, G.-L., Yu, R.-Q., 2015. DNAzyme-based biosensors and nanodevices. Chem. Commun. 51, 979–995. https://doi.org/10.1039/C4CC06855F
Good, B.T., Bowman, C.N., Davis, R.H., 2006. An effervescent reaction micropump for portable microfluidic systems. Lab. Chip 6, 659–666. https://doi.org/10.1039/B601542E
Gorkin, R., Park, J., Siegrist, J., Amasia, M., Lee, B.S., Park, J.-M., Kim, J., Kim, H., Madou, M., Cho, Y.-K., 2010. Centrifugal microfluidics for biomedical applications. Lab. Chip 10, 1758–1773. https://doi.org/10.1039/B924109D
Grotz, L.C., 1973. Blue-violet for nitrate ion. J. Chem. Educ. 50, 63.
Gubala, V., Harris, L.F., Ricco, A.J., Tan, M.X., Williams, D.E., 2012. Point of Care Diagnostics: Status and Future. Anal. Chem. 84, 487–515. https://doi.org/10.1021/ac2030199
Gui, L., Liu, J., 2004. Ice valve for a mini/micro flow channel. J. Micromechanics Microengineering 14, 242. https://doi.org/10.1088/0960-1317/14/2/011
Guo, X., Pethica, B.A., Huang, J.S., Prud'homme, R.K., 2004. Crystallization of Long-Chain n-Paraffins from Solutions and Melts As Observed by Differential Scanning Calorimetry. Macromolecules 37, 5638–5645. https://doi.org/10.1021/ma035848x
Guo, Y., Chen, J., Cheng, M., Monchaud, D., Zhou, J., Ju, H., 2017. A Thermophilic Tetramolecular G-Quadruplex/Hemin DNAzyme. Angew. Chem. Int. Ed. 56, 16636–16640. https://doi.org/10.1002/anie.201708964
Haiss, W., Thanh, N.T.K., Aveyard, J., Fernig, D.G., 2007. Determination of Size and Concentration of Gold Nanoparticles from UV−Vis Spectra. Anal. Chem. 79, 4215–4221. https://doi.org/10.1021/ac0702084
Hänscheid, T., 1999. Diagnosis of malaria: a review of alternatives to conventional microscopy. Clin. Lab. Haematol. 21, 235–245. https://doi.org/10.1046/j.1365-2257.1999.00220.x
Hauck, T.S., Giri, S., Gao, Y., Chan, W.C.W., 2010. Nanotechnology diagnostics for infectious diseases prevalent in developing countries. Adv. Drug Deliv. Rev., Nanotechnology Solutions for Infectious Diseases in Developing Nations 62, 438–448. https://doi.org/10.1016/j.addr.2009.11.015
Hébert, B., Bergeron, J., Potworowski, E.F., Tijssen, P., 1993. Increased PCR sensitivity by using paraffin wax as a reaction mix overlay. Mol. Cell. Probes 7, 249–252. https://doi.org/10.1006/mcpr.1993.1036

Heskins, M., Guillet, J.E., 1968. Solution Properties of Poly(N-isopropylacrylamide). J. Macromol. Sci. Part - Chem. 2, 1441–1455. https://doi.org/10.1080/10601326808051910
Esterbauer, H., 1996. Estimation of peroxidative damage. A critical review. Pathol. Biol. (Paris) 44, 25–28.
He, Y., Zhang, Y.H., Yeung, E.S., 2001. Capillary-based fully integrated and automated system for nanoliter polymerase chain reaction analysis directly from cheek cells. J. Chromatogr. A, 14th International Symposium on Microscale Separations and Analysis 924, 271–284. https://doi.org/10.1016/S0021-9673(01)00828-7
Howard, F.B., Frazier, J., Miles, H.T., 1977. Stable and metastable forms of poly(G). Biopolymers 16, 791–809. https://doi.org/10.1002/bip.1977.360160407
Hua, X., Zhou, Z., Yuan, L., Liu, S., 2013. Selective collection and detection of MCF-7 breast cancer cells using aptamer-functionalized magnetic beads and quantum dots based nano-bio-probes. Anal. Chim. Acta 788, 135–140. https://doi.org/10.1016/j.aca.2013.06.001
Hu, J., Wang, S., Wang, L., Li, F., Pingguan-Murphy, B., Lu, T.J., Xu, F., 2014. Advances in paper-based point-of-care diagnostics. Biosens. Bioelectron. 54, 585–597. https://doi.org/10.1016/j.bios.2013.10.075
Hung, Y.-L., Hsiung, T.-M., Chen, Y.-Y., Huang, Y.-F., Huang, C.-C., 2010. Colorimetric Detection of Heavy Metal Ions Using Label-Free Gold Nanoparticles and Alkanethiols. J. Phys. Chem. C 114, 16329–16334. https://doi.org/10.1021/jp1061573
Hu, X., Yuan, Q., 2018. Colorimetric Sandwich Assays for Nucleic Acid Detection, in: Biosensors Based on Sandwich Assays. Springer, Singapore, pp. 93–106.
Idota, N., Kikuchi, A., Kobayashi, J., Akiyama, Y., Sakai, K., Okano, T., 2006. Thermal Modulated Interaction of Aqueous Steroids Using Polymer-Grafted Capillaries. Langmuir 22, 425–430. https://doi.org/10.1021/la051968h
Idota, N., Kikuchi, A., Kobayashi, J., Sakai, K., Okano, T., 2005. Microfluidic Valves Comprising Nanolayered Thermoresponsive Polymer-Grafted Capillaries. Adv. Mater. 17, 2723–2727. https://doi.org/10.1002/adma.200402068
Inoue, T., Hisatsugu, Y., Ishikawa, R., Suzuki, M., 2004a. Solid–liquid phase behavior of binary fatty acid mixtures: 2. Mixtures of oleic acid with lauric acid, myristic acid, and palmitic acid. Chem. Phys. Lipids 127, 161–173. https://doi.org/10.1016/j.chemphyslip.2003.10.013
Inoue, T., Hisatsugu, Y., Yamamoto, R., Suzuki, M., 2004b. Solid–liquid phase behavior of binary fatty acid mixtures: 1. Oleic acid/stearic acid and oleic acid/behenic acid mixtures. Chem. Phys. Lipids 127, 143–152. https://doi.org/10.1016/j.chemphyslip.2003.09.014
Ito, Y., Hasuda, H., 2004. Immobilization of DNAzyme as a thermostable biocatalyst. Biotechnol. Bioeng. 86, 72–77. https://doi.org/10.1002/bit.20041
Jarlier, V., Nicolas, M.-H., Fournier, G., Philippon, A., 1988. Extended Broad-Spectrum β-Lactamases Conferring Transferable Resistance to Newer β-Lactam Agents in Enterobacteriaceae: Hospital Prevalence and Susceptibility Patterns. Rev. Infect. Dis. 10, 867–878. https://doi.org/10.1093/clinids/10.4.867

Jayasena, S.D., 1999. Aptamers: an emerging class of molecules that rival antibodies in diagnostics. Clin. Chem. 45, 1628–1650.
Jenjob, S., Sunintaboon, P., Inprakhon, P., Anantachoke, N., Reutrakul, V., 2012. Chitosan-functionalized poly(methyl methacrylate) particles by spinning disk processing for lipase immobilization. Carbohydr. Polym. 89, 842–848. https://doi.org/10.1016/j.carbpol.2012.04.019
Jiang, J., He, Y., Yu, X., Zhao, J., Cui, H., 2013. A homogeneous hemin/G-quadruplex DNAzyme based turn-on chemiluminescence aptasensor for interferon-gamma detection via in-situ assembly of luminol functionalized gold nanoparticles, deoxyribonucleic acid, interferon-gamma and hemin. Anal. Chim. Acta 791, 60–64. https://doi.org/10.1016/j.aca.2013.06.048
Jiang, L., Mancuso, M., Lu, Z., Akar, G., Cesarman, E., Erickson, D., 2014. Solar thermal polymerase chain reaction for smartphone-assisted molecular diagnostics. Sci. Rep. 4, srep04137. https://doi.org/10.1038/srep04137
Jiang, Y., Li, B., Milligan, J.N., Bhadra, S., Ellington, A.D., 2013. Real-Time Detection of Isothermal Amplification Reactions with Thermostable Catalytic Hairpin Assembly. J. Am. Chem. Soc. 135, 7430–7433. https://doi.org/10.1021/ja4023978
Jin, L.-Y., Dong, Y.-M., Wu, X.-M., Cao, G.-X., Wang, G.-L., 2015. Versatile and Amplified Biosensing through Enzymatic Cascade Reaction by Coupling Alkaline Phosphatase in Situ Generation of Photoresponsive Nanozyme. Anal. Chem. 87, 10429–10436. https://doi.org/10.1021/acs.analchem.5b02728
Jozwiakowski, M.J., Jones, D.M., Franz, R.M., 1990. Characterization of a Hot-Melt Fluid Bed Coating Process for Fine Granules. Pharm. Res. 7, 1119–1126. https://doi.org/10.1023/A:1015972007342
Kaboev, O.K., Luchkina, L.A., Tret'iakov, A.N., Bahrmand, A.R., 2000. PCR hot start using primers with the structure of molecular beacons (hairpin-like structure). Nucleic Acids Res. 28, e94–e94. https://doi.org/10.1093/nar/28.21.e94
Kaushick, A.M., Yuan, Z., Noyes, R.M., 1986. A simple demonstration of a gas evolution oscillator. J. Chem. Educ. 63, 76. https://doi.org/10.1021/ed063p76
Keen, P.H.R., Slater, N.K.H., Routh, A.F., 2014. Encapsulation of Amylase in Colloidosomes. Langmuir 30, 1939–1948. https://doi.org/10.1021/la4047897
Kellogg, D.E., Rybalkin, I., Chen, S., Mukhamedova, N., Vlasik, T., Siebert, P.D., Chenchik, A., 1994. TaqStart Antibody: "hot start" PCR facilitated by a neutralizing monoclonal antibody directed against Taq DNA polymerase. BioTechniques 16, 1134–1137.
Kermekchiev, M.B., Tzekov, A., Barnes, W.M., 2003. Cold-sensitive mutants of Taq DNA polymerase provide a hot start for PCR. Nucleic Acids Res. 31, 6139–6147. https://doi.org/10.1093/nar/gkg813
Klouda, L., Mikos, A.G., 2008. Thermoresponsive hydrogels in biomedical applications. Eur. J. Pharm. Biopharm., Interactive Polymers for Pharmaceutical and Biomedical Applications 68, 34–45. https://doi.org/10.1016/j.ejpb.2007.02.025

Knezevic, Z., Gosak, D., Hraste, M., Jalsenjako, I., 1998. Fluid-bed microencapsulation of ascorbic acid. J. Microencapsul. 15, 237–252. https://doi.org/10.3109/02652049809006853

Kong, D.-M., Cai, L.-L., Shen, H.-X., 2010. Quantitative detection of Ag^{+} and cysteine using G-quadruplex–hemin DNAzymes. Analyst 135, 1253–1258. https://doi.org/10.1039/B925168E

Kong, L.X., Parate, K., Abi-Samra, K., Madou, M., 2015. Multifunctional wax valves for liquid handling and incubation on a microfluidic CD. Microfluid. Nanofluidics 18, 1031–1037. https://doi.org/10.1007/s10404-014-1492-x

Kosman, J., Juskowiak, B., 2011. Peroxidase-mimicking DNAzymes for biosensing applications: A review. Anal. Chim. Acta 707, 7–17. https://doi.org/10.1016/j.aca.2011.08.050

Kourilov, V., Steinitz, M., 2002. Magnetic-bead enzyme-linked immunosorbent assay verifies adsorption of ligand and epitope accessibility. Anal. Biochem. 311, 166–170. https://doi.org/10.1016/S0003-2697(02)00405-0

Kubota, R., Labarre, P., Weigl, B.H., Li, Y., Haydock, P., Jenkins, D.M., 2013. Molecular diagnostics in a teacup: Non-Instrumented Nucleic Acid Amplification (NINA) for rapid, low cost detection of *Salmonella enterica*. Chin. Sci. Bull. 58, 1162–1168. https://doi.org/10.1007/s11434-012-5634-9

LaBarre, P., Gerlach, J., Wilmoth, J., Beddoe, A., Singleton, J., Weigl, B., 2010. Non-instrumented nucleic acid amplification (NINA): Instrument-free molecular malaria diagnostics for low-resource settings, in: 2010 Annual International Conference of the IEEE Engineering in Medicine and Biology. Presented at the 2010 Annual International Conference of the IEEE Engineering in Medicine and Biology, pp. 1097–1099. https://doi.org/10.1109/IEMBS.2010.5627346

LaBarre, P., Hawkins, K.R., Gerlach, J., Wilmoth, J., Beddoe, A., Singleton, J., Boyle, D., Weigl, B., 2011. A Simple, Inexpensive Device for Nucleic Acid Amplification without Electricity—Toward Instrument-Free Molecular Diagnostics in Low-Resource Settings. PLOS ONE 6, e19738. https://doi.org/10.1371/journal.pone.0019738

Lafleur, L.K., D. Bishop, J., K. Heiniger, E., P. Gallagher, R., D. Wheeler, M., Kauffman, P., Zhang, X., C. Kline, E., R. Buser, J., Kumar, S., A. Byrnes, S., J. Vermeulen, N.M., K. Scarr, N., Belousov, Y., Mahoney, W., J. Toley, B., D. Ladd, P., R. Lutz, B., Yager, P., 2016. A rapid, instrument-free, sample-to-result nucleic acid amplification test. Lab. Chip 16, 3777–3787. https://doi.org/10.1039/C6LC00677A

Latibari, S.T., Mehrali, M., Mehrali, M., Mahlia, T.M., Metselaar, H.S., 2013. Synthesis, characterization and thermal properties of nanoencapsulated phase change materials via sol–gel method. Energy 61, 664–672. https://doi.org/10.1016/j.energy.2013.09.012

Lee, B.S., Lee, J.-N., Park, J.-M., Lee, J.-G., Kim, S., Cho, Y.-K., Ko, C., 2009. A fully automated immunoassay from whole blood on a disc. Lab. Chip 9, 1548–1555. https://doi.org/10.1039/B820321K

Lee, C.-Y., Chang, C.-L., Wang, Y.-N., Fu, L.-M., 2011. Microfluidic Mixing: A Review. Int. J. Mol. Sci. 12, 3263–3287. https://doi.org/10.3390/ijms12053263
Lee, H., Park, T.G., 2008. Conjugation of Trypsin by Temperature-Sensitive Polymers Containing a Carbohydrate Moiety: Thermal Modulation of Enzyme Activity. Biotechnol. Prog. 14, 508–516. https://doi.org/10.1021/bp9701224
Lee, S.H., Noort, D. van, Lee, J.Y., Zhang, B.-T., Park, T.H., 2009. Effective mixing in a microfluidic chip using magnetic particles. Lab. Chip 9, 479–482. https://doi.org/10.1039/B814371D
Lee, T.Y., Choi, T.M., Shim, T.S., Frijns, R.A.M., Kim, S.-H., 2016. Microfluidic production of multiple emulsions and functional microcapsules. Lab. Chip 16, 3415–3440. https://doi.org/10.1039/C6LC00809G
Lequin, R.M., 2005. Enzyme Immunoassay (EIA)/Enzyme-Linked Immunosorbent Assay (ELISA). Clin. Chem. 51, 2415–2418. https://doi.org/10.1373/clinchem.2005.051532
Li, B., Liu, T., Hu, L., Wang, Y., Gao, L., 2013. Fabrication and Properties of Microencapsulated Paraffin@SiO2 Phase Change Composite for Thermal Energy Storage. ACS Sustain. Chem. Eng. 1, 374–380. https://doi.org/10.1021/sc300082m
Li, T., Dong, S., Wang, E., 2009a. G-Quadruplex Aptamers with Peroxidase-Like DNAzyme Functions: Which Is the Best and How Does it Work? Chem. – Asian J. 4, 918–922. https://doi.org/10.1002/asia.200900019
Li, T., Dong, S., Wang, E., 2009b. Label-Free Colorimetric Detection of Aqueous Mercury Ion (Hg_{2+}) Using Hg_{2+}-Modulated G-Quadruplex-Based DNAzymes. Anal. Chem. 81, 2144–2149. https://doi.org/10.1021/ac900188y
Li, T., Wang, E., Dong, S., 2010. Lead(II)-Induced Allosteric G-Quadruplex DNAzyme as a Colorimetric and Chemiluminescence Sensor for Highly Sensitive and Selective Pb_{2+} Detection. Anal. Chem. 82, 1515–1520. https://doi.org/10.1021/ac902638v
Li, T., Wang, E., Dong, S., 2009c. G-Quadruplex-based DNAzyme as a sensing platform for ultrasensitive colorimetric potassium detection. Chem. Commun. 0, 580–582. https://doi.org/10.1039/B815814B
Li, T., Wang, E., Dong, S., 2008. Chemiluminescence thrombin aptasensor using high-activity DNAzyme as catalytic label. Chem. Commun. 0, 5520–5522. https://doi.org/10.1039/B809296F
Liang, X., Wei, H., Cui, Z., Deng, J., Zhang, Z., You, X., Zhang, X.-E., 2010. Colorimetric detection of melamine in complex matrices based on cysteamine-modified gold nanoparticles. Analyst 136, 179–183. https://doi.org/10.1039/C0AN00432D
Liao, S.-C., Peng, J., Mauk, M.G., Awasthi, S., Song, J., Friedman, H., Bau, H.H., Liu, C., 2016. Smart cup: A minimally-instrumented, smartphone-based point-of-care molecular diagnostic device. Sens. Actuators B Chem. 229, 232–238. https://doi.org/10.1016/j.snb.2016.01.073
Lillis, L., Siverson, J., Lee, A., Cantera, J., Parker, M., Piepenburg, O., Lehman, D.A., Boyle, D.S., 2016. Factors influencing Recombinase polymerase

amplification (RPA) assay outcomes at point of care. Mol. Cell. Probes 30, 74–78. https://doi.org/10.1016/j.mcp.2016.01.009
Lin, Y., Jayasena, S.D., 1997. Inhibition of multiple thermostable DNA polymerases by a heterodimeric aptamer. J. Mol. Biol. 271, 100–111. https://doi.org/10.1006/jmbi.1997.1165
Liu, B., Yang, J., Zhang, Z., Yang, J., Li, D., 2018. A phase change microactuator based on paraffin wax/expanded graphite/nickel particle composite with induction heating. Sens. Actuators Phys. 275, 129–136. https://doi.org/10.1016/j.sna.2018.04.006
Liu, C., G. Mauk, M., Hart, R., Qiu, X., H. Bau, H., 2011. A self-heating cartridge for molecular diagnostics. Lab. Chip 11, 2686–2692. https://doi.org/10.1039/C1LC20345B
Liu, C., Wang, C., Li, Y., Rao, Z., 2017. Preparation and characterization of sodium thiosulfate pentahydrate/silica microencapsulated phase change material for thermal energy storage. RSC Adv. 7, 7238–7249. https://doi.org/10.1039/C6RA28056K
Liu, M., Hui, C.Y., Zhang, Q., Gu, J., Kannan, B., Jahanshahi-Anbuhi, S., Filipe, C.D.M., Brennan, J.D., Li, Y., 2016. Target-Induced and Equipment-Free DNA Amplification with a Simple Paper Device. Angew. Chem. 128, 2759–2763. https://doi.org/10.1002/ange.201509389
Liu, R.H., Bonanno, J., Yang, J., Lenigk, R., Grodzinski, P., 2004. Single-use, thermally actuated paraffin valves for microfluidic applications. Sens. Actuators B Chem. 98, 328–336. https://doi.org/10.1016/j.snb.2003.09.037
Liu, T., Nie, G., Zhang, X., Liu, W., Zhang, W., Wang, Y., Zhang, D., Wang, J., 2014. Development of a Detection Kit Based on G-Quadruplex DNAzyme for Detection of Lead(II) Ion in Food Samples. Food Anal. Methods 1133–1140. https://doi.org/10.1007/s12161-014-9990-8
Liu, W., Das, J., H. Mepham, A., R. Nemr, C., H. Sargent, E., O. Kelley, S., 2018. A fully-integrated and automated testing device for PCR-free viral nucleic acid detection in whole blood. Lab. Chip. https://doi.org/10.1039/C8LC00371H
Liu, W., Saint, D.A., 2002. Validation of a quantitative method for real time PCR kinetics. Biochem. Biophys. Res. Commun. 294, 347–353. https://doi.org/10.1016/S0006-291X(02)00478-3
Liu, Y., Meng, S., Mu, L., Jin, G., Zhong, W., Kong, J., 2008. Novel renewable immunosensors based on temperature-sensitive PNIPAAm bioconjugates. Biosens. Bioelectron. 24, 710–715. https://doi.org/10.1016/j.bios.2008.06.041
Li, W., Li, Y., Liu, Z., Lin, B., Yi, H., Xu, F., Nie, Z., Yao, S., 2016. Insight into G-quadruplex-hemin DNAzyme/RNAzyme: adjacent adenine as the intramolecular species for remarkable enhancement of enzymatic activity. Nucleic Acids Res. 44, 7373–7384. https://doi.org/10.1093/nar/gkw634
Lizardi, P.M., Huang, X., Zhu, Z., Bray-Ward, P., Thomas, D.C., Ward, D.C., 1998. Mutation detection and single-molecule counting using isothermal rolling-circle amplification. Nat. Genet. 19, 225–232. https://doi.org/10.1038/898
Logu, A.D., Uda, P., Pellerano, M.L., Pusceddu, M.C., Saddi, B., Schivo, M.L., 2001. Comparison of Two Rapid Colorimetric Methods for Determining Resistance of Mycobacterium tuberculosis to Rifampin, Isoniazid, and Streptomycin in

Liquid Medium. Eur. J. Clin. Microbiol. Infect. Dis. 20, 33–39. https://doi.org/10.1007/PL00011234
Loh, B.Y., Vuong, N.K., Chan, S., Lau, C.T., 2011. Automated Mobile pH Reader on a Camera Phone. IAENG Int. J. Comput. Sci. 38, 268–274.
Londe, G., Chunder, A., Wesser, A., Zhai, L., Cho, H.J., 2008. Microfluidic valves based on superhydrophobic nanostructures and switchable thermosensitive surface for lab-on-a-chip (LOC) systems. Sens. Actuators B Chem., Transducers '07/Eurosensors XXI 132, 431–438. https://doi.org/10.1016/j.snb.2007.10.052
Lucius, M., Falatach, R., McGlone, C., Makaroff, K., Danielson, A., Williams, C., Nix, J.C., Konkolewicz, D., Page, R.C., Berberich, J.A., 2016. Investigating the Impact of Polymer Functional Groups on the Stability and Activity of Lysozyme–Polymer Conjugates. Biomacromolecules 17, 1123–1134. https://doi.org/10.1021/acs.biomac.5b01743
Luo, Y., 2007. Preparation of MnO2 nanoparticles by directly mixing potassium permanganate and polyelectrolyte aqueous solutions. Mater. Lett. 61, 1893–1895. https://doi.org/10.1016/j.matlet.2006.07.165
Lutz, B., Liang, T., Fu, E., Ramachandran, S., Kauffman, P., Yager, P., 2013. Dissolvable fluidic time delays for programming multi-step assays in instrument-free paper diagnostics. Lab Chip 13, 2840–2847. https://doi.org/10.1039/C3LC50178G
Lutz, J.-F., Akdemir, Ö., Hoth, A., 2006. Point by Point Comparison of Two Thermosensitive Polymers Exhibiting a Similar LCST: Is the Age of Poly(NIPAM) Over? J. Am. Chem. Soc. 128, 13046–13047. https://doi.org/10.1021/ja065324n
Mackaplow, M.B., Zarraga, I.E., Morris, J.F., 2006. Rotary spray congealing of a suspension: Effect of disk speed and dispersed particle properties. J. Microencapsul. 23, 793–809. https://doi.org/10.1080/09687860600945446
Madsen, M.H., Feidenhans'l, N.A., Hansen, P.-E., Garnæs, J., Dirscherl, K., 2014. Accounting for PDMS shrinkage when replicating structures. J. Micromechanics Microengineering 24, 127002. https://doi.org/10.1088/0960-1317/24/12/127002
Mairal, T., Özalp, V.C., Sánchez, P.L., Mir, M., Katakis, I., O'Sullivan, C.K., 2008. Aptamers: molecular tools for analytical applications. Anal. Bioanal. Chem. 390, 989–1007. https://doi.org/10.1007/s00216-007-1346-4
Mamanee, W., Tuantranont, A., Afzulpurkar, N.V., Porntheerapat, N., Rahong, S., Wisitsoraat, A., 2006. PDMS Based Thermopnuematic Peristaltic Micropump for Microfluidic Systems. J. Phys. Conf. Ser. 34, 564. https://doi.org/10.1088/1742-6596/34/1/093
Martinez, A.W., Phillips, S.T., Butte, M.J., Whitesides, G.M., 2007. Patterned Paper as a Platform for Inexpensive, Low-Volume, Portable Bioassays. Angew. Chem. Int. Ed. 46, 1318–1320. https://doi.org/10.1002/anie.200603817
Martinez, A.W., Phillips, S.T., Whitesides, G.M., Carrilho, E., 2010. Diagnostics for the Developing World: Microfluidic Paper-Based Analytical Devices. Anal. Chem. 82, 3–10. https://doi.org/10.1021/ac9013989

Ma, X., Chen, Z., Zhou, J., Weng, W., Zheng, O., Lin, Z., Guo, L., Qiu, B., Chen, G., 2014. Aptamer-based portable biosensor for platelet-derived growth factor-BB (PDGF-BB) with personal glucose meter readout. Biosens. Bioelectron. 55, 412–416. https://doi.org/10.1016/j.bios.2013.12.041

Ma, Z., Jia, X., Hu, J., Zhang, G., Zhou, F., Liu, Z., Wang, H., 2013. Dual-Responsive Capsules with Tunable Low Critical Solution Temperatures and Their Loading and Release Behavior. Langmuir 29, 5631–5637. https://doi.org/10.1021/la400025j

Mazzone, P.J., Hammel, J., Dweik, R., Na, J., Czich, C., Laskowski, D., Mekhail, T., 2007. Diagnosis of lung cancer by the analysis of exhaled breath with a colorimetric sensor array. Thorax 62, 565–568. https://doi.org/10.1136/thx.2006.072892

Mellema, M., Van Benthum, W. a. J., Boer, B., Von Harras, J., Visser, A., 2006. Wax encapsulation of water-soluble compounds for application in foods. J. Microencapsul. 23, 729–740. https://doi.org/10.1080/02652040600787900

Mize, P.D., Hoke, R.A., Lin, C.P., Reardon, J.E., Schulte, T.H., 1989. Dual-enzyme cascade—An amplified method for the detection of alkaline phosphatase. Anal. Biochem. 179, 229–235. https://doi.org/10.1016/0003-2697(89)90120-6

Mohr, W.D., Saxton, R.L., Jepson, C.H., 1957. Mixing in Laminar-Flow Systems. Ind. Eng. Chem. 49, 1855–1856. https://doi.org/10.1021/ie50575a030

Molawi, K., Studer, A., 2007. Reversible switching of substrate activity of poly-N-isopropylacrylamide peptide conjugates. Chem. Commun. 0, 5173–5175. https://doi.org/10.1039/B713083J

Monteux, C., Marlière, C., Paris, P., Pantoustier, N., Sanson, N., Perrin, P., 2010. Poly(N-isopropylacrylamide) Microgels at the Oil−Water Interface: Interfacial Properties as a Function of Temperature. Langmuir 26, 13839–13846. https://doi.org/10.1021/la1019982

Morita, T., Sakamura, Y., Horikiri, Y., Suzuki, T., Yoshino, H., 2000. Protein encapsulation into biodegradable microspheres by a novel S/O/W emulsion method using poly(ethylene glycol) as a protein micronization adjuvant. J. Controlled Release 69, 435–444. https://doi.org/10.1016/S0168-3659(00)00326-6

Nakayama, S., Sintim, H.O., 2009a. Biomolecule detection with peroxidase - mimicking DNAzymes ; expanding detection modality with fluorogenic compounds. Mol. Biosyst. 6, 95–97. https://doi.org/10.1039/B916228C

Nakayama, S., Sintim, H.O., 2012. Investigating the interactions between cations, peroxidation substrates and G-quadruplex topology in DNAzyme peroxidation reactions using statistical testing. Anal. Chim. Acta 747, 1–6. https://doi.org/10.1016/j.aca.2012.08.008

Nakayama, S., Sintim, H.O., 2009b. Colorimetric split G-quadruplex probes for nucleic acid sensing: improving reconstituted DNAzyme's catalytic efficiency via probe remodeling. J. Am. Chem. Soc. 131, 10320–10333. https://doi.org/10.1021/ja902951b

Nelson, K.E., Bruesehoff, P.J., Lu, Y., 2005. *In Vitro* Selection of High Temperature Zn2+-Dependent DNAzymes. J. Mol. Evol. 61, 216–225. https://doi.org/10.1007/s00239-004-0374-3

Neo, J.L., Kamaladasan, K., Uttamchandani, M., 2012. G-Quadruplex Based Probes for Visual Detection and Sensing. Curr. Pharm. Des. 18, 2048–2057. https://doi.org/doi:10.2174/138161212799958341

Ness, J.V., Ness, L.K.V., Galas, D.J., 2003. Isothermal reactions for the amplification of oligonucleotides. Proc. Natl. Acad. Sci. 100, 4504–4509. https://doi.org/10.1073/pnas.0730811100

New England Biolabs, 2017. WarmStart® LAMP Kit (DNA & RNA).

Newmyer, S.L., Sun, J., Loehr, T.M., Ortiz de Montellano, P.R., 1996. Rescue of the horseradish peroxidase His-170-->Ala mutant activity by imidazole: importance of proximal ligand tethering. Biochemistry (Mosc.) 35, 12788–12795. https://doi.org/10.1021/bi9609331

Ngai, T., Behrens, S.H., Auweter, H., 2005. Novel emulsions stabilized by pH and temperature sensitive microgels. Chem. Commun. 0, 331–333. https://doi.org/10.1039/B412330A

Nie, J., Zhang, D.-W., Tie, C., Zhou, Y.-L., Zhang, X.-X., 2014. G-quadruplex based two-stage isothermal exponential amplification reaction for label-free DNA colorimetric detection. Biosens. Bioelectron. 56, 237–242. https://doi.org/10.1016/j.bios.2014.01.032

Noma, T., Sode, K., Ikebukuro, K., 2006. Characterization and application of aptamers for *Taq* DNA polymerase selected using an evolution-mimicking algorithm. Biotechnol. Lett. 28, 1939–1944. https://doi.org/10.1007/s10529-006-9178-4

Notomi, T., Okayama, H., Masubuchi, H., Yonekawa, T., Watanabe, K., Amino, N., Hase, T., 2000. Loop-mediated isothermal amplification of DNA. Nucleic Acids Res. 28, e63–e63. https://doi.org/10.1093/nar/28.12.e63

Obzansky, D.M., Rabin, B.R., Simons, D.M., Tseng, S.Y., Severino, D.M., Eggelte, H., Fisher, M., Harbron, S., Stout, R.W., Paolo, M.J.D., 1991. Sensitive, colorimetric enzyme amplification cascade for determination of alkaline phosphatase and application of the method to an immunoassay of thyrotropin. Clin. Chem. 37, 1513–1518.

O'Donnell, P.B., McGinity, J.W., 1997. Preparation of microspheres by the solvent evaporation technique. Adv. Drug Deliv. Rev., Biodegradable Microspheres/Therapeutic Peptide Delivery 28, 25–42. https://doi.org/10.1016/S0169-409X(97)00049-5

Ogden, S., Klintberg, L., Thornell, G., Hjort, K., Bodén, R., 2014. Review on miniaturized paraffin phase change actuators, valves, and pumps. Microfluid. Nanofluidics 17, 53–71. https://doi.org/10.1007/s10404-013-1289-3

Ozcan, A., 2014. Mobile phones democratize and cultivate next-generation imaging, diagnostics and measurement tools. Lab. Chip 14, 3187–3194. https://doi.org/10.1039/C4LC00010B

Pal, R., Yang, M., Johnson, B.N., Burke, D.T., Burns, M.A., 2004. Phase Change Microvalve for Integrated Devices. Anal. Chem. 76, 3740–3748. https://doi.org/10.1021/ac0352934

Pan, D., Liu, M., Li, F., Chen, Q., Liu, X., Liu, Y., Zhang, Z., Huang, W., Li, B., 2018. Formation mechanisms of solid in water in oil compound droplets in a

horizontal T-junction device. Chem. Eng. Sci. 176, 254–263. https://doi.org/10.1016/j.ces.2017.10.049
Papanicolaou, G.A., Medeiros, A.A., 1990. Discrimination of extended-spectrum beta-lactamases by a novel nitrocefin competition assay. Antimicrob. Agents Chemother. 34, 2184–2192.
Pavlov, V., Xiao, Y., Gill, R., Dishon, A., Kotler, M., Willner, I., 2004. Amplified Chemiluminescence Surface Detection of DNA and Telomerase Activity Using Catalytic Nucleic Acid Labels. Anal. Chem. 76, 2152–2156. https://doi.org/10.1021/ac035219l
Phillips, E.A., Shen, R., Zhao, S., Linnes, J.C., 2016. Thermally actuated wax valves for paper-fluidic diagnostics. Lab. Chip 16, 4230–4236. https://doi.org/10.1039/C6LC00945J
Pickering, S.U., 1907. Emulsions. J. Chem. Soc. Trans. 91, 2001–2021. https://doi.org/10.1039/CT9079102001
Pielichowski, K., Flejtuch, K., 2003. Differential Scanning Calorimetry Study of Blends of Poly(ethylene glycol) with Selected Fatty Acids. Macromol. Mater. Eng. 288, 259–264. https://doi.org/10.1002/mame.200390022
Piepenburg, O., Williams, C.H., Stemple, D.L., Armes, N.A., 2006. DNA Detection Using Recombination Proteins. PLoS Biol 4, e204. https://doi.org/10.1371/journal.pbio.0040204
Pollet, J., Strych, U., Willson, R.C., 2012. A peroxidase-active aptazyme as an isothermally amplifiable label in an aptazyme-linked oligonucleotide assay for low-picomolar IgE detection. The Analyst 137, 5710. https://doi.org/10.1039/c2an36201e
Porstmann, B., Porstmann, T., 1988. Chromogenic Substrates for Enzyme Immunoassay, in: Ngo, T.T. (Ed.), Nonisotopic Immunoassay. Springer US, pp. 57–84.
Pourmohamadian, H., Sheikhzadeh, G.A., Rahimi-Nasrabadi, M., Tabrizi, H.B., 2017. Fabrication and characterization of microencapsulated PA with SiO2 shell through sol–gel synthesis via sodium silicate precursor. J. Mater. Sci. Mater. Electron. 28, 9990–9997. https://doi.org/10.1007/s10854-017-6756-2
Power, J.F., Schepers, J.S., 1989. Nitrate contamination of groundwater in North America. Agric. Ecosyst. Environ., Effects of Agriculture on Groundwater 26, 165–187. https://doi.org/10.1016/0167-8809(89)90012-1
Priye, A., Bird, S.W., Light, Y.K., Ball, C.S., Negrete, O.A., Meagher, R.J., 2017. A smartphone-based diagnostic platform for rapid detection of Zika, chikungunya, and dengue viruses. Sci. Rep. 7, 44778. https://doi.org/10.1038/srep44778
Priye, A., Wong, S., Bi, Y., Carpio, M., Chang, J., Coen, M., Cope, D., Harris, J., Johnson, J., Keller, A., Lim, R., Lu, S., Millard, A., Pangelinan, A., Patel, N., Smith, L., Chan, K., Ugaz, V.M., 2016. Lab-on-a-Drone: Toward Pinpoint Deployment of Smartphone-Enabled Nucleic Acid-Based Diagnostics for Mobile Health Care. Anal. Chem. 88, 4651–4660. https://doi.org/10.1021/acs.analchem.5b04153
PureTemp, http://www.puretemp.com/.

Rackus, D.G., Shamsi, M.H.,Wheeler, A.R., 2015. Electrochemistry, biosensors and microfluidics: a convergence of fields. Chem. Soc. Rev. 44, 5320–5340. https://doi.org/10.1039/C4CS00369A

Ramos, J., Imaz, A., Forcada, J., 2012. Temperature-sensitive nanogels: poly(N -vinylcaprolactam) versus poly(N -isopropylacrylamide). Polym. Chem. 3, 852–856. https://doi.org/10.1039/C2PY00485B

Ramsden, W., 1904. Separation of solids in the surface-layers of solutions and "suspensions" (observations on surface-membranes, bubbles, emulsions, and mechanical coagulation).—Preliminary account. Proc. R. Soc. Lond. 72, 156–164. https://doi.org/10.1098/rspl.1903.0034

Buser, J.R., Zhang, X., Byrnes, S.A., Ladd, P.D., Heiniger, E.K., Wheeler, M.D., Bishop, J.D., Englund, J.A., Lutz, B., Weigl, B.H., Yager, P., 2016. A disposable chemical heater and dry enzyme preparation for lysis and extraction of DNA and RNA from microorganisms. Anal. Methods 8, 2880–2886. https://doi.org/10.1039/C6AY00107F

Reid, M.S., Le, X.C., Zhang, H., 2018. Exponential isothermal amplification of nucleic acids and amplified assays for proteins, cells, and enzyme activities. Angew. Chem. Int. Ed.

Reinhold E. Samuel, .Kashappa-Goud H Desai, Li, Z., F, O.K., P, S.S., 2012. Self-Healing Microencapsulation of Biomacromolecules without Organic Solvents. Angew. Chem. Int. Ed. 51, 10800–10803. https://doi.org/10.1002/anie.201206387

Restaino, S.M., White, I.M., 2018. Real-time multiplexed PCR using surface enhanced Raman spectroscopy in a thermoplastic chip. Lab. Chip 18, 832–839. https://doi.org/10.1039/C7LC01227F

Rida, A., Gijs, M.A.M., 2004. Manipulation of Self-Assembled Structures of Magnetic Beads for Microfluidic Mixing and Assaying. Anal. Chem. 76, 6239–6246. https://doi.org/10.1021/ac049415j

Rissin, D.M., Kan, C.W., Campbell, T.G., Howes, S.C., Fournier, D.R., Song, L., Piech, T., Patel, P.P., Chang, L., Rivnak, A.J., Ferrell, E.P., Randall, J.D., Provuncher, G.K., Walt, D.R., Duffy, D.C., 2010. Single-molecule enzyme-linked immunosorbent assay detects serum proteins at subfemtomolar concentrations. Nat. Biotechnol. 28, 595–599. https://doi.org/10.1038/nbt.1641

Roda, A., Mirasoli, M., Michelini, E., Di Fusco, M., Zangheri, M., Cevenini, L., Roda, B., Simoni, P., 2016. Progress in chemical luminescence-based biosensors: A critical review. Biosens. Bioelectron., 30th Anniversary Issue 76, 164–179. https://doi.org/10.1016/j.bios.2015.06.017

Roembke, B.T., Nakayama, S., Sintim, H.O., 2013. Nucleic acid detection using G-quadruplex amplification methodologies. Methods 64 3, 185–98.

Roy, D., Brooks, W.L.A., Sumerlin, B.S., 2013. New directions in thermoresponsive polymers. Chem. Soc. Rev. 42, 7214–7243. https://doi.org/10.1039/C3CS35499G

Roy, I., Gupta, M.N., 2003. Smart Polymeric Materials: Emerging Biochemical Applications. Chem. Biol. 10, 1161–1171. https://doi.org/10.1016/j.chembiol.2003.12.004

Ruscito, A., DeRosa, M.C., 2016. Small-Molecule Binding Aptamers: Selection Strategies, Characterization, and Applications. Front. Chem. 4. https://doi.org/10.3389/fchem.2016.00014

Ryu, H.W., Woo, S.W., Shin, B.C., Kim, S.D., 1992a. Prevention of supercooling and stabilization of inorganic salt hydrates as latent heat storage materials. Sol. Energy Mater. Sol. Cells, Special Issue on Heat Storage Materials 27, 161–172. https://doi.org/10.1016/0927-0248(92)90117-8

Ryu, H.W., Woo, S.W., Shin, B.C., Kim, S.D., 1992b. Prevention of supercooling and stabilization of inorganic salt hydrates as latent heat storage materials. Sol. Energy Mater. Sol. Cells, Special Issue on Heat Storage Materials 27, 161–172. https://doi.org/10.1016/0927-0248(92)90117-8

Saiki, R.K., Gelfand, D.H., Stoffel, S., Scharf, S.J., Higuchi, R., Horn, G.T., Mullis, K.B., Erlich, H.A., 1988. Primer-directed enzymatic amplification of DNA with a thermostable DNA polymerase. Science 239, 487–491.

Sakai, S., Hashimoto, I., Kawakami, K., 2008. Production of cell-enclosing hollow-core agarose microcapsules via jetting in water-immiscible liquid paraffin and formation of embryoid body-like spherical tissues from mouse ES cells enclosed within these microcapsules. Biotechnol. Bioeng. 99, 235–243. https://doi.org/10.1002/bit.21624

Sapan, C.V., Lundblad, R.L., Price, N.C., 1999. Colorimetric protein assay techniques. Biotechnol. Appl. Biochem. 29, 99–108. https://doi.org/10.1111/j.1470-8744.1999.tb00538.x

Sarı, A., Alkan, C., Bilgin, C., 2014. Micro/nano encapsulation of some paraffin eutectic mixtures with poly(methyl methacrylate) shell: Preparation, characterization and latent heat thermal energy storage properties. Appl. Energy 136, 217–227. https://doi.org/10.1016/j.apenergy.2014.09.047

Sarı, A., Alkan, C., Döğüşcü, D.K., Kızıl, Ç., 2015. Micro/nano encapsulated n-tetracosane and n-octadecane eutectic mixture with polystyrene shell for low-temperature latent heat thermal energy storage applications. Sol. Energy 115, 195–203. https://doi.org/10.1016/j.solener.2015.02.035

Sather, A.C., Lee, H.G., Colombe, J.R., Zhang, A., Buchwald, S.L., 2015. Dosage delivery of sensitive reagents enables glove-box-free synthesis. Nature 524, 208–211. https://doi.org/10.1038/nature14654

Schild, H.G., 1992. Poly(N-isopropylacrylamide): experiment, theory and application. Prog. Polym. Sci. 17, 163–249. https://doi.org/10.1016/0079-6700(92)90023-R

Sears, J.F., Khan, A.S., 2003. Single-tube fluorescent product-enhanced reverse transcriptase assay with Ampliwax^{TM} (STF-PERT) for retrovirus quantitation. J. Virol. Methods 108, 139–142. https://doi.org/10.1016/S0166-0934(02)00287-2

Seiffert, S., Thiele, J., Abate, A.R., Weitz, D.A., 2010. Smart Microgel Capsules from Macromolecular Precursors. J. Am. Chem. Soc. 132, 6606–6609. https://doi.org/10.1021/ja102156h

Sema, M., Alemu, A., Bayih, A.G., Getie, S., Getnet, G., Guelig, D., Burton, R., LaBarre, P., Pillai, D.R., 2015. Evaluation of non-instrumented nucleic acid amplification by loop-mediated isothermal amplification (NINA-LAMP) for

the diagnosis of malaria in Northwest Ethiopia. Malar. J. 14, 44. https://doi.org/10.1186/s12936-015-0559-9
Sener, G., Uzun, L., Denizli, A., 2014. Colorimetric Sensor Array Based on Gold Nanoparticles and Amino Acids for Identification of Toxic Metal Ions in Water. ACS Appl. Mater. Interfaces 6, 18395–18400. https://doi.org/10.1021/am5071283
Seok, Y., Byun, J.-Y., Mun, H., Kim, M.-G., 2014. Colorimetric detection of PCR products of DNA from pathogenic bacterial targets based on a simultaneously amplified DNAzyme. Microchim. Acta 181, 1965–1971. https://doi.org/10.1007/s00604-014-1297-3
Shen, L., A. Hagen, J., Papautsky, I., 2012. Point-of-care colorimetric detection with a smartphone. Lab. Chip 12, 4240–4243. https://doi.org/10.1039/C2LC40741H
Shimron, S., Wang, F., Orbach, R., Willner, I., 2012. Amplified Detection of DNA through the Enzyme-Free Autonomous Assembly of Hemin/G-Quadruplex DNAzyme Nanowires. Anal. Chem. 84, 1042–1048. https://doi.org/10.1021/ac202643y
Shin, H.K., Park, M., Kim, H.-Y., Park, S.-J., 2015. Thermal property and latent heat energy storage behavior of sodium acetate trihydrate composites containing expanded graphite and carboxymethyl cellulose for phase change materials. Appl. Therm. Eng. 75, 978–983. https://doi.org/10.1016/j.applthermaleng.2014.10.035
Shumayrikh, N., Huang, Y.C., Sen, D., 2015. Heme activation by DNA: isoguanine pentaplexes, but not quadruplexes, bind heme and enhance its oxidative activity. Nucleic Acids Res. 43, 4191–4201. https://doi.org/10.1093/nar/gkv266
Sia, S.K., Kricka, L.J., 2008. Microfluidics and point-of-care testing. Lab. Chip 8, 1982. https://doi.org/10.1039/b817915h
Silverman, S.K., 2016. Catalytic DNA: Scope, Applications, and Biochemistry of Deoxyribozymes. Trends Biochem. Sci. 41 7, 595–609.
Sim, W.Y., Yoon, H.J., Jeong, O.C., Yang, S.S., 2003. A phase-change type micropump with aluminum flap valves. J. Micromechanics Microengineering 13, 286. https://doi.org/10.1088/0960-1317/13/2/317
Singleton, J., Zentner, C., Buser, J., Yager, P., LaBarre, P., Weigl, B.H., 2013. Instrument-free exothermic heating with phase change temperature control for paper microfluidic devices. Proc. SPIE 8615, 86150R. https://doi.org/10.1117/12.2005928
Siu, V.S., Feng, J., Flanigan, P.W., Palmore, G.T.R., Pacifici, D., 2014. A “plasmonic cuvette”: dye chemistry coupled to plasmonic interferometry for glucose sensing. Nanophotonics 3, 125–140. https://doi.org/10.1515/nanoph-2013-0057
Song, J., Mauk, M.G., Hackett, B.A., Cherry, S., Bau, H.H., Liu, C., 2016. Instrument-Free Point-of-Care Molecular Detection of Zika Virus. Anal. Chem. 88, 7289–7294. https://doi.org/10.1021/acs.analchem.6b01632
Song, S., Dong, L., Qu, Z., Ren, J., Xiong, C., 2014. Microencapsulated capric–stearic acid with silica shell as a novel phase change material for thermal

energy storage. Appl. Therm. Eng. 70, 546–551. https://doi.org/10.1016/j.applthermaleng.2014.05.067
S. Satarkar, N., Biswal, D., Zach Hilt, J., 2010. Hydrogel nanocomposites: a review of applications as remote controlled biomaterials. Soft Matter 6, 2364–2371. https://doi.org/10.1039/B925218P
Stefan, L., Denat, F., Monchaud, D., 2012. Insights into how nucleotide supplements enhance the peroxidase-mimicking DNAzyme activity of the G-quadruplex/hemin system. Nucleic Acids Res. 40, 8759–8772. https://doi.org/10.1093/nar/gks581
Stojanovic, M.N., de Prada, P., Landry, D.W., 2001. Aptamer-Based Folding Fluorescent Sensor for Cocaine. J. Am. Chem. Soc. 123, 4928–4931. https://doi.org/10.1021/ja0038171
Sugihara, S., Ohashi, M., Ikeda, I., 2007. Synthesis of Fine Hydrogel Microspheres and Capsules from Thermoresponsive Coacervate. Macromolecules 40, 3394–3401. https://doi.org/10.1021/ma062365v
Sun, B.J., Shum, H.C., Holtze, C., Weitz, D.A., 2010. Microfluidic Melt Emulsification for Encapsulation and Release of Actives. ACS Appl. Mater. Interfaces 2, 3411–3416. https://doi.org/10.1021/am100860b
Sun, H., Chen, H., Zhang, X., Liu, Y., Guan, A., Li, Q., Yang, Q., Shi, Y., Xu, S., Tang, Y., 2016. Colorimetric detection of sodium ion in serum based on the G-quadruplex conformation related DNAzyme activity. Anal. Chim. Acta 912, 133–138. https://doi.org/10.1016/j.aca.2016.01.041
Suzuki, K., Yumura, T., Tanaka, Y., Akashi, M., 2001. Thermo-responsive release from interpenetrating porous silica–poly(N-isopropylacrylamide) hybrid gels. J. Controlled Release 75, 183–189. https://doi.org/10.1016/S0168-3659(01)00393-5
Taguchi, Y., Yamamoto, R., Saito, N., Tanaka, M., 2014. Preparation of Microcapsules Containing Aqueous Solution of Azur B with Melting Dispersion Cooling Method and Application to DNA Amplification Detector. J. Encapsulation Adsorpt. Sci. 04, 15. https://doi.org/10.4236/jeas.2014.41003
Tang, G., Zhao, C., Gao, J., Tan, H., 2016. Colorimetric detection of hydrogen sulfide based on terbium-G-quadruplex-hemin DNAzyme. Sens. Actuators B Chem. 237, 795–801. https://doi.org/10.1016/j.snb.2016.06.162
Tang, J., Hou, L., Tang, D., Zhang, B., Zhou, J., Chen, G., 2012. Hemin/G-quadruplex-based DNAzyme concatamers as electrocatalysts and biolabels for amplified electrochemical immunosensing of IgG1. Chem. Commun. 48, 8180–8182. https://doi.org/10.1039/C2CC33390B
Tang, J., Lee, M.F.X., Zhang, W., Zhao, B., Berry, R.M., Tam, K.C., 2014. Dual Responsive Pickering Emulsion Stabilized by Poly[2-(dimethylamino)ethyl methacrylate] Grafted Cellulose Nanocrystals. Biomacromolecules 15, 3052–3060. https://doi.org/10.1021/bm500663w
Tang, L., Liu, Y., Ali, M.M., Kang, D.K., Zhao, W., Li, J., 2012. Colorimetric and Ultrasensitive Bioassay Based on a Dual-Amplification System Using Aptamer and DNAzyme. Anal. Chem. 84, 4711–4717. https://doi.org/10.1021/ac203274k

Tanner, N.A., Zhang, Y., Evans Jr, T.C., 2012. Simultaneous multiple target detection in real-time loop-mediated isothermal amplification. Biotechniques 53, 81–89.
Teller, C., Willner, I., 2010. Functional nucleic acid nanostructures and DNA machines. Curr. Opin. Biotechnol. 21 4, 376–91.
Tombelli, S., Minunni, M., Mascini, M., 2007. Aptamers-based assays for diagnostics, environmental and food analysis. Biomol. Eng. 24, 191–200. https://doi.org/10.1016/j.bioeng.2007.03.003
Travascio, P., Li, Y., Sen, D., 1998. DNA-enhanced peroxidase activity of a DNA aptamer-hemin complex. Chem. Biol. 5, 505–517. https://doi.org/10.1016/S1074-5521(98)90006-0
Trzebicka, B., Szweda, R., Kosowski, D., Szweda, D., Otulakowski, Ł., Haladjova, E., Dworak, A., 2017. Thermoresponsive polymer-peptide/protein conjugates. Prog. Polym. Sci., Topical Volume on Biomaterials 68, 35–76. https://doi.org/10.1016/j.progpolymsci.2016.12.004
Tseng, C.-C., Yang, R.-J., Ju, W.-J., Fu, L.-M., 2018. Microfluidic paper-based platform for whole blood creatinine detection. Chem. Eng. J. 348, 117–124. https://doi.org/10.1016/j.cej.2018.04.191
Tsuji, S., Kawaguchi, H., 2008. Thermosensitive Pickering Emulsion Stabilized by Poly(N-isopropylacrylamide)-Carrying Particles. Langmuir 24, 3300–3305. https://doi.org/10.1021/la701780g
Tuerk, C., Gold, L., 1990. Systematic evolution of ligands by exponential enrichment: RNA ligands to bacteriophage T4 DNA polymerase. Science 249, 505–510. https://doi.org/10.1126/science.2200121
Vashist, S.K., Luppa, P.B., Yeo, L.Y., Ozcan, A., Luong, J.H.T., 2015. Emerging Technologies for Next-Generation Point-of-Care Testing. Trends Biotechnol. 33, 692–705. https://doi.org/10.1016/j.tibtech.2015.09.001
Velders, A.H., Schoen, C., Saggiomo, V., 2018. Loop-mediated isothermal amplification (LAMP) shield for Arduino DNA detection. BMC Res. Notes 11, 93. https://doi.org/10.1186/s13104-018-3197-9
Vladisavljević, G.T., Al Nuumani, R., Nabavi, S.A., 2017. Microfluidic Production of Multiple Emulsions. Micromachines 8, 75. https://doi.org/10.3390/mi8030075
Volk, A., Kähler, C.J., 2018. Density model for aqueous glycerol solutions. Exp. Fluids 59, 75. https://doi.org/10.1007/s00348-018-2527-y
Vreeland, W.N., Locascio, L.E., 2003. Using Bioinspired Thermally Triggered Liposomes for High-Efficiency Mixing and Reagent Delivery in Microfluidic Devices. Anal. Chem. 75, 6906–6911. https://doi.org/10.1021/ac034850j
Wahed, A.A.E., Patel, P., Faye, O., Thaloengsok, S., Heidenreich, D., Matangkasombut, P., Manopwisedjaroen, K., Sakuntabhai, A., Sall, A.A., Hufert, F.T., Weidmann, M., 2015. Recombinase Polymerase Amplification Assay for Rapid Diagnostics of Dengue Infection. PLOS ONE 10, e0129682. https://doi.org/10.1371/journal.pone.0129682
Wang, C., Wu, J., Zong, C., Ju, H., Yan, F., 2011. Highly sensitive rapid chemiluminescent immunoassay using the DNAzyme label for signal amplification. Analyst 136, 4295–4300. https://doi.org/10.1039/C1AN15512A

Wang, W., Zhang, M.-J., Chu, L.-Y., 2014. Functional polymeric microparticles engineered from controllable microfluidic emulsions. Acc. Chem. Res. 47 2, 373–84.
Wang, X., Lin, G., Cui, G., Zhou, X., Liu, G.L., 2017. White blood cell counting on smartphone paper electrochemical sensor. Biosens. Bioelectron. 90, 549–557. https://doi.org/10.1016/j.bios.2016.10.017
Wang, X., Lu, X., Chen, J., 2014. Development of biosensor technologies for analysis of environmental contaminants. Trends Environ. Anal. Chem. 2, 25–32. https://doi.org/10.1016/j.teac.2014.04.001
Wen, Y., Xu, Y., Mao, X., Wei, Y., Song, H., Chen, N., Huang, Q., Fan, C., Li, D., 2012. DNAzyme-Based Rolling-Circle Amplification DNA Machine for Ultrasensitive Analysis of MicroRNA in Drosophila Larva. Anal. Chem. 84, 7664–7669. https://doi.org/10.1021/ac300616z
Whitesides, G.M., 2006. The origins and the future of microfluidics. Nature 442, 368. https://doi.org/10.1038/nature05058
Willner, I., Shlyahovsky, B., Zayats, M., Willner, B., 2008. DNAzymes for sensing, nanobiotechnology and logic gate applications. Chem. Soc. Rev. 37 6, 1153–65.
Wong, G., Wong, I., Chan, K., Hsieh, Y., Wong, S., 2015. A Rapid and Low-Cost PCR Thermal Cycler for Low Resource Settings. PLOS ONE 10, e0131701. https://doi.org/10.1371/journal.pone.0131701
World Health Organization, 2018. Model List of Essential In Vitro Diagnostics, First. ed.
World Health Organization, 2013. World health report 2013: Research for universal health coverage.
Wu, H., Liu, Y., Wang, H., Wu, J., Zhu, F., Zou, P., 2016. Label-free and enzyme-free colorimetric detection of microRNA by catalyzed hairpin assembly coupled with hybridization chain reaction. Biosens. Bioelectron. 81, 303–308. https://doi.org/10.1016/j.bios.2016.03.013
Wu, H., Zhang, K., Liu, Y., Wang, H., Wu, J., Zhu, F., Zou, P., 2015. Binding-induced and label-free colorimetric method for protein detection based on autonomous assembly of hemin/G-quadruplex DNAzyme amplification strategy. Biosens. Bioelectron. 64, 572–578. https://doi.org/10.1016/j.bios.2014.09.096
Xiao, Y., Pavlov, V., Niazov, T., Dishon, A., Kotler, M., Willner, I., 2004. Catalytic Beacons for the Detection of DNA and Telomerase Activity. J. Am. Chem. Soc. 126, 7430–7431. https://doi.org/10.1021/ja031875r
Xu, J., Qian, J., Li, H., Wu, Z.-S., Shen, W., Jia, L., 2016. Intelligent DNA machine for the ultrasensitive colorimetric detection of nucleic acids. Biosens. Bioelectron. 75, 41–47. https://doi.org/10.1016/j.bios.2015.08.015
Xu, Y., Li, D., Cheng, W., Hu, R., Sang, Y., Yin, Y., Ding, S., Ju, H., 2016. Chemiluminescence imaging for microRNA detection based on cascade exponential isothermal amplification machinery. Anal. Chim. Acta 936, 229–235. https://doi.org/10.1016/j.aca.2016.07.007

Yager, P., Domingo, G.J., Gerdes, J., 2008. Point-of-Care Diagnostics for Global Health. Annu. Rev. Biomed. Eng. 10, 107–144. https://doi.org/10.1146/annurev.bioeng.10.061807.160524

Yang, B., Lin, Q., 2007. A latchable microvalve using phase change of paraffin wax. Sens. Actuators Phys., International Mechanical Engineering congress and Exposition 2005 134, 194–200. https://doi.org/10.1016/j.sna.2006.07.017

Yang, C., Lates, V., Prieto-Simón, B., Marty, J.-L., Yang, X., 2012. Aptamer-DNAzyme hairpins for biosensing of Ochratoxin A. Biosens. Bioelectron. 32, 208–212. https://doi.org/10.1016/j.bios.2011.12.011

Yang, L., Du, F., Chen, G., Yasmeen, A., Tang, Z., 2014. A novel colorimetric PCR-based biosensor for detection and quantification of hepatitis B virus. Anal. Chim. Acta 840, 75–81. https://doi.org/10.1016/j.aca.2014.05.032

Yang, X., Fang, C., Mei, H., Chang, T., Cao, Z., Shangguan, D., 2011. Characterization of G-Quadruplex/Hemin Peroxidase: Substrate Specificity and Inactivation Kinetics. Chem. – Eur. J. 17, 14475–14484. https://doi.org/10.1002/chem.201101941

Yang, X., Li, T., Li, B., Wang, E., 2010. Potassium -sensitive G-quadruplex DNA for sensitive visible potassium detection. Analyst 135, 71–75. https://doi.org/10.1039/B913036E

Yang, Z.-H., Zhuo, Y., Yuan, R., Chai, Y.-Q., 2015. Amplified Thrombin Aptasensor Based on Alkaline Phosphatase and Hemin/G-Quadruplex-Catalyzed Oxidation of 1-Naphthol. ACS Appl. Mater. Interfaces 7, 10308–10315. https://doi.org/10.1021/acsami.5b00988

Yan, L., Zhou, J., Zheng, Y., Gamson, A.S., Roembke, B.T., Nakayama, S., Sintim, H.O., 2014. Isothermal amplified detection of DNA and RNA. Mol. Biosyst. 10, 970–1003. https://doi.org/10.1039/C3MB70304E

Yolken, R.H., 1982. Enzyme Immunoassays for the Detection of Infectious Antigens in Body Fluids: Current Limitations and Future Prospects. Rev. Infect. Dis. 4, 35–68. https://doi.org/10.1093/clinids/4.1.35

Yoo, J.-C., Choi, Y.J., Kang, C.J., Kim, Y.-S., 2007. A novel polydimethylsiloxane microfluidic system including thermopneumatic-actuated micropump and Paraffin-actuated microvalve. Sens. Actuators Phys., Selected Papers From the Asia-Pacific Conference of Transducers and Micro-Nano Technology (APCOT 2006) 139, 216–220. https://doi.org/10.1016/j.sna.2007.04.056

Yuan, Y., Yuan, R., Chai, Y., Zhuo, Y., Ye, X., Gan, X., Bai, L., 2012. Hemin/G-quadruplex simultaneously acts as NADH oxidase and HRP-mimicking DNAzyme for simple, sensitive pseudobienzyme electrochemical detection of thrombin. Chem. Commun. 48, 4621–4623. https://doi.org/10.1039/C2CC31423A

Yuan, Y., Zhang, N., Tao, W., Cao, X., He, Y., 2014. Fatty acids as phase change materials: A review. Renew. Sustain. Energy Rev. 29, 482–498. https://doi.org/10.1016/j.rser.2013.08.107

Yu, C., Mutlu, S., Selvaganapathy, P., Mastrangelo, C.H., Svec, F., Fréchet, J.M.J., 2003. Flow Control Valves for Analytical Microfluidic Chips without Mechanical Parts Based on Thermally Responsive Monolithic Polymers. Anal. Chem. 75, 1958–1961. https://doi.org/10.1021/ac026455j

Zalba, B., Marín, J.M., Cabeza, L.F., Mehling, H., 2003. Review on thermal energy storage with phase change: materials, heat transfer analysis and applications. Appl. Therm. Eng. 23, 251–283. https://doi.org/10.1016/S1359-4311(02)00192-8

Zang, Y., Lei, J., Ling, P., Ju, H., 2015. Catalytic Hairpin Assembly-Programmed Porphyrin–DNA Complex as Photoelectrochemical Initiator for DNA Biosensing. Anal. Chem. 87, 5430–5436. https://doi.org/10.1021/acs.analchem.5b00888

Zarket, B.C., Raghavan, S.R., 2017. Onion-like multilayered polymer capsules synthesized by a bioinspired inside-out technique. Nat. Commun. 8, 193. https://doi.org/10.1038/s41467-017-00077-7

Zeng, Y., Hu, J., Long, Y., Zhang, C., 2013. Sensitive Detection of DNA Methyltransferase Using Hairpin Probe-Based Primer Generation Rolling Circle Amplification-Induced Chemiluminescence. Anal. Chem. 85, 6143–6150. https://doi.org/10.1021/ac4011292

Zhang, J., Gao, Q., Chen, P., Chen, J., Chen, G., Fu, F., 2011. A novel Tb3+-promoted G-quadruplex-hemin DNAzyme for the development of label-free visual biosensors. Biosens. Bioelectron. 26, 4053–4057. https://doi.org/10.1016/j.bios.2011.03.029

Zhang, K., Wu, W., Guo, K., Chen, J., Zhang, P., 2010. Synthesis of Temperature-Responsive Poly(N-isopropyl acrylamide)/Poly(methyl methacrylate)/Silica Hybrid Capsules from Inverse Pickering Emulsion Polymerization and Their Application in Controlled Drug Release. Langmuir 26, 7971–7980. https://doi.org/10.1021/la904841m

Zhang, L., Zhu, J., Li, T., Wang, E., 2011. Bifunctional Colorimetric Oligonucleotide Probe Based on a G-Quadruplex DNAzyme Molecular Beacon. Anal. Chem. 83, 8871–8876. https://doi.org/10.1021/ac2006763

Zhang, T., Wang, Y., Shi, H., Yang, W., 2012. Fabrication and performances of new kind microencapsulated phase change material based on stearic acid core and polycarbonate shell. Energy Convers. Manag., IREC 2011, The International Renewable Energy Congress 64, 1–7. https://doi.org/10.1016/j.enconman.2012.04.011

Zhao, B., Ranguelova, K., Jiang, J., Mason, R.P., 2011. Studies on the photosensitized reduction of resorufin and implications for the detection of oxidative stress with Amplex Red. Free Radic. Biol. Med. 51, 153–159. https://doi.org/10.1016/j.freeradbiomed.2011.03.016

Zhao, B., Summers, F.A., Mason, R.P., 2012. Photooxidation of Amplex red to resorufin: Implications of exposing the Amplex red assay to light. Free Radic. Biol. Med. 53, 1080–1087. https://doi.org/10.1016/j.freeradbiomed.2012.06.034

Zhao, W., Schafer, S., Choi, J., Yamanaka, Y.J., Lombardi, M.L., Bose, S., Carlson, A.L., Phillips, J.A., Teo, W., Droujinine, I.A., Cui, C.H., Jain, R.K., Lammerding, J., Love, J.C., Lin, C.P., Sarkar, D., Karnik, R., Karp, J.M., 2011. Cell-surface sensors for real-time probing of cellular environments. Nat. Nanotechnol. 6, 524–531. https://doi.org/10.1038/nnano.2011.101

Zhao, Y., Shum, H.C., Adams, L.L.A., Sun, B., Holtze, C., Gu, Z., Weitz, D.A., 2011. Enhanced Encapsulation of Actives in Self-Sealing Microcapsules by Precipitation in Capsule Shells. Langmuir 27, 13988–13991. https://doi.org/10.1021/la2034774

Zhou, M., Diwu, Z., Panchuk-Voloshina, N., Haugland, R.P., 1997. A Stable Nonfluorescent Derivative of Resorufin for the Fluorometric Determination of Trace Hydrogen Peroxide: Applications in Detecting the Activity of Phagocyte NADPH Oxidase and Other Oxidases. Anal. Biochem. 253, 162–168. https://doi.org/10.1006/abio.1997.2391

Zhou, M., Liu, Y., Tu, Y., Tao, G., Yan, J., 2012. DNAzyme-based turn-on chemiluminescence assays in homogenous media. Biosens. Bioelectron. 35, 489–492. https://doi.org/10.1016/j.bios.2012.03.013

Zhou, W., Huang, P.-J.J., Ding, J., Liu, J., 2014. Aptamer-based biosensors for biomedical diagnostics. Analyst 139, 2627–2640. https://doi.org/10.1039/C4AN00132J

Zhou, X.-H., Kong, D.-M., Shen, H.-X., 2010a. G-quadruplex–hemin DNAzyme-amplified colorimetric detection of Ag+ ion. Anal. Chim. Acta 678, 124–127. https://doi.org/10.1016/j.aca.2010.08.025

Zhou, X.-H., Kong, D.-M., Shen, H.-X., 2010b. Ag^{+} and Cysteine Quantitation Based on G-Quadruplex−Hemin DNAzymes Disruption by Ag^{+}. Anal. Chem. 82, 789–793. https://doi.org/10.1021/ac902421u

Zieringer, M.A., Carroll, N.J., Abbaspourrad, A., Koehler, S.A., Weitz, D.A., 2015. Microcapsules for Enhanced Cargo Retention and Diversity. Small 11, 2903–2909. https://doi.org/10.1002/smll.201403175

Zimbres, F.M., Tárnok, A., Ulrich, H., Wrenger, C., 2013. Aptamers: Novel Molecules as Diagnostic Markers in Bacterial and Viral Infections? BioMed Res. Int. 2013. https://doi.org/10.1155/2013/731516

Zoppe, J.O., Venditti, R.A., Rojas, O.J., 2012. Pickering emulsions stabilized by cellulose nanocrystals grafted with thermo-responsive polymer brushes. J. Colloid Interface Sci. 369, 202–209. https://doi.org/10.1016/j.jcis.2011.12.011